A changing North: The implications of high-volume groundwater extraction and reduced water availability on sub-arctic peatland hydrology, connectivity, and geochemistry

by

Nicole Elizabeth Balliston

A thesis

presented to the University of Waterloo

in fulfillment of the

thesis requirement for the degree of

Doctor of Philosophy

in

Geography

Waterloo, Ontario, Canada, 2022

Examining Committee Membership

The following individuals served on the Examining Committee for this thesis. The decision of the Examining Committee is by majority vote.

External Examiner   Dr. Jim Buttle

               Professor, Trent University

Supervisor   Dr. Jonathan Price

               Professor, University of Waterloo

Internal Member   Dr. Colin McCarter

               Post-doctoral Fellow, McMaster University

Internal-external Member   Dr. Brian Branfireun

               Professor, University of Western Ontario

Other Member(s)   Dr. Fereidoun Rezanezhad

               Research Associate Professor, University of Waterloo

Author's Declaration

This thesis consists of material all of which I authored or co-authored: see Statement of Contributions included in the thesis. This is a true copy of the thesis, including any required final revisions, as accepted by my examiners.

I understand that my thesis may be made electronically available to the public.

Statement of Contributions

This thesis is structured in manuscript format. Chapter 2 has been accepted in, Chapter 3 has been submitted to, and Chapter 4 will be submitted to peer-reviewed academic journals; the finalized publications may differ from the chapters presented here based on comments received during the peer review process.

Nicole Balliston used a previously developed monitoring network, and a combination of her own collected data and data collected through pre-existing monitoring programs. Nicole Balliston was responsible for all data compilation, analysis and interpretation with feedback and assistance from Dr. J. Price as thesis advisor. Nicole Balliston wrote the first draft of all chapters and thesis advisor Dr. J. Price provided editorial comments and feedback thereafter in the writing process.

Chapter 2 is accepted for publication as:

Balliston, N. E & Price, J. S (*accepted April 6, 2022*) Beyond fill and spill: Hydrological connectivity in a sub-arctic bog-fen-tributary complex in the Hudson Bay Lowlands, Canada. Hydrological Processes HYP-21-0911

Nicole Balliston was solely responsible for the data analysis and writing of the first draft of this manuscript. Dr. Price was responsible for feedback and generally minor edits thereafter. Feedback was also provided by two anonymous peer reviewers during the peer review process.

Chapter 3 is submitted as:

Balliston, N. E. & Price, J. S (submitted March 20, 2022). Landscape scale subsidence and alterations to hydrophysical structure and function in mine-dewatered peatlands in the Hudson Bay Lowlands. Submitted to Water Resources Research 2022WR032408

Nicole Balliston was solely responsible for the data analysis and writing of the first draft of this manuscript. Dr. J. Price was responsible for feedback and generally minor edits thereafter.

Chapter 4 has been prepared but not yet submitted as:

Balliston., N. E., Sutton, O., & Price, J. Hydrological and geochemical changes in disturbed sub-arctic patterned peatlands induced by mine dewatering

Nicole Balliston was responsible for the majority of data analysis and manuscript preparation. As advisor, Dr. J. Price provided guidance on data analysis and generally minor edits during manuscript preparation. Dr. Sutton assisted through the development a 1-D diffusive calcium transport model, and through his editorial comments during the manuscript preparation process.

By signing below, I indicate that I am in agreement with the evaluation of the

roles and contributions of the various authors expressed above.

J. Price   O. Sutton

Abstract

Patterned bog and fen peatlands of the Hudson Bay Lowlands (HBL) currently make up 90% of land cover in this region and form one of the largest continuous peatland complexes in the world. A globally significant storage of carbon, these peatlands are also unique ecosystems and perform valuable water regulation mechanisms in HBL watersheds. At present, the HBL region faces the increasing dual threats of resource extraction operations and increasing temperatures due to climate change, both of which may reduce water availability. In spite of their global significance, there is a dearth of information on the temporal and spatial patterns of hydrological connectivity across HBL peatland complexes, as well as the relative importance and variability of meteorological parameters. Further, studies attempting to characterize the effects of reduced water availability on hydrological structure and function in HBL peatland complexes are extremely limited. Such information is required to better understand the trajectory of these systems under future disturbance scenarios.

To this end, hydrological (i.e., streamflow and groundwater levels), meteorological (i.e., precipitation, snow depth, evapotranspiration, and temperature) and hydrogeological/geochemical (i.e., porewater samples, peat depth, surface elevation, and hydrophysical properties) data were collected from both disturbed and undisturbed peatland complexes in the HBL between 2007 and 2018. Disturbed peatlands were located within the de-watering radius of the De Beers Victor Diamond Mine, located 90 km west of Attawapiskat. The undisturbed peatlands studied here were mainly within a bog-fen-tributary complex ~30 km south of the impacted transect, monitored by the Ministry of Environment, Conservation and Parks.

Within the unimpacted peatland complex hydrological connectivity (the ease of water movement across the landscape) was generally highest in the spring, due to freshet, and fall, due to lower evapotranspiration losses. However, water transfer between peatland units occurred all year, including overwinter drainage through deeper unfrozen peat. Shoulder season temperatures were particularly important controls on hydrology by defining the length of the unfrozen season and partitioning snowmelt between peatland storage (if frost tables were absent) or streamflow (where frost tables were present). This region is projected to have greater temperature fluctuations, and longer unfrozen periods in the future, which will likely increase evapotranspiration and the frequency of snowmelt/ frost thaw desynchronization. The modelling of hydrological connectivity under this future scenario is recommended to better understand the long-term effects within this landscape.

Within the peatlands of the mine impacted transect, large downward vertical gradients lowered water tables beyond the range of natural variability. Where depleted storage was observed subsidence of up to 15 cm occurred and was higher in peatlands with thin underlying marine sediment aquitard or where pre-consolidation pressures were low (i.e., fens). Where subsidence was measured, there was generally an accompanying decline in lateral hydraulic conductivity (K_{sat}); this drove bog-fen-tributary flowpaths deeper into the peat profile, thereby potentially reducing the amount of solute-rich waters that reached the surface of at downgradient fens. This altered hydrophysical state may limit further water losses in the future, however, the reduction of solute at the surface may shift these systems away from nutrient dependent fen vegetation towards ombrotrophic bogs.

Hydrological connectivity is the ease of lateral water transfer downgradient that links runoff from peatlands to streamflow in downgradient channels; a state of hydrological connection occurs within patterned peatlands when the high transmissivity near surface is saturated. Where storage was depleted along the mine impacted transect, the proportion of time impacted peatlands spent in a hydrologically connected state was significantly reduced. Large bog-fen and fen-tributary gradients initially facilitated large water fluxes despite lower watertables, however reductions in water flux and even fen-tributary flux reversals occurred during the latter six years. In the downgradient tributaries, reduced lateral water inputs resulted in a lower normalized streamflow when compared to the unimpacted system, particularly in the latter half of the study period. In the majority of impacted peatlands, depleted water storage allowed for solute-poor precipitation to enter deeper in the peat profile while limiting the upwards advection of solute rich waters under fens. Post dewatering, the slow advection at depth and upwards diffusion of solute from the source (underlying marine sediment) may take decades or centuries for some solute concentrations (e.g., calcium) to recover within the most impacted locations. This may shift fens towards nutrient poor bogs; however, the equilibrium state of these peatlands is currently unknown. Future research should focus on applying the responses to disturbance here to different locations and scales of peatland complex in order to better understand the cumulative effects of these anthropogenic disturbances on the trajectory of these systems.

Acknowledgements

When I finished my undergraduate degree back in 2013, I swore I would run far away from academia and never look back. 9 years later facing the end of this PhD I have never been happier to prove myself wrong. To everyone and everything that made learning fun again, and who sparked my love of all things peatland, thank you for showing me my calling.

To all of those who supported me in the field, from the De Beers Victor Mine staff to my many wonderful and hardworking field assistants, thank you for making even the wettest, soggiest, buggiest moments happy memories. And to those who set up my PhD field site before me and formed the foundation of the amazing dataset I had the opportunity to work with, thank you for your time and effort. My work stands on the shoulders of giants, and I am honored to continue on the Victor legacy from those who walked (and fell off of) the boardwalks before me.

To my amazing colleagues at the Wetlands Hydrology Lab and beyond, thank you for your patience, your assistance, and your comradery both in person and in this crazy digital world we've found ourselves in. That we managed to hold together a community in such isolating and trying times is a testament to our strength as researchers and as friends. In particular, a huge thank you to Tasha-Leigh Gauthier; I cannot put into words how grateful I am for our many long musings and eventful field adventures. I look forward to tackling the many complexities of peatland science with you and having a blast along the way.

To my supervisor Dr. Jonathan Price, thanks for taking a chance on me when I cold emailed you back in 2014, and for keeping me around all these years. My life changed the moment I boarded that first flight to Victor, and I feel lucky to love this work just as today as my first day in the field. I've learned how to be a better scientist and a leader, and you have pushed me to achieve far beyond what I thought capable. Thank you as well to committee members Dr. Brian Branfireun, Dr. Colin McCarter and Dr. Fereidoun Rezanezhad as well as my external examiner Dr. Jim Buttle for your support in this process.

Last but certainly not least, to my friends and family (both human and otherwise!) thank you for reminding me that I am more than just my work. For forcing me to take breaks and enjoy the world outside this PhD. For getting me through this thesis during a pandemic with some semblance of sanity intact. And for allowing me to stop and take moss samples every time we go on a hike together. Most

importantly, thank you to my wife Lauren, for both lifting me up and keeping me grounded, and for always fueling me with your unconditional love and support during this long and trying adventure. I am honored to spend the rest of my life saving the world with you, one day at a time.

Dedication

To my wife Lauren, who spent the better part of the last two years trapped in a house with me and still wants to stick around.

Table of Contents

List of Figures

List of Tables

Chapter 1

Introduction

The patterned bog and fen peatlands of the Hudson Bay Lowlands (HBL), constituting 90% of land cover in this region, form one of the largest continuous peatland complexes in the world (Rouse *et al.,* 1992). A globally significant storage of carbon (Loisel *et al.,* 2021), these peatlands are also unique ecosystems and perform valuable water regulation mechanisms in HBL watersheds. Outflow from these peatland complexes provides a substantial portion of both higher and lower order tributary discharge (Orlova & Branfireun, 2014), influences stream geochemistry (Richardson *et al.,* 2012; Rouse *et al.,* 1992), and buffers salt-water intrusion from the saline oceanic waters at the coast (Price *et al.,* 1989). Despite their prominence and global significance, the remoteness of this landscape has left a dearth of knowledge on the hydrological processes and feedbacks that regulate water quality and quantity in HBL peatland complexes. With the combined effects of climate change (IPCC, 2022) and the increasing demand for resource extraction in this area, there is a growing need to better understand peatland hydrological and hydrogeochemical feedbacks in these complexes in both natural and disturbed states.

Peat accumulation has been occurring in the HBL region for over 5000 years (Glaser *et al.,* 2004b). Favorable conditions for accumulation were first initiated after the retreat of the Tyrell-sea due to isostatic uplift, leaving a flat, poorly drained landscape underlain by low permeability marine sediment (MS) (Lee, 1959; Price & Woo, 1988). Limited drainage through this MS layer, coupled with a cool and moist climate (Rouse *et al.,* 1992), resulted in the long-term maintenance of high-water table conditions (Glaser *et al.,* 2004; Reeve *et al.,* 2000). In this waterlogged environment, decomposition was slowed thus favoring the accumulation of organic material. Presently, the regional average peat depth is 2.4 meters and increases from the coast inland, roughly mimicking the successional pathway from coastal marsh to the patterned bog and fen complexes (Glaser *et al.,* 2004a, b; Riley, 2011).

In the HBL, patterned bogs form the topographical highs in the landscape, with thicker peat deposits and elevated (1-2 m) surfaces compared to downgradient fens (Difebo *et al.,* 2015). During high water table conditions, a high transmissivity layer near the surface of the bogs is saturated and water is shuttled quickly downgradient to fens and surface water features in a process typically referred to as "fill and spill" (Spence & Woo, 2003; Balliston & Price, 2018; McCarter & Price,

2017). Fens, in turn, act as water conveyance mechanisms where pools orient perpendicular to flow between higher ridges, forming a conveyer-like pattern in the landscape (Price, 1994; Glaser, 1989; Price & Maloney, 1994). During high water table conditions, fen pools connect across higher ridges, shuttling water downgradient to surface water features (McCarter & Price, 2017; Quinton & Roulet, 1998; Spence & Woo, 2003). In both bogs and fens, the degree of decomposition increases with depth (Hayward & Clymo, 1982), typically resulting in peat that has higher bulk density, lower total and effective porosity (Rezanezhad *et al.,* 2016), and lower transmissivity (Balliston *et al.,* 2018; McCarter & Price, 2017) at depth. When water tables fall below the high transmissivity layer near the surface, flow must travel through this deeper and typically lower conductivity peat, greatly lowering the rate at which water is transferred downgradient (McCarter & Price, 2017).

The amount of water transferred along bog-fen-tributary flowpaths (i.e., degree of hydrological connectivity) is temporally dynamic, with 50-75% of runoff occurring during high flow periods (Quinton & Roulet, 1998; Orlova & Branfireun, 2014) which can occur over <15% of the unfrozen season (Quinton & Roulet, 1998). Variability within and between seasons is high, however, and there is a lack of information on the temporal and spatial patterns of connectivity across bog-fen-tributary systems in the HBL region, particularly over consecutive years. Further, the relative influence of differing meteorological fluxes (e.g., rainfall, snowmelt, evapotranspiration) has been understudied, making it difficult to understand the impacts of disturbance vs. natural variability in hydrological fluxes. Knowledge regarding the effects of reduced water availability on hydrological structure and function in HBL peatland complexes is also limited. One case study on the effects of large volume groundwater extraction was presented at the De Beers Victor Diamond Mine, located ~90 km of Attawapiskat in the James Bay Lowland (JBL), which was actively dewatered for 12 years (Itasca Denver, 2017). In the first year of dewatering, a ~1.5 km transect was instrumented within the radius of mine dewatering to assess the impact of deep aquifer depressurization on peatland hydrological structure and function (Whittington & Price, 2012a).

Over the first five years of dewatering, deep seepage fluxes (i.e., downwards movement of water from overlying peat towards the MS layer) increased by up to an order of magnitude within mine-impacted peatlands, from <0.1 mm/day pre-impact (HCL, 2004) to up to 4 mm/day (Whittington & Price, 2012a, b). Areas with increased downwards flux corresponded to lower water tables and an average surface consolidation of 7 cm, with more pronounced impacts in peatlands with a thinner underlying MS confining layer (Whittington & Price, 2012a, b; Leclair *et al.,* 2015). In unimpacted

2

peatlands, when water tables decline near surface peat undergoes reversible consolidation though a process known as "mire breathing" (Ingram, 1983), where the surface of the peatland rises and falls in tandem with the water table due to the highly porous (Berry & Poskitt, 1972) and elastic structure (Price & Schlotzhauer, 1999; Kellner & Halldin, 2002). This allows for regulation of water storage and alleviation of moisture stress during low water availability (Fritz, 2006), increasing water content at the surface (Roulet, 1991; Whittington & Price, 2006). The amount of reversible consolidation relative to subsidence (i.e., irreversible consolidation) within mine impacted peatlands, however, is currently unknown. It is also unclear if subsidence continued to proceed for the remainder of the mine dewatering, and if this resulted in observable changes in peat hydro physical structure or altered bog-fen-tributary flowpaths. Such information is paramount to understanding the long-term changes to the hydrological functioning of these peatland complexes, particularly after dewatering concludes.

In unimpacted peatland complexes, porewater geochemistry is closely linked with the mixing of water sources along bog-fen-tributary flowpaths. The upgradient bogs are ombrotrophic, receiving precipitation-sourced water, low in nutrients and major ions (Sjors, 1963; Glaser *et al.,* 2004). A portion of the water which enters bog storage is advected downwards towards the MS layer, before inflecting upwards near the peat/MS interface due to the low hydraulic conductivity in the latter (Reeve *et al.,* 2000; 2001). Along this advective flowpath, waters are enriched with decomposition products and MS derived ions which diffuse upwards (Glaser *et al.,* 2004; Orlova & Branfireun, 2014). Solute enriched water is then upwelled at the surface of downgradient fens, mixing with solute-poor waters that travel across the high transmissivity near surface during high water table conditions. During the first five years of mine dewatering, depleted water storage in the mine-impacted peatlands (Whittington & Price, 2012, Leclair *et al.,* 2015) suggests a disruption in the near surface flow of water between bogs and fens. Limited isotopic analysis suggests that this may increase the amount of solute-poor water (i.e., precipitation sourced) entering deeper into the peat profile (Perras, 2016). The effects of the disruption of these flow pathways on the composition of porewater within the peat profile and in different peatlands along the impacted transect is, however, uncertain. As fen vegetation is reliant on minimum concentrations of solutes, changes in porewater geochemistry at the surface has implications on the trajectory of these systems long after dewatering has ceased.

1.1 Objectives

The goal of this research is to better understand the hydrological functioning of patterned peatland complexes within the HBL landscape related to changes in water availability, both in unimpacted and in mine-impacted systems. The objectives of this dissertation are thus to:

1. Gain a better understanding of undisturbed peatland complex hydrology though the assessment of seasonal and annual changes in water storage and transmission within an undisturbed bog-fen-tributary complex, and determine how this influences the degree and timing of hydrological connectivity across the landscape,

2. Quantify the changes in peatland hydrological structure and function in bog and fen peatlands in a mine impacted landscape over the lifespan of the mine, and contrast to unimpacted peatland complexes, and

3. Assess the changes in water storage and transmission within and between peatlands in a mine impacted landscape and the resulting changes to peatland hydrological connectivity and hydrogeochemistry, relative to unimpacted peatland complexes.

1.1.1 Organization of Thesis

This thesis has been structured in fulfillment of the manuscript option at the University of Waterloo. Chapter 1 provides an introduction to, and context for, the thesis as well as the goal and objectives of this research. Each objective is then addressed within the following three chapters. Chapter 2 focuses on the hydrological functioning of an unimpacted bog-fen-tributary complex to better understand hydrological feedbacks related to seasonal and annual variations in water availability. Chapters 3 and 4 focus on mine-impacted peatlands, first on the physical changes to the peat profile and the resulting alterations in hydrological functioning, then on the direct consequences of dewatering and the associated changes in water quality and quantity in mine-impacted peatlands.

The conclusions of this thesis are in Chapter 5, followed by three appendices: Appendix A contains supplementary figures and tables related to Chapter 2, Appendix B contains supplementary figures and tables related to Chapter 3, and Appendix C contains supplementary figures and tables related to Chapter 4.

Chapter 2

Beyond fill and spill: Hydrological connectivity in a sub-arctic bog-fen-tributary complex in the Hudson Bay Lowlands, Canada

2.1 Summary

Patterned bog and fen peatlands, which dominate the landscape in the Hudson Bay Lowlands (HBL), act as important water storage and conveyance features in this region. In spite of their hydrological importance, there are currently no studies that define and characterize the thresholds of bog-fen-tributary hydrological connectivity in the HBL or their relation to seasonal and annual changes in water fluxes. To this end, hydrological (i.e., streamflow and groundwater levels) and meteorological (i.e., precipitation, snow depth, evapotranspiration, and temperature) data were collected at a 4.8 km^2 bog-fen-tributary complex between 2007 and 2018. Connectivity thresholds were best characterized into three states (disconnected, connected, and high activity) that incorporated 41, 47, and 12% of the study period and 4, 18, and 78% of runoff, respectively. Runoff generally peaked in the spring due to snowmelt, while connectivity was highest in the peatlands in the fall months when precipitation exceeded evapotranspiration due to cooling temperatures. Warmer than average spring temperatures accelerated snowmelt rate faster than frost table thaw rate in the fen; this reduced the amount of meltwater that entered storage, increased drainage from bog to fen and decreased overall connectivity in the unfrozen season. Cooler than average spring temperatures delayed bog connection and ground thaw; the late frost melt provided a source of water to the bogs after melt into the late spring and early summer. This study provides a basis for the modelling of peatland hydrological connectivity in the region in the drier conditions anticipated with climatic warming and regional resource extraction.

2.2 Introduction

In the James Bay Lowland (JBL), the southeastern portion of the larger Hudson Bay Lowlands (HBL), patterned peatland complexes perform important water storage and conveyance functions within the landscape (Glaser *et al.,* 2004a). Peat accumulation has been favoured in this area for over 5000 years (Glaser *et al.,* 2004b) due to a flat regional landscape (Price & Woo, 1988), cool and moist climate (Rouse *et al.,* 1992), and a layer of low permeability marine sediment deposited during the regional inundation of the Tyrell sea after glacial retreat ~8500 cal yr BP (Lee, 1959; Price &

5

Woo, 1988). Present day average peat depth is 2.4 m, though highly spatially variable, and is generally higher in bogs than in fens (Glaser *et al.,* 2004b). Along the peat profile, hydraulic conductivity is highest at the surface in the poorly decomposed, variably saturated acrotelm (Ingram, 1978), with reported values as high as 10^2-10^3 m/day in the top 30 cm of the peat profile (Balliston *et al.,* 2018; McCarter & Price, 2017). The transition between the acrotelm and the fully saturated catotelm (Ingram, 1978) below is marked by increasing decomposition and bulk density (Hayward & Clymo, 1982), decreasing total and effective porosity (Rezanezhad *et al.,* 2016), and decreasing saturated hydraulic conductivity by up to 3 orders of magnitude (Balliston *et al.,* 2018; McCarter & Price, 2017). Hydraulic conductivity in the marine sediment below the peat profile is low compared to that in the peat ($1x10^{-3}$ m/day), limiting drainage (Whittington & Price, 2013).

Presently, peatlands generate up to 50% of the discharge of the higher order tributaries of the Attawapiskat River, which is one of the largest rivers of the JBL (Orlova & Branfireun, 2014), as well as a large percentage of low and higher order tributary baseflow (Richardson *et al*. 2012). Downgradient, higher order streams drain into James Bay, buffering saltwater intrusion inland (Price *et al.,* 1989). The HBL region is facing the dual threat of increasing pressure for resource extraction and rapidly shifting temperature and precipitation patterns due to climate change (IPCC, 2013); both have the potential to reduce water availability in this region. It is therefore paramount to understand the hydrological connectivity (i.e., the ease of lateral water transfer downgradient that links runoff from peatlands to streamflow in downgradient channels) of patterned peatland complexes across the landscape to determine the probable function of these systems under water limited scenarios that are likely in the future.

At a broad scale, water movement in patterned peatland complexes is governed by the topographical arrangement of peatland forms across the landscape and their differing hydrological attributes and antecedent moisture conditions (Siegel & Glaser, 2006). Both bogs and fens in this area are patterned (i.e., form mosaics of high and low microtopography) and are *Sphagnum* dominated; each have distinct roles in the landscape.

Patterned bogs are domed with disorganized pools at their crest and a hummock hollow microtopography, sometimes featuring poor fen water tracks along the steeper edges (Glaser *et al.,* 2004a; Price, 1994). Compared to local fens, domed bogs have slightly elevated (~1-2 m) surfaces (Difebo *et al.,* 2015) and thicker peat deposits (Glaser *et al.,* 2004a), resulting in higher water table

elevations but deeper water tables. Patterned bogs act mainly as water storage features and source-water areas for downgradient fens (Price & Maloney, 1994). During periods of high water table elevation, such as spring melt, bog water tables reside in the near-surface, high transmissivity layer in hollows (Oosterwoud *et al.*, 2017) and sometimes above the surface in interconnected hollows (Balliston *et al.,* 2018), readily releasing water to fens and surface water systems. During low water table conditions, water transfer is restricted to the saturated zone of deeper peat, which has relatively low hydraulic conductivity (Balliston & Price, 2018; McCarter & Price, 2017).

Downgradient patterned fens are commonly characterized by an alternating ridge/pool topography oriented perpendicular to the direction of flow, with decreasing pool sizes along the flowpath (Price, 1994), which typically drain into surface water features or larger channel fens (Glaser, 1989; Price & Maloney, 1994; Ulanowski, 2014). During wet periods, elevated water tables reach a given threshold at which time adjacent fen pools connect across ridges (Price & Maloney, 1994; Quinton & Roulet, 1998), especially in localized low elevation pathways (McCarter & Price, 2017), and shuttle water towards downgradient surface waters in a process known as "fill and spill" (McCarter & Price, 2017; Quinton & Roulet, 1998; Spence & Woo, 2003). During dry, relatively low water table periods, near surface connectivity is reduced while flow continues at a much slower rate through deeper, lower hydraulic conductivity peat (Balliston & Price, 2018; McCarter & Price, 2017).

The role of antecedent moisture conditions in filling bog and fen storage is important due to the large storage capacity of the hollows and pools within the microtopography (Oosterwoud *et al.*, 2017; Quinton & Roulet, 1998; Quinton *et al.*, 2003). In a patterned fen peatland in northern Quebec, 77% of peatland runoff occurred during periods of high connection, though this represented only 14% of the study period (Quinton & Roulet, 1998). In the JBL area, surface water from upgradient peatlands contributed 53-57% of streamflow during high flow periods and 52-67% during low flow periods, while deeper groundwater contributed <20% at higher order tributaries and <10% at lower order tributaries over a single monitoring season (April-October) (Orlova & Branfireun, 2014). The functioning of these systems during overwinter conditions is less well studied, though historically has been considered a period of hydrological inactivity. Frost table position with respect to the water table controls the available peat water storage capacity, being nil in frozen saturated peat (Price & FitzGibbon, 1987). When snowmelt occurs while frost tables are present, a greater proportion of melt is redirected to runoff due to the impermeability of frozen saturated peat (Perras, 2016; Price, 1987; Quinton & Roulet, 1998; Woo, 1986). Frost table depth and thickness are highly variable in sub-arctic

peatlands (Price & FitzGibbon, 1987; Quinton & Roulet, 1998) and the dynamics between connectivity and frost not well studied.

Though the general roles of bog and fen peatlands as water storage and conveyance features is known, and that high water table conditions facilitate bog-fen connectivity (McCarter & Price, 2017; Price & Maloney, 1994) there are currently a lack of studies that define the water table and streamflow connectivity thresholds in patterned bog-fen-tributary systems, or characterize the timing, magnitude, or variability of water fluxes as a function of connectivity across multiple seasons and consecutive years. The determination of hydrological connectivity and water level thresholds have been applied to other Canadian peatlands in permafrost (Connon *et al.,* 2015), sub-arctic Canadian Shield (Spence *et al.,* 2011), boreal plains (Goodbrand *et al.,* 2019), montane regions (Streich & Westbrook, 2020), and coastal plains (Price *et al.,* 1991), but has not been conducted in patterned peatland complexes of the HBL. One nearby study calculated vertical and lateral fluxes in two bog-fen-tributary complexes within a mine impacted zone (Leclair *et al.,* 2015), however this was limited to one to two years of spring and summer analysis (May-August). One study demonstrated hydrological connectivity as a function of water table in a sub-arctic fen (McCarter and Price, 2017) over a single summer season through hydrological forcing with pumped water input. However, the natural variability of connectivity as a function of meteorological conditions, as well as water table depths associated with this threshold across a bog-fen-tributary system, has not been characterized. Establishing baseline peatland complex hydrology, connectivity thresholds, and seasonal and annual behaviour is needed to better understand how these systems respond to variations in water availability within the context of a warming climate.

Determining the applicability of "fill and spill" connectivity to patterned peatland complexes, and assessing the related hydrological thresholds, is broadly applicable to peatlands, and in particular patterned peatlands elsewhere, such as those located in Northern Alberta (Vitt *et al.*, 2003), Labrador (Foster & King*,* 1984; Price & Maloney, 1994;), the northern USA (Siegel, 1983), Scotland, Sweden, and Siberia (Eppinga *et al.,* 2010). The goal of this research is to better understand the seasonal and annual variability of where water is stored and transmitted through a bog-fen-tributary complex, and how this influences the degree and timing of hydrological connectivity across the landscape. The specific objectives are to 1) characterize snowmelt, rainfall, evapotranspiration , and frost table formation and thaw, and how this relates to water storage and distribution across a bog-fen-tributary system over a 10-year study period, 2) define the thresholds for landscape connectivity along the

topographical gradient of a bog-fen-tributary system and how it relates to streamflow generation, and 3) relate seasonal and annual changes in water storage and distribution within the peatland complex to the frequency and variability of landscape connectivity.

2.3 Study Site

The study site is a 4.8 km^2 sub-watershed of the 204 km^2 Tributary 5 drainage basin (Richardson *et al*., 2012) in the HBL (52°41'42.15"N, 83°56'42.13"W, Figure 2.1b), ~14 km south of the De Beers Group of Companies Victor Mine. Average temperatures in January and July (climate normals from 1981-2010) are -22.4 ℃ and 17.1 ℃ at Lansdowne House (300 km southwest), and -20.7 ℃ and 15.4 ℃ at Moosonee (250 km southeast). 30-year average yearly precipitation totals are 700 and 681 mm at Lansdowne House and Moosonee, respectively, with 30 and 35% falling as snow (Environment Canada, 2020a, 2020b).

Designated a Ministry of Environment, Conservation and Parks reference site (MOEref), the main instrumented portion of the study site includes a ~1 km long boardwalk spanning two eddy covariance towers (Figure 2.1a), situated on a 0.51 km^2 domed bog and a 2.5 km^2 ribbed fen, respectively. The study site is beyond the zone of influence of aquifer dewatering associated with the mine (Itasca Denver, 2016). The domed bog is *Sphagnum* dominated with sparse cover of stunted trees (*Picea mariana and Larix laricina)* and shrubs (Ulanowski, 2014). The ribbed fen is dominated by *Sphagnum* and stunted *Larix lariciana* in the topographical highs, and sedges (*Carex lasiocarpa*) and horsetail (*Equisetum fluviatile)* in the topographical lows (Ulanowski, 2014). Further site details are described in Ulanowski (2014) and Harris (2020). The boardwalk runs along the bog transect in the system, beginning at the bog dome (Bog$_{dome}$) to the bog outlet (Bog$_{out}$) where it meets the moderate rich ribbed fen (Fen$_{mid}$) (Figure 2.1c). The upper fen transect begins in the upgradient portion of the ribbed fen (Fen$_{up}$) and ends at Fen$_{mid}$. The lower fen transect begins at Fen$_{mid}$ and ends to where the fen meets Trib 5 (Fen$_{out}$).

Local (peatland) groundwater flow patterns generally follow the topography of the peat surface (Emili & Price, 2006). Within the bog, the slope decreases from 0.0020 m/m between Bog$_{dome}$ and Bog$_{out}$, to 0.0016 m/m between Bog$_{out}$ and Fen$_{mid}$. Within the fen there is a 0.0015 m/m slope along the upper fen transect, increasing to 0.0019 m/m along the lower fen transect. The gradient increases markedly to 0.05 m/m between Fen$_{out}$ and Trib 5. In both the bog and fen, low microtopes (hollows and pools, respectively) are generally 20-30 cm lower than the high microtopes (hummocks and

ridges, respectively), with greater differences in the open water portions of the ribbed fen where pool bottoms can be over 1 m lower than adjacent ridges. Due to the relatively flat landscape, and 1 to >3 m thick marine sediment aquitard below the peat column (Whittington & Price, 2013), there is poor connectivity to the regional aquifer (Whittington & Price, 2012), the Silurian limestone bedrock of the Upper and Lower Attawapiskat formations (Martini, 1981; McDonald, 1989). Regionally, the exchange of water between the peat and underlying aquitard results in an average annual recharge of ~3-30 mm (Leclair *et al.,* 2015).
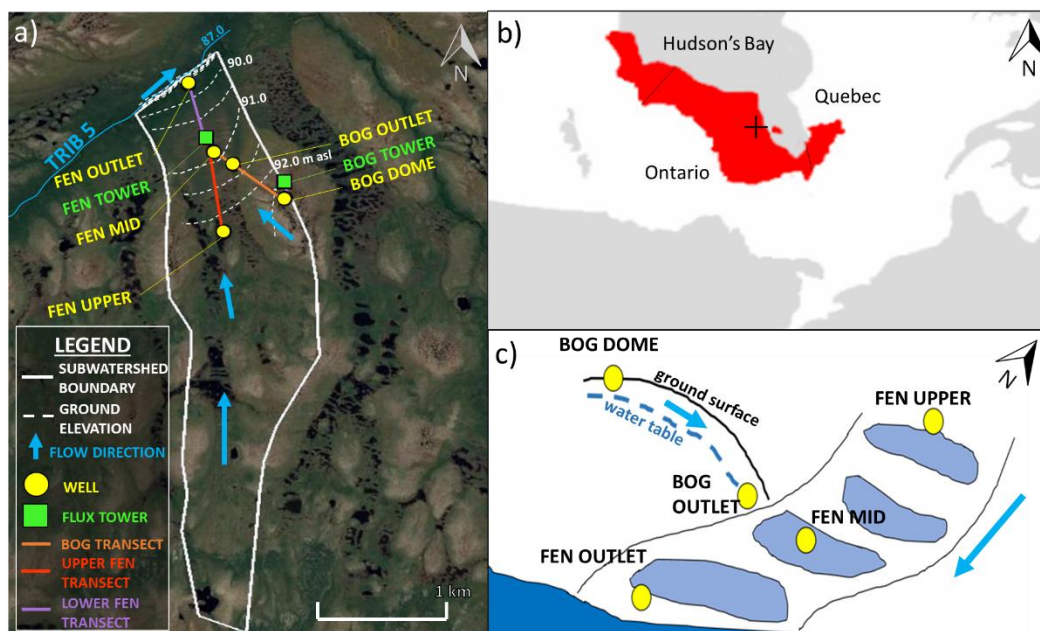
Figure 2.1. a) flow boundaries and instrumented portion of the MOEref study site located b) 90 km west of Attawapiskat in the James Bay Lowland, the southern sub-section of the Hudson Bay Lowlands (red area). The instrumented portion c) includes two flowpaths which lead from the bog dome to the fen outlet along a series of cascading pools (light blue), and the upgradient portion of a large ribbed fen to the fen outlet.

2.4 Methods

The overall study period was from 2007-2018, however not all sources of data were available for the entire study period. Table 2.1 summarizes each main data source, data types collected, and the period of data availability.

Table 2.1. Summary of meteorological and hydrological data sources, the variables measured, and the time interval of data availability

	Variables	Data Collection Period
MOEref bog (CA-ARB) and fen (CA-ARF) flux towers (https://ameriflux.lbl.gov)	meteorological variables, snow depth	2011-2015
	soil temperature	2012-2018
MOEref bog and fen transect	water table elevations	2011-2012, 2018
De Beers Victor Mine Meteorological Station and Monitoring Data	meteorological variables, water table elevations streamflow Trib 5A streamflow Trib 5	2007-2018 2007-2018 2007-2018 2007-2015
University of Waterloo high intensity data collection	water table elevations	May 2011-Oct 2011- Jun 2012-Sep 2012, Aug 2017- Aug 2019
	streamflow at Trib5$_{MOE}$	May 2011- Oct 2011- May 2012-Sep 2012
Environment Canada Stations (Moosonee & Lansdowne House)	snow depth, meteorological variables	2007-2018

2.4.1 Meterological Data

The bog and fen flux towers located at MOEref have recorded half hourly precipitation, air temperature, snow depth, net radiation (Q^*), ground heat flux (Q_G), and actual evapotranspiration (*AET)* since 2011; data were available between 2011 and 2015 from the Ameriflux database (https://ameriflux.lbl.gov, Todd & Humphreys, 2018a and 2018b). Simple linear regression between MOEref towers and the De Beers Victor Mine meteorological station (16 km north), instrumented since 2007, provided a good fit for temperature (r^2=0.97, p<0.01) and precipitation during non-frozen periods (r^2=0.99, p<0.01). Data from this secondary station were transformed using this regression for periods outside the 2011-2015 window. Half hourly Q^* was also gap-filled by combining the readings from the two MOEref towers using tower-specific regression relationships.

Overwinter precipitation was not regularly recorded at the MOEref towers nor at the Victor MET station. Snow water equivalence (*SWE*) was thus unavailable, precluding water balance closure. However, the MOEref snow depth was used to determine the timing and relative magnitude of snow accumulation and melt. Snow depth data were gap-filled and extended beyond the available period using Moosonee (290 km southeast) and Lansdowne House (280 km southwest) Environment Canada weather station observations. Data gaps were present in all three datasets, therefore the most complete dataset (Moosonee) was regressed and transformed against MOEref bog (r^2=0.9, p<0.01) and gap-filled using regressed and transformed Lansdowne House data (r^2=0.9, p<0.01). Though the three locations are varying distances inland, the large and non-local nature of winter storms in this area as well as the flatness of this landscape suggest the use of single point measurements in this terrain are adequate (Whittington *et al.*, 2012).

2.4.2 Evapotranspiration Data

Actual evapotranspiration (*AET*) was measured at each MOEref flux tower using the eddy covariance (EC) technique. EC instrumentation installed 7 m above the bog and fen surface were used to measure half hourly latent heat (L_E) fluxes (W m^{-2}) and converted to *AET* (mm) using the latent heat of vaporization (for more instrumentation and data processing details, see Helbig *et al.,* 2019 and Humphreys *et al.,* 2014). Gap-filling *AET* was accomplished with a two-step process. First, a regression relationship between $Q*$ and L_E (unique to each tower) was used to gap-fill *AET* during the 2011-2015 period (r^2=0.77 and 0.71, p<0.01 for the bog and fen, respectively). After this, any remaining half-hours, including the period beyond the MOEref measurements, were gap-filled using monthly regressions between non-gap-filled half hourly equilibrium *ET* (ET_{eq}) and *AET*. Equilibrium *ET* was calculated as (Priestley & Taylor, 1972)

$$ET_{eq} = \frac{\Delta}{\Delta - \gamma}\left(Q* - Q_g\right) \qquad (2.1)$$

where Δ is the slope of the saturation vapour pressure vs. air temperature curve and γ is the psychrometric constant. Monthly regressions were made between bog and fen ET_{eq} and *AET* during the seasons with notable fluxes (April-September) and months outside the growing season were grouped (Jan-Mar), with r^2 between 0.7 and 0.8 for both bog and fen for all regressions (p<0.01).

2.4.3 Frost Table Depth and Thickness

Soil profile temperature data were available at four locations (bog hummock, bog hollow, fen ridge, and fen pool/low lawn) at the MOE flux towers between 2012-2018. Each location represents a microtope (characteristic microtopographic feature) with the hummock/ridge representing topographic highs and hollow/pool topographic lows. Temperature probes were instrumented at depths 2, 5, 10, 20, 50, 100, and 150 cm in fen locations, and 2, 5, 10, 20, 50, and 100 cm in bog locations. For this analysis, frost was considered to be present between depths where soil temperatures were consistently (i.e., >24 hours consecutively) below 0 ℃ in these profiles.

2.4.4 Tributary Streamflow

Trib 5 stage data were logged hourly directly downgradient of Fen_{out} (herein referred to as $Trib5_{MOE}$-Figure A1) from 2011-2012 using a submersible pressure transducer (Ulanowski, 2014), however streamflow measurements were not recorded there. Both stage and streamflow data were collected near the outlet of a first order headwater stream of Trib 5 ($Trib5A_{out}$) ~1.5 km downgradient of MOEref as part of the Victor Mine environmental monitoring program between 2007-2018. Stage data were logged hourly at $Trib5A_{out}$ using a submersible pressure transducer, and stage-streamflow measurements were taken manually using a SonTek FlowTracker Acoustic Doppler Velocimeter at a monthly interval (Orlova & Branfireun, 2014). Due to the limited availability of stage data (Table 2.1) and absence of streamflow data at $Trib5_{MOE,}$ stage, data were regressed between $Trib5_{MOE}$(y) and $Trib5A_{out}$(x) to determine the closeness of fit between these two locations. The fit was statistically significant (p<0.01) and a 1:1 ratio (r^2=0.94, y=1.004x), therefore $Trib5A_{out}$ stage data were used without transformation at $Trib5_{MOE}$. Due to the difference in catchment area upgradient of these two locations (140 and 29.9 km^2 at $Trib5_{MOE}$ and $Trib5A_{out}$, respectively; Figure A1; Richardson *et al.,* 2012) $Trib5A_{out}$ streamflow was normalized to a runoff depth for comparison with other hydrological variables at MOEref. An implicit assumption of this approach is that each 1 m^2 of peatland contributes similar amounts of runoff at $Trib5A_{out}$ and $Trib5_{MOE}$ at a landscape scale. Runoff values were valid for the limits of the stage discharge curve at $Trib5A_{out}$ (flows under 2 m^3/s normalized to 5.8 mm/d). To verify the applicability of streamflow analysis at different catchment scales, additional data were obtained from a De Beers environmental monitoring gauge station located ~5 km downgradient at the outlet of the 204 km^2 Trib 5 watershed ($Trib5_{out}$; Figure A1). Data were available between 2007-2015 and collected at the same frequency as at $Trib5A_{out}$. $Trib5_{out}$ stage (x) was

regressed against Trib5A$_{out}$(y) due to the longer period of data availability of the latter (Table 2.1). Data fit was significant (p<0.01; r^2=0.88, y=0.80x) suggesting there is a high degree of cross-correlation throughout these nested catchments.

2.4.5 Groundwater Data

To record water table, MOEref was instrumented with 13 2" PVC wells (Figure A2) that were fitted with a geotextile liner, slotted along 150 cm depth starting at the peat surface, and fitted with a Solinst^{TM} Levelogger pressure transducer, logged hourly over the data collection period (Table 2.1). Each well was developed after installation and prior to monitoring, to ensure screens were not blocked. Data were compensated for atmospheric pressure during both monitoring periods using Solinst^{TM} Barologger measurements and QA/QC'd with manual measurements.

Five of 13 wells were selected for further analysis to represent average water table behaviour over each landscape unit (Figure 2.1a,c); water tables within the non-selected wells were of intermediate water table depth and behavior to those selected and were significantly correlated (Figure A2). Gaps in data outside the high intensity monitoring periods were filled using four monitoring wells instrumented in 2007 as part of the Victor Diamond Mine environmental monitoring program (Table 2.1) and logged hourly using Solinst^{TM} Levelogger pressure transducers. Selected Victor wells were of matching landscape unit types (bog dome, bog outlet, upper fen, and fen outlet) and were located within 5 km of MOEref. Linear regressions were conducted and fitted datasets were compared to manual water level elevations collected at MOEref outside the high intensity monitoring periods, to assess accuracy (Table A1).

Lateral hydraulic gradients were calculated along three separate subsections of the MOEref transect to represent flow potential and flow direction along the bog (*Bog$_{dome}$-Bog$_{out}$*), along the fen (*Fen$_{up}$-Fen$_{out}$*), and at the bog/fen interface (*Bog$_{out}$-Fen$_{mid}$*), using logged water tables. Positive gradients indicate flow from the higher elevation unit to the lower elevation unit (e.g., positive *Bog$_{dome}$-Bog$_{out}$* indicates flow from Bog$_{dome}$ to Bog$_{out}$).

2.4.6 Establishing Streamflow and Water Table Connectivity Thresholds

Landscape connectivity was assessed using 24-hr changes in runoff at Trib5$_{MOE}$ as an indirect measure of "fill and spill" threshold exceedance. When the system is highly connected (i.e., during water conveyance periods) water moves quickly from the bog headwaters through to the stream, and

14

thus runoff will increase or decrease quickly in response to hydrological inputs. Conversely, during low connectivity periods, runoff will remain relatively consistent since hydrological inputs are predominately held in storage.

For the purposes of this paper, the periods are defined as the predominantly frozen period from November 1st to March 31st (herein defined as winter), the spring freshet period from April 1st to May 31st (spring), the growing season between June 1st and August 31st (summer), and the senescence period of September 1st to October 31st (fall).

Average water table depth for each unit was plotted against runoff and the equation for the line of best fit plotted for unfrozen months (frozen months were excluded due to the confounding effects of frost table). Water table depth connectivity thresholds were determined for each peatland unit based on characteristics of the curves of 24-hour change in runoff vs. runoff magnitude, as illustrated later with the data. Three runoff thresholds were identified (high activity, connected, and disconnected) using the equations from the lines of best fit.

2.5 Results

2.5.1 Seasonal and Annual Variability in Meteorological and Hydrological Variables

Over the study period, average temperatures in January and July (-20.2 and 16.1 ℃, respectively) (Figure 2.2a) were within the range of the 30-year climate normals reported at Moosonee and Lansdowne House. The average total rainfall over the non-frozen season (391 mm) was ~50-100 mm lower than climate normals, however this is in part attributable to the exclusion of rain which may have fallen during the frozen season at the study site. Trends in temperature and precipitation were difficult to discern across years due to the large amount of variability present. Of note, the period between spring 2013 and spring 2014 was cooler and drier than average, while the spring and summer of 2015 was warmer and wetter (Figure 2.3a, c).

Average air temperature generally decreased below 0 °C in November and increased above 0 °C in April (Figure 2.2a), corresponding to the beginning and end of the winter period (as defined herein). Variation in temperature between years (Figure 2.3a) was greatest during the winter shoulder months (December and March), with a 15 and 20 °C difference between the warmest and coldest December (2015 and 2013) and March (2010 and 2014), respectively. In contrast, there was <5 °C difference

between the warmest/coldest years during the summer months. The variability in average temperature over winter months influenced the number of unfrozen (above 0 °C) days, with 7 unfrozen days in winter in both warmer years (2015 and 2010) and no unfrozen days in winter in colder years (2013 and 2014).

The accumulation of snow (Figure 2.2a) generally started in November, though in some years began as early as October and as late as December (Figure 2.3b). An earlier start date did not correlate with higher snow depth, however due to large melt events in many years. Correspondingly, though generally snowmelt began in April (Figure 2.2a) in some years, it occurred as early as February and as late as May (Figure 2.3b). An earlier melt start did not correspond to an earlier melt end, as shown by the late presence of snow in 2017 despite having the 3rd earliest melt start (Figure 2.3b).

The period in which precipitation fell as rain generally spanned from May to October (Figure 2.2a). Year over year variability in rainfall was large (Figure 2.3c); the rainiest year (2009 with 583 mm) had 2.6 times the rainfall of the driest (2013 with 223 mm). July and September generally contributed the most to this variability with a 140 and 151 mm difference in the wettest and driest July and September, respectively. There was no clear relationship between when rainfall occurred and the total yearly rainfall, as the wettest year on record had an even distribution of rainfall (17-19% in each month from June-September) while the second wettest had 55% of rainfall in July and August alone.

Patterns in *AET* generally follow that of air temperature; increasing above zero in April and declining to negligible values in November (Figure 2.2a). On average, *AET* exceeded rainfall between May-July resulting in a water deficit, while cooler temperatures and lower *AET* in early fall (September) resulted in a water surplus (Figure 2.2a). The differences in annual cumulative *AET* over the unfrozen period was less than that of precipitation (Figure 3c, d); the year with the lowest *AET* (2008) differed from the highest (2011) by only 98 mm compared to the 360 mm difference with rainfall. The largest monthly *AET* values occurred during June and July, which were also the months primarily responsible for differences in annual total *AET*. Winter sublimation was not measured directly, however was incorporated into the snow depth measurements.

Generally, bog water tables were deeper than those in the fen, and the fen water tables remained above the surface for the majority of the year (Figure 2.2b). Water table positions in all peatland units followed a similar annual cycle (small standard deviations in Figure 2.2b). With the exception of

16

Fen$_{up}$ (where water table position remained relatively constant), water tables dropped by ~10 cm overwinter. Each spring, water tables rose by ~25 cm in Fen$_{out}$, Fen$_{mid}$, and Bog$_{dome}$. Fen$_{up}$ was less responsive, however, rising by <5 cm. From spring to summer, mean water table positions dropped before recovering in the fall except for Bog$_{out}$ which declined consistently to winter (Figure 2.2b). Hydraulic gradients varied seasonally in response to the water table changes (Figure 2.2c). Overwinter gradients were constant as most water tables declined. The unique lack of overwinter drainage in Fen$_{up}$ resulted in a small increase in the *Fen$_{up}$- Fen$_{mid}$* gradient while others remained stable (light gray line in Figure 2.2c). In spring, a notable delay in Bog$_{out}$ water table response in the spring compared to Fen$_{mid}$ (Figure 2.2b) resulted in a flow reversal between these two units in May (gradient reversal shown in Figure 2.2c). The spring Bog$_{out}$-Fen$_{mid}$ reversal was highly variable between years (Figure 2.3e), reaching magnitudes as high as summer values some years (2007, 2008, and 2014), while gradient reversals did not occur at all in others (2010-2013). Conversely, Fen$_{up}$-Fen$_{mid}$ and Bog$_{dome}$-Bog$_{out}$ gradients varied little year to year (not shown), where the standard deviation was <5% of the mean for all months (Figure 2.2c). Late spring to end of fall hydraulic gradients returned to pre-snowmelt values, though the Bog$_{out}$-Fen$_{mid}$ gradient still varied 20-40% between years (Figure 2.3e).

   Runoff at Trib5$_{MOE}$ (Figure 2.2d) was generally lowest overwinter (declining to average values of ~0.04 mm/day in February) and highest during snowmelt (increasing to ~3 mm/ day in May). In all years but three, over 50% of runoff occured between April and June (steep increases in Figure 2.3f). In some years (e.g., 2009), a second notable contribution to runoff occured in late summer (August) or early fall (October). Total yearly runoff (end of year totals in Figure 2.3f) was more variable than all other variables in the system, with a 300% difference between the years with the highest (2015) and lowest (2010) runoff.
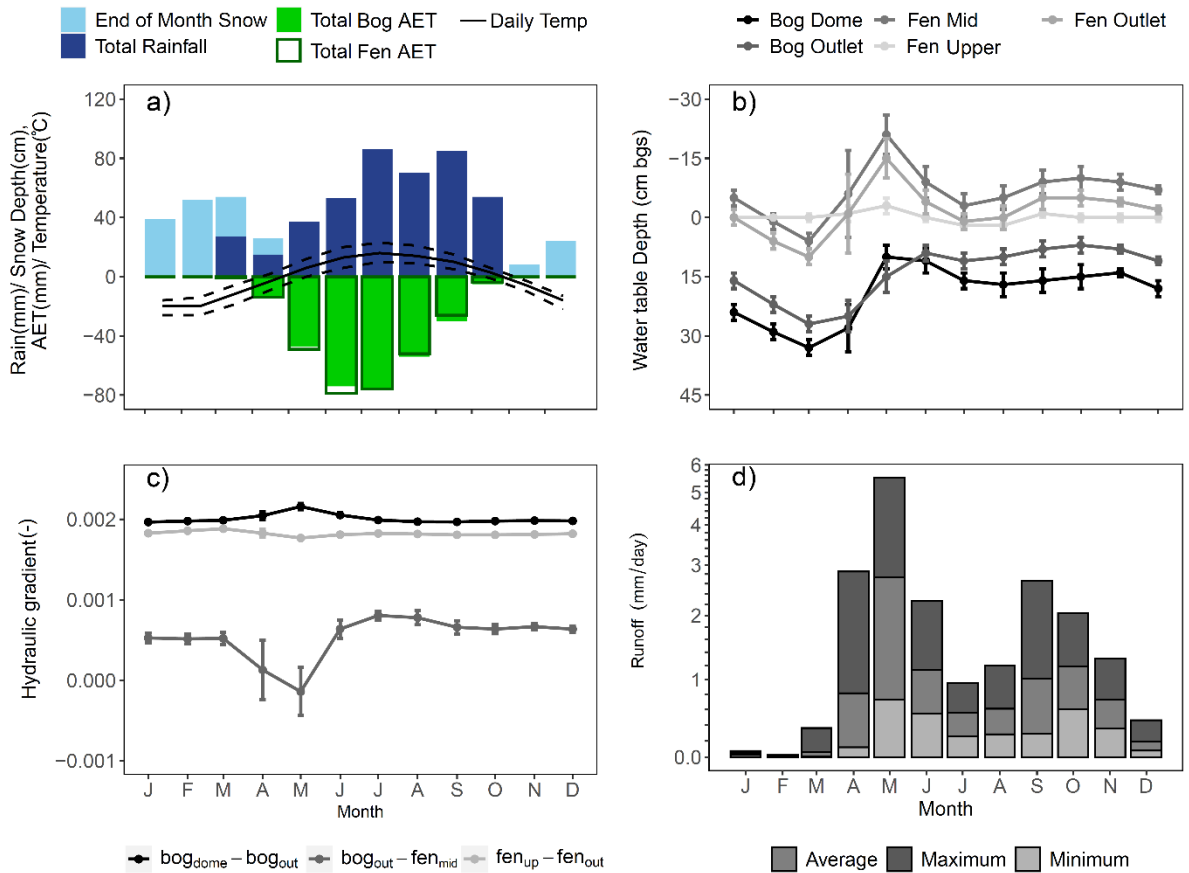
Figure 2.2. (a) Monthly averages for all days between 2007-2018 for selected meteorological variables as well as daily maximum and minimum temperature (dashed lines), (b) water table average depth ± standard deviation, (c) average hydraulic gradients that drive flow across peatland units ± standard deviation, and (d) daily maximum, mean, and minimum runoff.
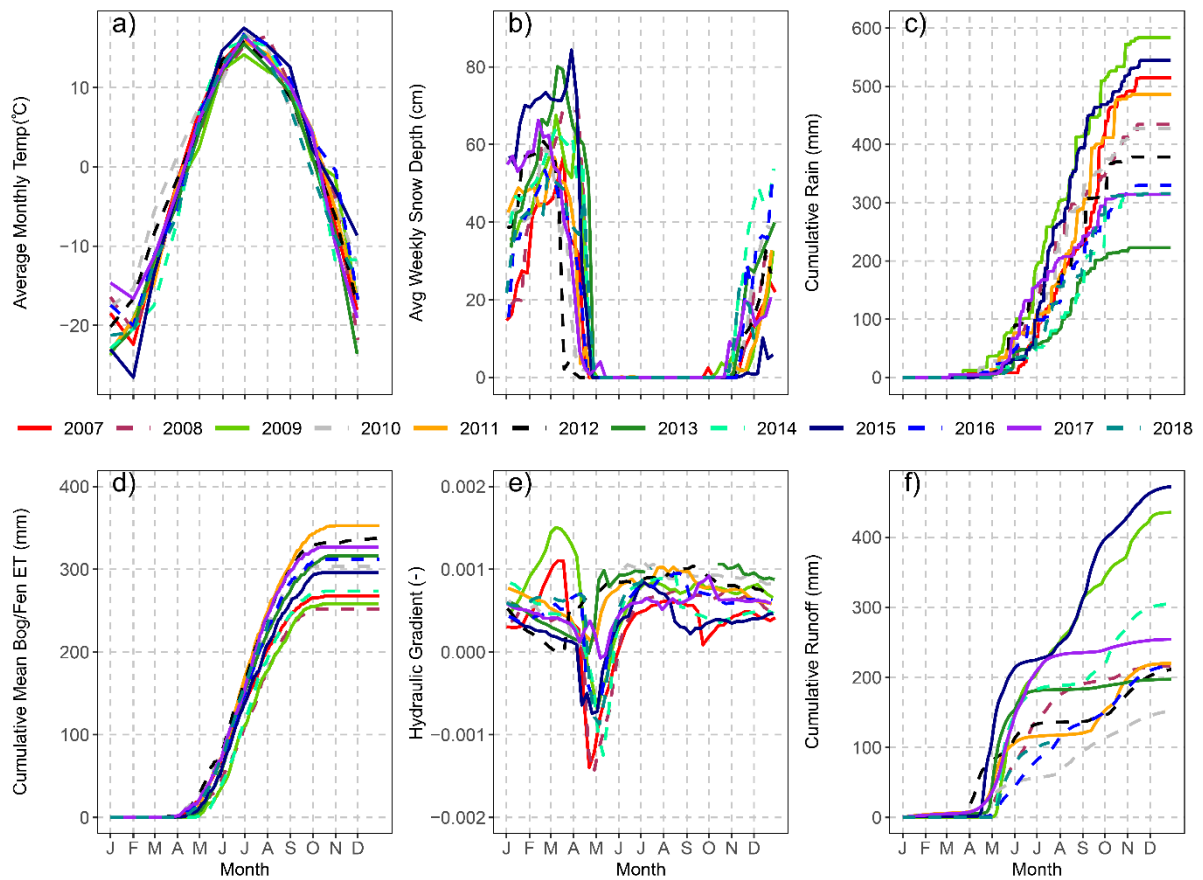
Figure 2.3. (a) Mean monthly temperature, (b) mean weekly snow depth, (c) daily cumulative rain, (d) daily cumulative *AET* averaged over the bog and fen, (e) weekly averaged *Bog_out*-*Fen_mid* gradient, and (f) daily cumulative runoff.

2.5.2 Frost Table Dynamics

Frost was present in at least part of the landscape for over 50% of the year (Figure 2.4), forming from the surface downwards in all microtopes. Frost table thickening occurred earlier in the fen microtopes, reaching the peak depth (~20-50 cm) by the end of December, while peaks were not reached in the bog hummock until mid-January or February. Uniquely, in the bog hollow frost did not begin to form until December in most years and did not peak until February or March. Timing of frost formation was strongly year dependent; 2013 had the earliest formation in all microtopes, over a week early in all microtopes and 40 days early in the bog hollow, while 2016 had the latest formation where the bog hollow was 7 weeks later than average and the remaining microtopes two weeks later

than average. The depth and thickness of the frost table was further complicated by near-surface melt events early in the frost season, which occurred between October and December in 2011 and 2015 at all microtopes but the bog hollow.

Measurable frost thaw commenced, on average, in late April in the bog hollow, fen pool, and fen ridge, and about two weeks later in the bog hummock. Bog hummock thaw rates were consistently lower (0.8 ±0.5 cm/day) than bog hollow (1.5 ±0.6 cm/day), fen ridge (3.5 ±1.7 cm/day), and fen pool (2.3 ±0.9 cm/day). Due to the differential melt times, the bog hollow and fen ridge were generally frost free in the first week of May and the fen pool by the end of May, while the bog hummock had frost into the beginning of June. Thaw timing and duration were also highly year-dependent. In the bog hummock and fen ridge, 2011 and 2016 were the earliest thaw years, respectively, where near-surface thaw started 7 days earlier than average. In the fen pool and bog hollow, 2012 was the year with earliest thaw even though the time of thaw start was 14 days later than average in the fen pool.
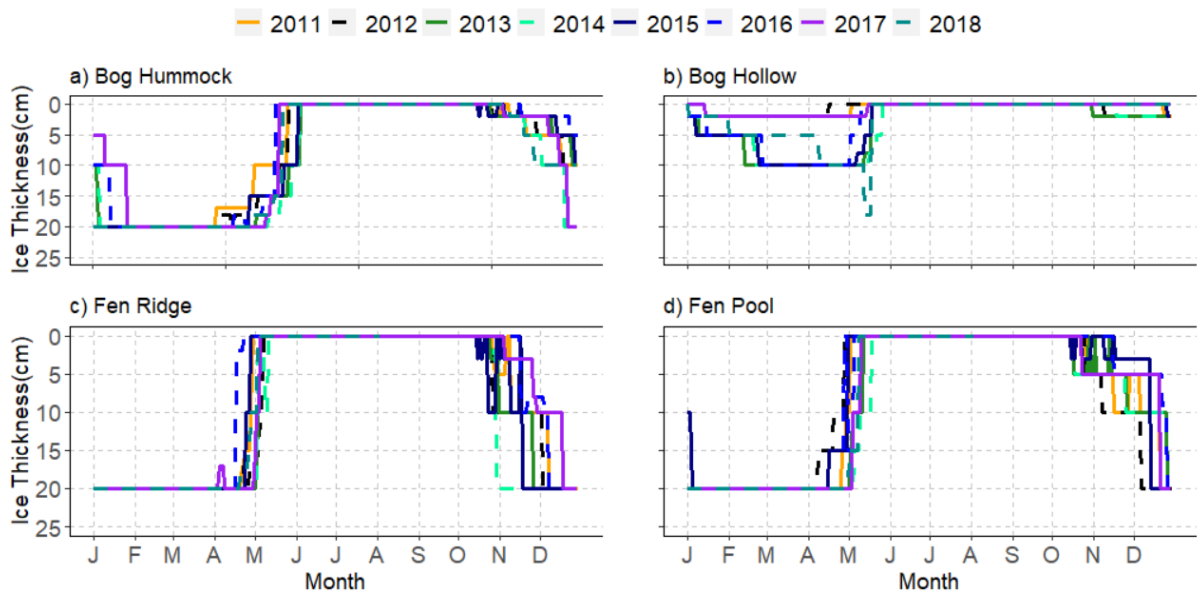
Figure 2.4. Frost table thickness from 2012-2018 in the instrumented a) bog hummock, b) bog hollow, c) fen ridge, and d) fen pool.

2.5.3 Bog-Fen-Tributary Connectivity Thresholds

2.5.3.1 Trib 5 Connectivity

As the recipient of all runoff in the bog-fen-tributary complex, the hydrological responsiveness (i.e., 24-hour runoff response) at $Trib5_{MOE}$ was used to establish connected and disconnected periods in the landscape. A total of 3438 observational days were incorporated into the runoff response analysis, which included data from both frozen and unfrozen periods. The 24-hour runoff response (Figure 2.5a) was near zero for runoff below 0.17 mm/ day; above this threshold response increased exponentially with increasing runoff. The system was therefore divided into disconnected and connected states, using 0.17 mm/day as the threshold runoff. Data above this threshold best fit a power law (Figure 2.5b), which follows the Pareto principle, in which the largest 20% of the independent variable (runoff) incorporates 80% of the output (i.e., of the sum of the 24-hour changes in runoff). A second threshold of system connectivity was thus assumed at the 80th percentile runoff (1.8 mm/ day), defined here as the "high activity" state, where response was disproportionally high.
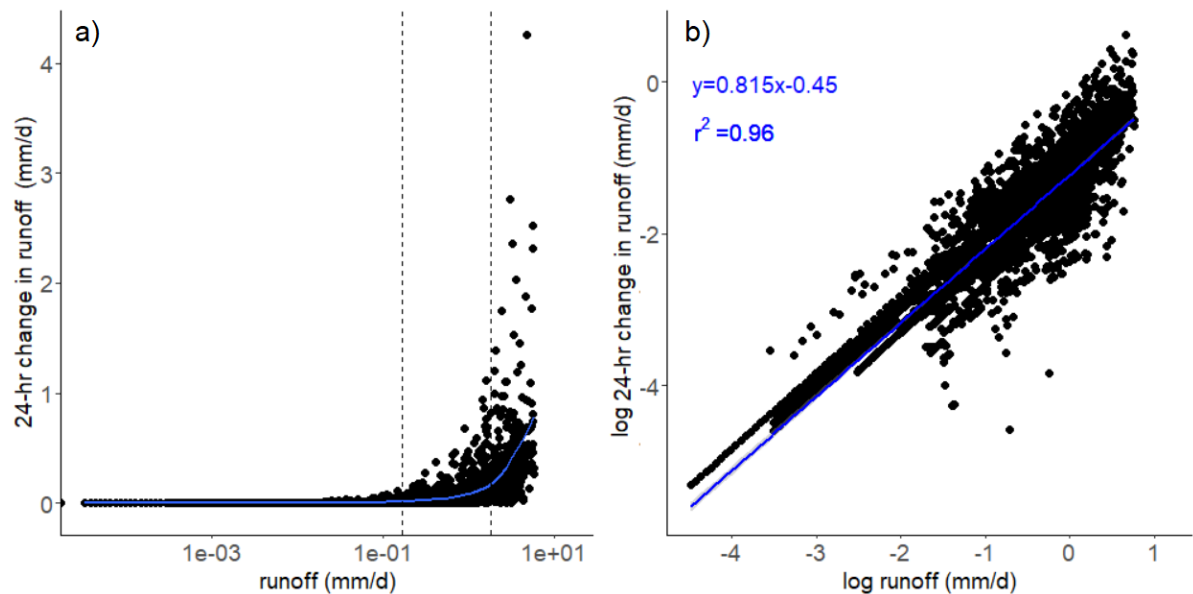
Figure 2.5. 24-hour runoff change as a function of daily runoff (a) and log-log plot of the same variables (b) fitted with a straight line representing a power function (blue) for values above the disconnection threshold. Dashed lines indicate the disconnected/connected (0.17 mm/day) and connected, high activity (1.8 mm/day) thresholds.

2.5.3.2 Subsurface Peatland Flow Connectivity

To determine the contribution of different upgradient landscape units to runoff, the sensitivity of runoff to water table position within each of the units must be defined. Only non-winter periods for each peatland unit were used for this analysis, as data during the winter period plotted off the otherwise linear relationship between water table and runoff (Figure 2.6, lines of best fit). The large scatter of data on the water table/ runoff plots, particularly in the bog units and in the spring season, suggests a range of potential water tables for the established runoff thresholds. Therefore, water table thresholds were selected where the corresponding runoff threshold was reached at least 50% of the time (i.e., at least 50% of data points for a given water table value plotted above horizontal dashed lines in Figure 2.6). Water table thresholds were shallowest in Fen_{out} (-10 and 10 cm below ground surface (bgs)) and deepest in Bog_{dome} (1 and 26 cm bgs) with intermediate values in Fen_{up} (-5 and 6 cm bgs) and Bog_{out} (0 to 16 cm bgs). Fen_{mid} thresholds were within 1 cm of those in Fen_{out} and thus are not shown.
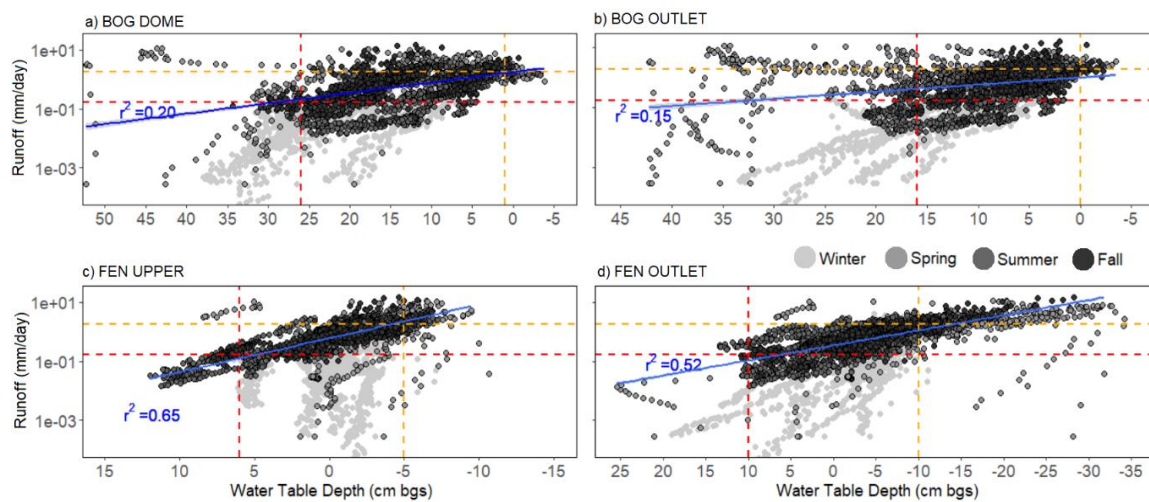
Figure 2.6. Daily a) bog dome, b) bog outlet, c) fen upper, and d) fen outlet water table depths (x axis) vs. tributary runoff (y axis) by season. Negative values indicate water table above the surface. Data from non-frozen seasons (circles with black outlines) were used to generate the line of best fit (blue, p<0.01), due to the non-linear behaviour of data from the frozen season (circles with no outline). Horizontal orange and red lines indicate the high activity and disconnected runoff thresholds, respectively, and vertical lines indicate corresponding water table thresholds.

22

2.5.3.3 Seasonal and interannual landscape connectivity

The proportion of time each unit was disconnected, connected, and in a high activity state over the study period is summarized in Table 2.2 for all seasons in the tributary ($Trib5_{MOE}$) and non-winter seasons in the peatland units. Figure 2.7 illustrates the yearly landscape connectivity patterns for each landscape unit over the relevant periods (Fen_{mid} showed the same patterns as Fen_{out} and is thus not shown). All peatland units spent most of the non-winter period in a connected or high activity state, and fen units were connected more often than bog units. Bog_{out} was the most disconnected unit in the non-winter season (24%) while Fen_{out} and Fen_{mid} were the least disconnected (5 and 4% respectively).

Winter was the period of most frequent disconnection for the tributary (i.e. Trib 5, 74%); runoff ceased by the end of March in 8 of 12 years. Water tables were disconnected at the beginning of spring in 9, 11, and 6 of 12 years in Bog_{dome}, Bog_{out}, and Fen_{out}, respectively. In contrast, due to its sustained water table, Fen_{up} was categorized as connected at the beginning of spring in all years. The beginning of spring snowmelt (yellow boxes- Figure 2.7) signaled the start of landscape reconnection, and spring had the highest proportion of high activity runoff in all units except in Bog_{out}, which was disconnected more in spring than any other season (Table 2.2). A high activity period in the tributary corresponded with high connectivity in Fen_{up} and Fen_{out} from late spring to early summer (April-June) in most years. In the majority of years, at least one peatland unit and the tributary disconnected during the summer season. Bog_{dome} was the most well-connected during this period, followed Fen_{mid} and Fen_{out} while Fen_{up} spent the greatest amount of time disconnected, fully disconnecting for a week or more in 5 out of the 10 years of data availability for this location.

All landscape units and the tributary reconnected briefly between October and November (except for 2013 when the fen and tributary remain partially disconnected) and in half of the years a second period of high activity occurred between September and November in the tributary and at least one peatland unit. The system re-entered a state of disconnection by the end of the unfrozen period.

Table 2.2. Proportion of time spent in disconnected (DIS), connected (CON), and high activity (HIGH) states from spring to fall for each peatland unit and for all seasons at Trib5$_{MOE}$ over the study period

		Winter (Nov-Mar)	Spring (Apr-May)	Summer (Jun-Aug)	Fall (Sep-Oct)	Non- winter (Apr-Oct)	Overall (Jan-Dec)
Total		41%	17%	25%	16%	59%	100%
Bog Dome	DIS	**-**	32	5	7	12	-
	CON	-	63	**93**	91	**85**	**-**
	HIGH	-	**5**	2	2	3	-
Bog Outlet	DIS	-	**59**	13	4	24	-
	CON	-	39	87	**94**	75	**-**
	HIGH	-	**2**	0	**2**	**1**	**-**
Fen Upgradient	DIS	-	2	**14**	8	9	-
	CON	**-**	77	83	86	**82**	**-**
	HIGH	-	**21**	3	6	9	-
Fen Mid	DIS	**-**	12	1	0	4	-
	CON	-	18	**72**	58	**52**	**-**
	HIGH	-	**70**	27	42	44	-
Fen Outlet	DIS	**-**	14	3	1	5	-
	CON	-	38	**90**	78	**73**	**-**
	HIGH	-	**48**	7	21	22	-
Trib5$_{MOE}$	DIS	**74**	28	27	12	19	41
	CON	25	37	63	**74**	**62**	**47**
	HIGH	1	**35**	10	15	19	12

24
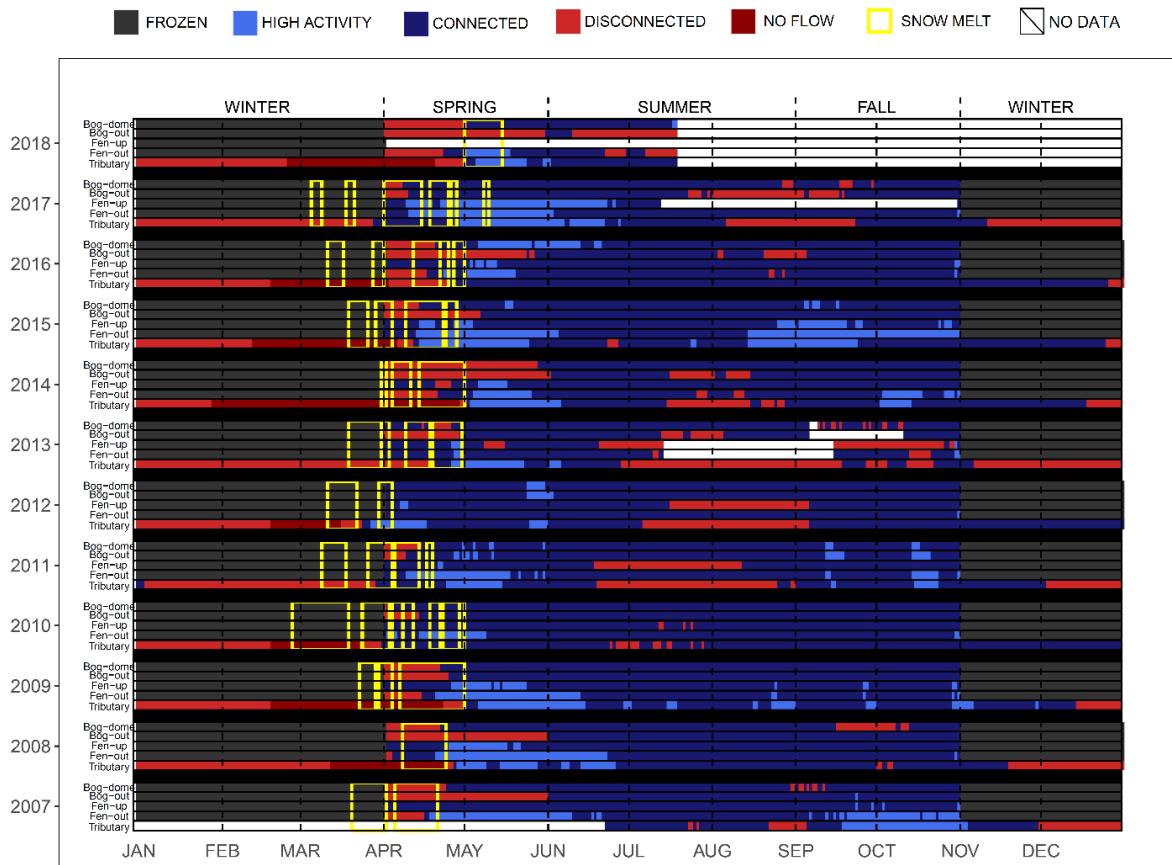
Figure 2.7. Timeline showing the connectivity states of Bog$_{dome}$, Bog$_{out}$, Fen$_{up}$, Fen$_{out}$, and the Trib5$_{MOE}$ (tributary) using established water table and runoff thresholds. Winter periods were excluded in peatland units due to the breakdown of runoff/water table relationships. Snowmelt periods are outlined in the yellow boxes. Fen$_{mid}$ follows the same temporal patterns as Fen$_{out}$ and was thus not included.

2.6 Discussion

The interaction between meteorological conditions and hydrological processes in this system are highly seasonal in nature; system functioning is best described within the context of these previously defined seasons.

2.6.1 Winter (November-March)

Overwinter hydrological functioning of the bog-fen-tributary complex was most controlled by the presence and thickness of frost tables within the peatland units. In both the bog and fen, the frost table extended downwards from the surface through the hydrologically transmissive upper layer (Figure 2.4; Price & FitzGibbon, 1987), which is generally near surface (top 0-15 cm) in this area (Balliston & Price, 2020; McCarter and Price, 2017). In the absence of near surface runoff, disconnection occurred at $Trib5_{MOE}$ by the end of each year despite apparently connected upgradient conditions (Figure 2.7). Non-negligible fluxes of water were, however, transported within the system below the freezing front, as evidenced by declining water tables in most peatland units (Figure 2.2b) and runoff presence until February or March in all years (Figure 2.7). This is consistent with winter baseflow conditions noted in another sub-arctic bog-fen system in which there was fen outflow all winter long (Price & FitzGibbon, 1987).

Overwinter drainage and frost table thickness varied between peatland units. Bog frost tables were thinner and formed later than those in the fen (Figure 2.4; Ulanowski, 2014) and, combined with a lack of upgradient inflow, resulted in a faster decline in water tables (Figure 2.2b). Though not measured here, studies in other northern peatlands have shown a correlation between higher localized snow depth and thinner frost tables as well as delayed formation of ground ice (Moore, 1987; Streich & Westbrook., 2020). Frost tables were thinnest at this site in bog hollows (Figure 2.4a), suggesting this may be an area of preferential snow accumulation. It is also possible that the higher moisture content and shallower water table in the bog hollow may delay frost formation due to the higher heat capacity of water compared to that in drier peat (Van Huizen *et al.*, 2022; Wright *et al.*, 2009).

In the fen, the earlier formation and thickening of frost in the ridges and pools (Figure 2.4c,d), extended the freezing front to the saturated zone, which impaired its ability to transmit runoff downgradient, especially in Fen_{up} (Figure 2.2b). The sustained level of water storage in Fen_{up} is likely enhanced by its low hydraulic gradient and a water-supply from upgradient peatlands (cf. Price, 1987). The hydrological activity in Fen_{mid} and Fen_{out} was more complex, with large overwinter decreases in water table (Figure 2.2b) despite the intersection of the freezing front and the saturated zone. The relatively large hydraulic gradients between Fen_{mid}, Fen_{out}, and $Trib5_{MOE}$ over winter (Figure 2.2c) may have forced drainage deeper in the fen profile in the absence of near-surface connectivity, despite relatively low hydraulic conductivity at depth. This is consistent with the two-year study of mine-impacted peatlands in this area, in which both bog and fen water tables declined

over winter. However, in that study this was attributed to enhanced deep seepage due to mine dewatering (Leclair *et al.,* 2015).

2.6.2 Spring (March-May)

Early spring, hydrology was primarily controlled by snowmelt (Figure 2.3b) and frost table thaw (Figure 2.4). In the tributary, total spring runoff was highly correlated to peak snow depth (r^2=0.82, p<0.01) and peak runoff occurred shortly after snow melt completion (Figures 2.2d and 2.3b,f), consistent with other rivers in the HBL region (Déry *et al.,* 2005), and other northern peatland-fed systems (Connon *et al.,* 2015; Goodbrand *et al.* 2019; Spence *et al.,* 2011; Streich *et al.,* 2020; Wells *et al.,* 2017) . No significant correlations were found between spring runoff and frost table melt likely due to the high complexity and landscale scale variability of frost thaw dynamics.

Some replenishment of overwinter storage deficits in the peatland units occurred each year (Figure 2.2b), consistent with past studies in the area (Leclair *et al.*, 2015). The amount of water entering storage in each peatland unit, however, was related to the synchrony between frost thaw and snow melt. Frost thaw (Figure 2.4) and thus water table reconnection (Figure 2.7) was earlier in the fen relative to the bog. This asynchrony of bog and fen water table reconnection was responsible for the decline, and in some years reversal, of the bog-fen gradient during late April to early May (Figures 2.2c and 2.3e). The number of days before bog reconnection during the spring freshet varied from year to year (Figure 2.7) and corresponded to the spring data points that deviated from linear water table/ runoff relationships (Figure 2.6). Here, data plotted first near-vertically (runoff increased while water tables remained low) and then near-horizontally (water tables filled after runoff had already peaked). This pattern was more prevalent in Bog$_{out}$ which reconnected last in all years (Figure 2.7). In all years, the later part of spring was highly connected and rainfall that occurred during this period was shuttled downgradient to Trib 5 due to the high water tables (Leclair *et al.,* 2015; McCarter *et al.,* 2017). Spring was also associated with the largest proportion of high activity runoff (Figure 2.7, Table 2.2), high-water tables in the fens (Figure 2.2b), and largest increases in cumulative runoff (Figure 2.3f), as was observed in other tributaries in the HBL area where the highest proportion of runoff was associated with peak runoff after melt (Richardson *et al.*, 2012).

2.6.3 Summer (June-August)

During the summer, the landscape underwent a period of drying and landscape disconnection (Figure 2.7) due to relatively high *AET* losses. Generally, years that experienced greater summer rainfall experienced longer periods of landscape connection and higher total runoff. In June there was a significant relationship between rainfall and total runoff (r^2=0.60, p<0.01), while in July and August, a significant relationship existed with the previous month's rainfall and not the current month (r^2=0.71, p<0.01 in July and r^2=0.65, p<0.01 in August). This offset is due to increasing *AET* losses that lowered water tables, decreased transmissivity, and therefore increased lag time to outflow (Leclair *et al.,* 2015). There were no statistically significant correlations between *AET* and runoff or connectivity, likely due to the much lower inter-year variability of *AET* compared to precipitation during these months. The high contribution of rainfall to runoff in this and other HBL tributaries was also noted by Orlova & Branfireun, (2014), who found precipitation sourced 50% of streamflow during wet periods (spring to early summer) and 42% during dry periods (mid summer and winter).

2.6.4 Fall (September-October)

Fall was a period of landscape reconnection in most years with the highest percentage of connectivity in all units except Fen$_{up}$ (Table 2.2). Reconnection occurred over a wide range of rainfall amounts (Figures 2.3c and 2.7) due to lower *AET* losses (Figures 2.2a and 2.3d). September and October rainfall correlated with total runoff in each month (r^2=0.49, p<0.01 and r^2=0.65, p<0.01, respectively) and wet summer conditions did not guarantee reconnection in the fall if fall rainfall was low (e.g., 2008).

As temperatures dropped below 0 °C between early and mid November, runoff began to decline and disconnect (Figures 2.3a and 2.3f), however, it was not synchronous with the degree of upgradient landscape connectivity (Figure 2.7) or frost formation (Figure 2.4). The rate of decline of runoff was relatively constant each year and the date of tributary disconnection correlated to the average daily runoff in the month prior to this period of decline (r^2=0.67, p<0.01).

2.6.5 Effects of abnormal spring and early winter temperatures on hydrological cycling

Years in which spring and early winter (November-December) ambient temperatures were abnormal had distinctive deviations in hydrogical functioning and connectivity, the details of which are described below and summarized in Figure 2.8.

Abnormally cold early winter and spring temperatures generally extended the frozen period (Figure 2.8). In early winter, low temperatures (e.g., 2013, Figure 2.3a) resulted in early frost table formation (Figure 2.4) and tributary disconnection (Figure 2.7). In spring, cold temperatures (e.g., 2014; Figure 2.3a) delayed snow and frost melt (Figure 2.4) and stream reconnection (Figure 2.7). When linearly regressed, snow melt start and end dates each correlated differently with average spring temperature (Figure A3; snow melt start $r^2=0.65$, $p<0.01$; melt end $r^2=0.70$, $p<0.01$). As a result, the melt window (i.e., duration of time between melt start and end) was shorter as average temperature decreased (Figure 2.8). This is likely because colder springs were associated with later but more consistent warming that caused faster melt (steep curve in April 2014; Figure 2.3b), whereas warmer springs often experienced temperature oscillations above and below zero (not shown), resulting in melt slowing (plateau in April 2011; Figure 2.3b) or even snow reaccumulation (snow events in March 2011 and 2012; Figure 2.3b). The effect of below average spring temperatures and a late but rapid snowmelt was observed in 2014 (3 ºC cooler than average), when melt started 22 days later and was 10 days faster than average (Figure 2.3b). Spring 2014 had the highest peak runoff over the study period (not shown) and was a notably hazardous year for flood risk in local northern communities (Khalafzai *et al.,* 2019), even though starting snow depth was average (Figure 2.3b). This late melt also influences summer connectivity (Figure 2.8), as delayed melt resulted in higher summer connectivity than years with earlier melt and similar rainfall amounts (i.e., 2013; Figures 2.3c and 2.7).

Abnormally warm early winter and spring temperatures generally shortened the frozen period. Warm November and December temperatures (e.g., 2015, Figure 2.3a) delayed frost table formation (Figure 2.4) and snow accumulation (Figure 2.3b), which delayed tributary disconnection (Figure 2.7). Warm spring temperatures (e.g., 2010 and 2012; Figure 2.3a) triggered premature snowmelt and frost thaw (Figures 2.3b, 2.4), though this was not consistent in some microtopes. There was a significant correlation between increased spring temperatures and earlier frost thaw dates in low microtopes (Figure A3; fen pool, $r^2=0.60$, $p<0.01$; bog hollow, $r^2=0.69$, $p<0.01$,). However, snowmelt

29

start and end occured 11 and 9 days earlier per 1°C increase in average spring temperature (Figure A3), while in fen pool and bog hollow microtopes, which melted first, thaw occurred 4 and 8 days earlier. As a result, warmer temperatures caused snowmelt while frost tables were generally present (Figure 2.8). The effects of snowmelt and thaw desynchronization was evident in 2012, when thin bog hollow frost (~2 cm, Figure 2.4) allowed meltwater ingress while both fen pool and ridge frost table were still at their thickest (Figure 2.4), reducing entry of snowmelt to fen ground storage (Figure 2.8), shown by the reduced high activity state in spring of this year (Figure 2.7). Melt that bypassed fen ground storage became surface runoff to the tributary, evidenced by early increases in runoff (Figure 2.3f) in the warmest springs of 2010 and 2012. This early loss of water to the downstream system had a similar effect to an abnormally low snowfall winter, with low peak spring runoff and poorly replenished water tables (see Orlova & Branfireun, 2014; Richardson *et. al.*, 2012 and Whittington *et al.*, 2012).

Similar "short-circuiting" behaviour of precpitation and snowmelt across the landscape in the presence of frost tables has been observed within other northern peatland dominated catchments. In the peat pleateaus of the Northwest Territories (Connon *et al.,* 2015) spring runoff reached its annual peak when frost tables prevented the entrance of meltwaters into the large storage capacity of thawed bog collapse features. However connectivity was low for the remainder of the year in these peat plateaus due to the isolating effect of permafrost. In a boreal montane fen system (Streich & Westbrook*.,* 2020), disproportionaly high runoff was generated during rain events where frost tables were present in the fen; the presence of frost also reduced the depletion of fen storage which preseved water levels into the summer. In the peatland complex studied here, the effects of spring temperature on snowmelt and ground thaw carried over to patterns in summer connectivity (Figure 2.7, 2.8). Abnormally warm spring months (e.g., 2010, 2012) or those with abnormally early melt (e.g., 2011) resulted in earlier Fen$_{up}$ and tributary disconnection (Figure 2.7). The effects of these conditions on broader peatland functioning were noted in 2010 as abnormally low runoff at the catchment scale (Richardson *et al.,* 2012) and visible dessication of *Sphagnum* mosses across the landscape (Orlova & Branfireun, 2014). If continued, long term declines in water table postion could result in vegetation species shifts, changes in decomposition rates (Hilbert *et al.,* 2000), and irreversible consolidation that could alter the hydrophysical structure of the peat profile (Whittington & Price, 2006). Lower water tables can also alter frost dynamics by decreasing the thermal heat capacity of the peat, which favours earlier and thicker frost table formation. This, in turn, combined with projected increasing

temperatures, may result in snow melt while frost tables are present (Figure 2.8), which could further exacerbate water storage deficits.
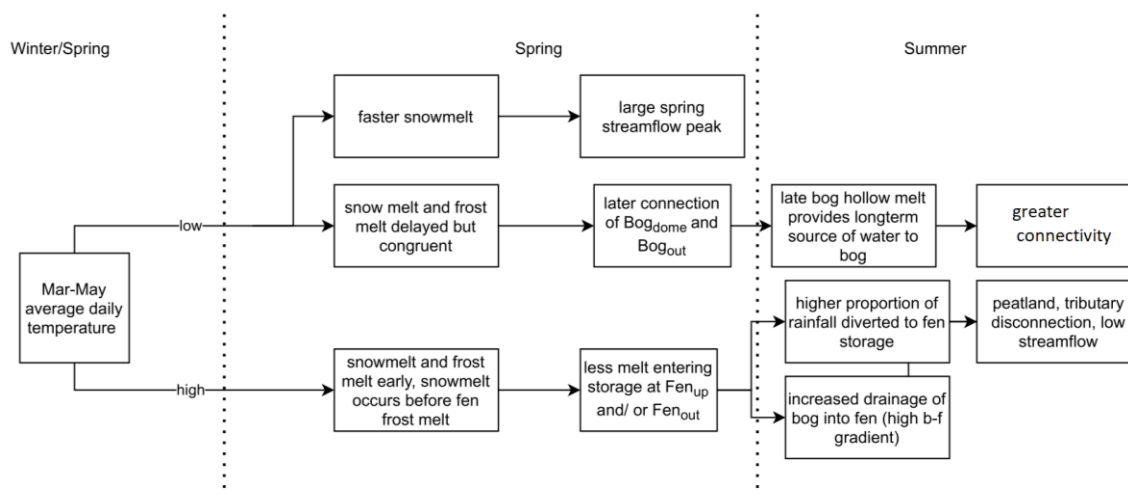
Figure 2.8. Flow diagram illustrating the cross seasonal impacts of abnormally low and abnormally high temperatures, the resulting changes in melt dynamics, and the resulting summer outcomes.

2.6.6 Redefining Connectivity Thresholds

In previous studies, hydrological connectivity in patterned peatlands (McCarter & Price, 2017; Quinton & Roulet, 1998) has been described as a binary "fill and spill" mechanism (Spence & Woo, 2003). In this system, 18 and 78% of runoff volume at $Trib5_{MOE}$ occurred during connected and high activity states defined here (Figure 2.5 a,b), which occurred over 47 and 12% of the study period (Table 2.2). This suggests that the three-phase model of connectivity is more useful than a binary fill-and-spill model, particularly when assessing runoff peaks and flood risk in tributaries due to the high proportion of total runoff occurring over a small proportion of the year. To assess the potential for use of these thresholds at different locations in nested catchments, the processes used to define connectivity thresholds at $Trib5_{MOE}$ was repeated at the highly autocorrelated $Trib5_{out}$. At this secondary gauge, 24-hour stream response was negligible (i.e., the tributary was disconnected) below runoff values of 0.20 mm/day, and in a high activity state above 1.5 mm/day (Figure A4). The similarity of these streamflow thresholds to those developed at MOEref in addition to the high correlation of stage between $Trib5_{out}$, $Trib5A_{out}$ and $Trib5_{MOE}$ suggests high scalability of this

analysis. The development of hydrological models would greatly aid in further assessing connectivity threshold scaling within a catchment, as well as the larger applicability to other catchments within this region.

The water table position associated with connected and high activity states was shallower in the fen units when compared to the bog units (Figure 2.6), since the higher position in the landscape of bogs (Figure 2.1 a,c) allows them to act as sources of water to fens during drier conditions. These water table depths are comparable to those defined in other northern peatland-dominated catchments. In a permafrost peatland system, bog-to-bog connectivity was associated with water table depths ~10 cm bgs (Connon *et al.,* 2015), while in boreal fens active groundwater contribution to downgradient tributaries occurred at water tables between 5-10 cm bgs (Goodbrand *et al.,* 2019), except for in extreme environments such as a montane fen underlain by well drained sediment, which contributed groundwater flow to water tables up to 90 cm bgs (Streich & Westbrook*,* 2020). It is likely that connectivity thresholds are landscape specific and defined by the local topography, peatland morphology and climate; the modelling of these systems would greatly aid in assessing the sensitivity of connectivity thresholds on system functioning in different environments. The breakdown of these thresholds during frozen periods, which occurred during ~40% of the year, limits applicability of threshold-based fill-and-spill models and requires the incorporation of processes outlined in Figure 2.8 to capture frozen period connectivity.

2.6.7 Limitations

Limitations

The five peatland units selected for this study, though generally representative of the landscape, are not fully exhaustive of the range of patterned peatland morophology found in the HBL. Most notably, the presence of ladder fens, which form on the slope of domed bogs, may complicate the transmissivity feedbacks of the system by providing additional near-surface high transmissivity flowpaths along the bog surface (McCarter & Price, 2017). This may be important for the tributary connectivity in locations where bog peatlands connect to tributaries directly, which should be investigated in future studies.

The determination of water table connectivity thresholds was complicated by a large degree of variability in the runoff /water table relationships. This is likely due to the hysteretic effect of water

table and runoff response to wetting and drying (Fitzgerald *et al.,* 2003), particularly in the bog where water tables are lower and frost was present later in the year. Water table hysteresis is likely important in short term fluctuations (e.g., the water table response after a single rainfall event will be higher where storage deficits have already been filled).

The use of normalized streamflow data required the assumption that, at a landscape scale, a unit area of peatland contributes equally to runoff. This intrinsically relies on the assumption that peatland morphology is homogeneous at the catchment scale, which may be complicated by the presence of larger fen water tracks in larger catchments (Richardson *et al.,* 2012). Though this may change the magnitude of normalized runoff at different systems, the highly consistent patterns in connectivity at different catchment scales observed here suggests this assumption is sufficient for the purposes of this study.

2.7 Conclusions and Recommendations

The hydrological connectivity of this bog-fen-tributary complex was found to be highly seasonal in nature and closely linked with the variable meteorological conditions present in this area. Over winter (November-March), the landscape underwent a period of snow accumulation and the freezing of the high-transmissivity near-surface peat. Declining runoff increased lateral hydraulic gradients between the peatlands and the tributary, which resulted in drainage from the deeper unfrozen layers of the bog and lower fen units. Conversely, smaller hydraulic gradients and drainage from upgradient bogs and fen allowed upper fen water tables to remain high and stable over winter. Spring snowmelt (April-May) released water stored over the winter as snow refilled overwinter deficits in ground water storage. Once water tables reached connectivity thresholds, or where frost prevented the downward movement of water, meltwater was then exported downstream to the tributary, peaking runoff . Increasing temperatures and *AET* from spring to summer (June-August) signaled the start of a drying period and disconnection, as water tables declined below the high transmissivity near-surface. Summer connectivity was highly dependent on the dynamic equilibrium between rainfall and *AET* until temperatures declined into fall. The system entered a second period of high connectivity briefly in early fall (September-October), before the formation of frost tables and snow accumulation began in the next yearly cycle.

The influence of abnormally warm or cold spring temperatures was determined to be extremely important in overall landscape connectivity. Abnormally cold spring temperatures resulted in

snowmelt that was delayed and thus able to enter the unfrozen ground. Cold springs often also correlated with more rapid snowmelt, which resulted in later but larger peaks in runoff, important for assessing flood risks. Abnormally warm springs resulted in earlier snow melt and increased the time between snowmelt and frost table thaw in the fen, reducing the amount of meltwater entering below ground fen storage. This resulted in earlier summer landscape disconnection and lower runoff. The implications of greater temperature fluctuations, as well as longer unfrozen periods, is likely to result in increased *AET*, more years with snowmelt and frost thaw desynchronization, and greater drainage of peatlands to the tributary during shoulder seasons. This should be studied in these systems in greater detail as it has the potential to influence frost table dynamics, species composition, decomposition rates, and may limit the ability of these systems to buffer other changes, such as drought. Connectivity thresholds developed here show potential to be scaled within nested catchments, suggesting a high degree of hydrological consistency in this part of the HBL landscape; the applicability of these thresholds across different watersheds should be further investigated to allow for the assessment of largescale changes on these systems.

2.8 Acknowledgments

Chapter 3

Landscape scale subsidence and alterations to hydrophysical structure and function in mine-dewatered peatlands in the Hudson Bay Lowlands

3.1 Summary

The depositional history of the Hudson Bay Lowlands (HBL) has created a low relief, poorly drained landscape, favouring the formation of one of the largest peatland complexes in the world. High volume dewatering associated with resource extraction in this area, such as the De Beers Victor Diamond Mine, tests the ability of the underlying confining layer to limit water losses in the peatlands above. This research quantifies the increase in effective stress related to mine dewatering and the resulting changes to peatland hydrophysical structure and function. One impacted and two unimpacted transects were instrumented for meteorological (precipitation and evapotranspiration) and hydrophysical (hydraulic head, hydraulic conductivity (K_{sat}), and surface elevation) monitoring over a 12-year period in the vicinity of the Victor Mine. Over this study period, the unimpacted peatlands operated within relative hydrological equilibrium, demonstrated through shallow water tables, negligible subsidence, and stable K_{sat}. Contrastingly, all impacted peatlands experienced increased downwards hydraulic gradients, deeper water tables, and measurable long-term subsidence (4-15 cm). Hydrological impacts were highest in bogs with a thin underlying confining layer even if they were further from the point of dewatering, highlighting the need for environmental monitoring programs which incorporate an assessment of aquitard thickness. Where subsidence occurred, associated decreases in K_{sat} deflected bog-fen-tributary flow-paths deeper, reducing the upwards transport of solute rich water to downgradient fens. The long-term effects of these landscape scale changes should be studied further, particularly since climate change in this region will potentially increase water deficits and further alter peatland connectivity.

3.2 Introduction

Due to the depositional history of the Hudson Bay Lowlands (HBL), conditions have been favorable for the development of one of the largest peatland complexes in the world (Rouse *et al.*, 1992). Broadly, these peatland complexes perform important water storage and conveyance functions

within the landscape (Glaser *et al.*, 2004a), and are a globally significant store of soil carbon (Loisel *et al.*, 2021).

The extensive accumulation of peat in this landscape is largely due to the relatively flat and thick low-permeability marine sediment (Price & Woo, 1988) deposited during a marine transgression associated with the melting of the Laurentide Ice sheet ~8,000 years ago (Lee, 1959). The relatively low vertical hydraulic conductivity of this layer limits deep seepage (Whittington & Price, 2013a). Combined with a relatively cool and wet climate, this facilitates a persistent high water table (Reeve *et al.*, 2000), favouring peat accumulation. With increasing pressure for resource extraction in this area, the confining ability of this aquitard will be tested due to the high-volume groundwater removal required to maintain mineable conditions in the bedrock below. A test case for the effects of largescale dewatering is the De Beers Group of Companies Victor Diamond Mine, located 90 km west of Attawapiskat in the HBL, which was actively dewatered for 12 years (Itasca Denver, 2017). Within the first five years of dewatering, deep seepage fluxes in the peat-covered landscape increased by up to an order of magnitude within the mine-impacted area from <0.1 mm/day pre-impact (HCl, 2004) to 1-4 mm/day after five years of dewatering (Whittington & Price, 2013). This resulted in lower water tables in both bog and fen peatlands (Leclair *et al.*, 2015), and an increased risk for surface desiccation and peat oxidation (Perras, 2016). Locations with a thinner layer of marine sediment within the zone of influence of the mine exhibited a greater increase in deep seepage within this time, suggesting these areas are at higher risk of long-term impacts (Leclair *et al.*, 2015; Whittington & Price, 2013).

Lower water tables, reduced pore water pressure, and increased downward water fluxes increased the effective stress on peat (Hobbs, 1986). Peat is highly compressible compared to mineral soils, therefore even relatively small decreases in pressure and associated increases in effective stress can result in substantial deformation of the peat structure (Ng & Eischens, 1983; Fox & Edil, 1996; Price *et al.*, 2005; Gofar & Sutejo, 2007). Below a pressure threshold (i.e., pre-consolidation pressure) this reduction is reversible. Normal seasonal variations in water pressure in peatlands, reflected in the water table position, create effective stresses below this threshold that are reversible, and can cause "mire breathing" (Ingram, 1983; Kellner & Halldin, 2002), in which the surface rises and falls. This swelling and subsidence can be relatively rapid and large due to the poorly decomposed near-surface peat, which has high elasticity (Price & Schlotzhauer, 1999; Kellner & Halldin, 2002), and a large pore volume (Berry & Poskitt, 1972). The process of mire breathing is considered a water

preservation mechanism (Fritz, 2006), allowing the surface to drop with declining water levels, and thus facilitating higher water contents in the near-surface peat than it would otherwise be (Roulet, 1991; Whittington & Price, 2006). Beyond the pre-consolidation pressure, volume changes are not fully reversible, which can cause permanent subsidence (Schothorst, 1977) and alter the hydraulic properties of the peat (Chow *et al.*, 1992; Price, 2003; Whittington & Price, 2006) due to the reshaping and reduction of pore volume (Liu *et al.*, 2020). Lowered water tables also increase oxygen availability in previously saturated peat, enhancing decomposition (which can be considered as tertiary consolidation) (Hilbert *et al.*, 2000; Belyea & Clymo, 2001), irreversibly altering particle shape and decreasing pore volume.

Reduced pore volume, whether reversible or irreversible, results in increased bulk density and water retention, and decreased saturated hydraulic conductivity (K_{sat}), specific yield, compressibility, and void ratio (Chow *et al.*, 1992; Oleszczuk *et al.*, 2000; Price, 2003). Higher density and lower hydraulic conductivity peat has lower effective porosity (Balliston & Price, 2020) and lower lateral and vertical water transmission below the water table (Whittington & Price, 2006; Price, 2003). In the patterned, highly hydrologically connected peatland complexes of the HBL, where peat consolidation associated with mine dewatering occurs, a shift to less transmissive peat near the surface may reduce landscape connectivity to the downgradient peatlands and tributaries, while similar changes at depth may reduce the vertical flux.

Initial studies at the Victor Diamond Mine reported peat and marine sediment subsidence of up to 7 and 34 cm, respectively (Whittington & Price, 2013). However, the longer-term consolidation behaviour, increase in vertical effective stress and the amount of long-term subsidence associated with mine dewatering, was not determined. Relating these impacts to peatland type, position in the landscape, and thickness of underlying marine sediment can provide guidance on identifying areas of high sensitivity to disturbance in future mining operations beyond simply identifying a dewatered radius. Further, assessing the changes to landscape connectivity and hydrological function can help characterize the long-term effects on these systems after dewatering has ceased. With the pressure to develop larger mining operations in this area (i.e., the Ring of Fire; Chong, 2014) and the accelerated pace of climate change in the north (IPCC, 2022) this information may be paramount in assessing the potential reduction in peatland resilience and connectivity due to these combined disturbances.

The goal of this research is to quantify the subsidence related to mine dewatering in bog and fen peatlands of the HBL and assess the resulting changes in peatland hydraulic and physical structure and function. The specific objectives are to 1) measure the seasonal and inter-annual changes in peat surface elevation and thickness and relate this to the thickness of the marine sediment layer, position on the landscape, peatland class (i.e., bog vs. fen), and weather conditions 2) determine spatial and temporal changes in depth-dependent hydraulic conductivity within the peat profile, and 3) assess the implications of changing topography and structure on hydrological flowpaths.

3.3 Study Sites

Research was conducted at one impacted site (Figure 3.1- Main Transect) and two unimpacted sites (Figure 3.1- MOEref and Bioherm Bog). The Main Transect is a 1.5 km transect within 1 km of the De Beers Group of Companies Victor Diamond Mine (herein referred to as the Victor Mine) (52°49'15''N, 83°53'00''W), Ontario which was in operation from 2007-2019. This transect was instrumented in 2007 and crosses five peatlands divided by peatland class according to the Canadian Wetland Classification System (CWCS; National Wetlands Working Group, 1997), herein referred to as Bogs 1-3 and Fens 1-2. According to the CWCS, Bogs 1-3 are of the domed form, Fen 1 transitions from a floating riparian fen sub-form to a stream riparian fen sub-form, and Fen 2 is of the stream riparian fen sub-form. Average peat thickness is 2.2, 1.7, and 2.4 m in Bogs 1-3, and 1.7 and 2.0 m in Fens 1 and 2, respectively. The thickness of the marine sediment (MS) varies across the transect (contours in Figure 3.1) increasing from Bog 1 to Bog 2 then decreasing again to Bog 3. Two bioherms (bedrock outcroppings where MS is absent) are located at the south and northmost points of the transect. The north and south branches of North Granny Creek (NNGC and NSGC) cross the transect at Fen 2 and Fen 1, respectively.
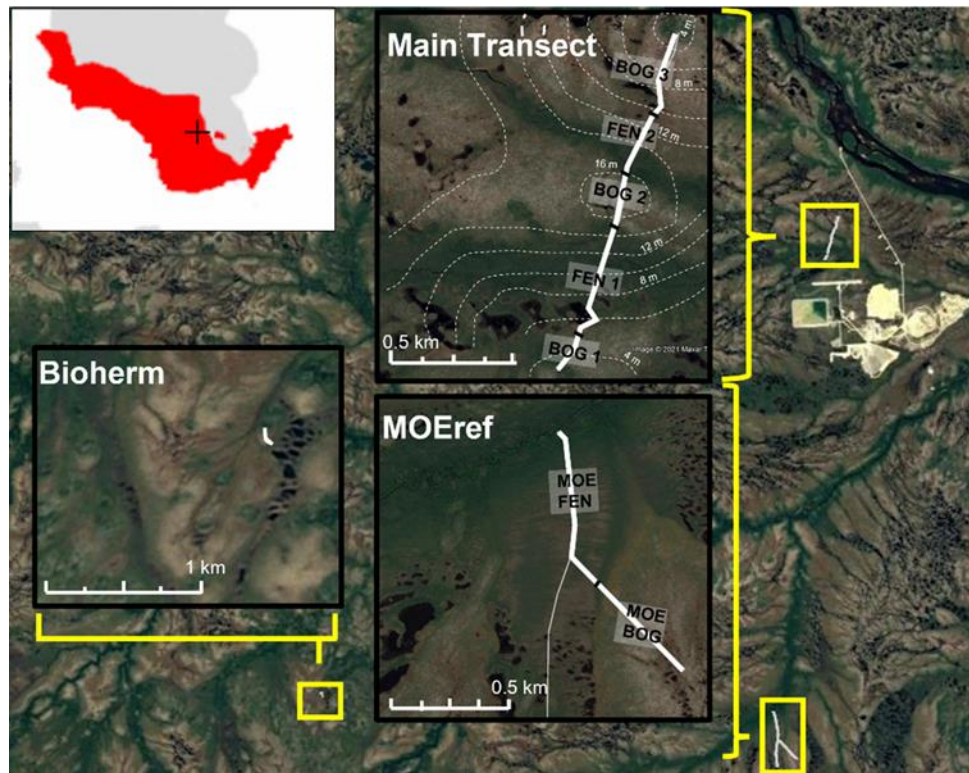
Figure 3.1. Location of the study sites within the Hudson Bay Lowlands, Ontario (top left), and in relation to the De Beers Group of Companies Victor Diamond mine (right). Transects (solid lines) and peatlands within each site are identified in map inlays, as well as marine sediment thickness contours (dashed lines) at the Main Transect.

The MOEref site is an undisturbed ~1.5 km transect instrumented in 2010, 14 km south of the zone of mine influence (Figure 3.1). MOEref spans two peatlands, a forested domed bog (MOE Bog) and a moderate-rich ribbed fen (MOE Fen) (Ulanowski & Branfireun, 2013). Peat thickness ranges from 2.0 to 2.3 m in the bog and decreases from bog to fen to a minimum of <0.5 m at the fen's northmost extent (Ulanowski, 2014). The Bioherm Bog has a single domed bog peatland located ~20 km southwest of the zone of mine influence and ~10 km west of MOEref (Figure 3.1). This peatland is instrumented along a 150 m transect starting ~25 m from a bioherm and extending outwards, with a peat thickness from 2.3 to 2.7 m (Leclair *et al.*, 2015). MS thickness was not established at MOEref or the Bioherm Bog.

3.4 Methods

3.4.1 Meteorological Parameters

Meteorological parameters were collected at a station (herein referred to as Victor station) instrumented within the vicinity of the Victor Mine in 2007, approximately ~2 km from the Main Transect. Actual evapotranspiration (*AET*) data were measured at two flux towers at MOEref and then fitted to equilibrium ET calculated using the Priestley-Taylor method with parameters collected at the Victor station (Priestley & Taylor, 1972). For more detailed methodology on the AET/ equillibrium ET regression see Chapter 2.

3.4.2 Site Instrumentation and Monitoring

In 2007, 18 monitoring nests were installed along the Main Transect, with two to four nests in each peatland (Figure 3.2a; installation details in Whittington & Price, 2013). Each monitoring nest comprised 2.54 cm inside diameter PVC pipe installations including a fully screened well, and piezometers with a 20 cm screened interval at the bottom; these included a 90 cm below ground surface (bgs) piezometer, a 150 cm bgs piezometer, and a piezometer installed just above the MS layer (Figure 3.2a). Shallow (300-350 cm bgs) and deep (450-600 cm bgs) MS piezometers were installed in seven nests within Bog 1, Fen 1, and Bog 3. A 1.27 cm diameter length of rebar (herein referred to as an elevation rod (ER)) was installed through the peat layer into the MS at all but a single nest in Fen 2. Stickup (the distance between the ground surface and the top of the pipe or ER) and water level depths were measured at all ER and pipes in all nests during monitoring events between 2007-2018 (for exact monitoring intervals and frequency see Table B1). MS water levels were only available until 2012 due to instrumentation failure. The elevation of the peat surface was not constant, as evidenced by changing stickup length in the piezometers and ERs. Measured water level depths below pipe top, were corrected using stickup values within the given pipe to obtain relative depths bgs as the peat surface rose and fell. An annual DGPS survey was used to determine the pipe-top elevations.

A total of 11 monitoring nests (2.54 cm inside diameter PVC pipes) were instrumented along the MOEref transect in 2011, six of which were installed into MOE Bog and five in MOE Fen (Figure 3.2b; installation details in Ulanowski, 2014). Each monitoring nest included a fully screened well and 20 cm screen length piezometers with the center of the screen at 100, 150 and 200 cm bgs.

MOEref was monitored intensively between 2011-2012 and again in 2018 (details in Table B1). An annual DGPS survey was used to determine the pipe-top elevations, as it was at all pipe-tops and elevation rods in this study. The second reference site (Bioherm Bog) was instrumented in 2008, with four nests including 100 cm, 150 cm, deep peat and MS piezometers (Figure 3.2c; for installation details see Leclair *et al.*, 2015). Wells were not installed in this transect and thus water levels were taken from a nearby domed bog monitored as part of the Victor Mine groundwater monitoring network, located <1 km west, and cross referenced to shallow piezometer values where available. Monitoring events at Bioherm Bog took place between 2008 and 2012 (details in Table B1). A datum of 600 cm bgs at each monitoring nest was used to calculate hydraulic head.
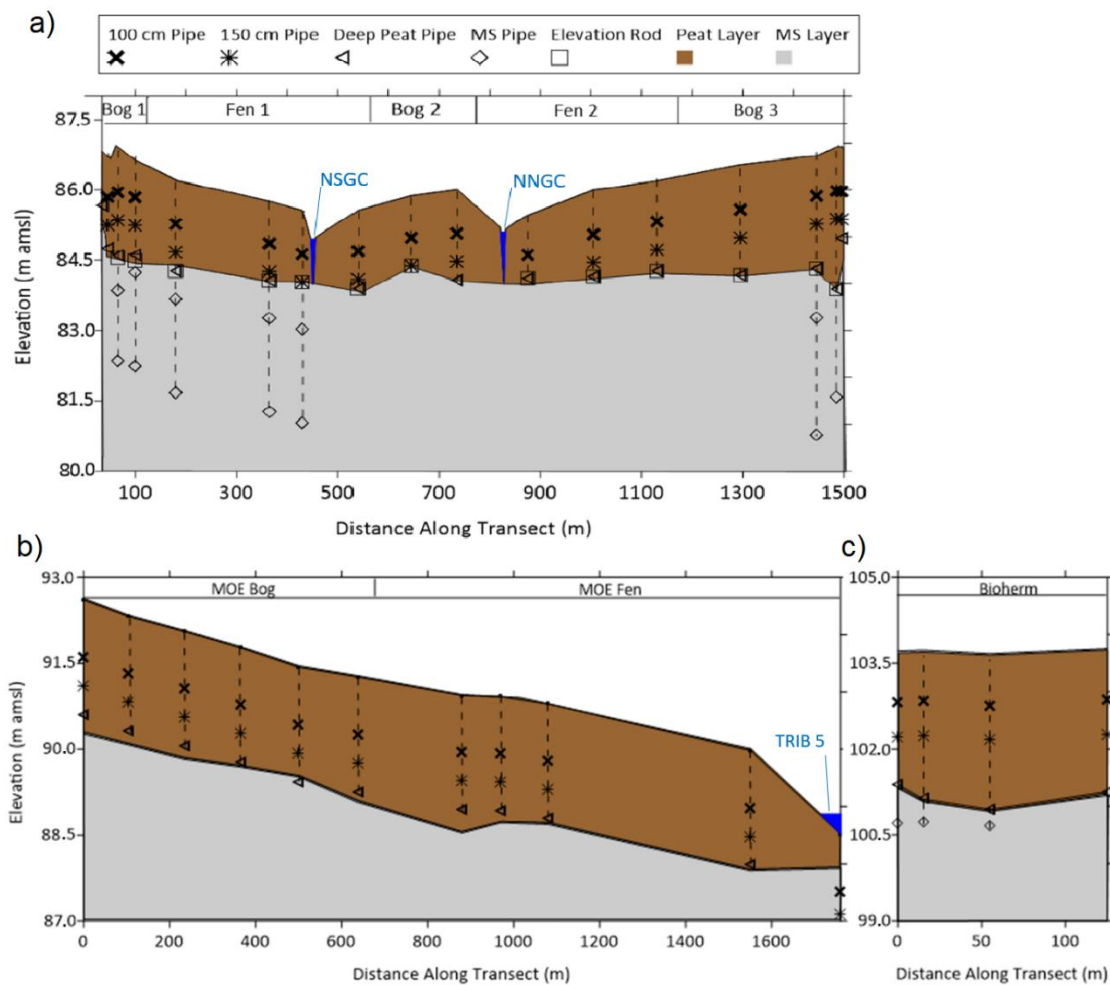
Figure 3.2. Monitoring nest installations and surface water features at a) the impacted Main Transect, and the unimpacted b) MOEref and c) Bioherm Bog

41

3.4.3 Peat Thickness Measurements

Total peat thickness was measured using a hand auger, where soil was extracted until 1 cm or more of MS was retrieved. Peat thickness measurements were taken at 38 locations at the Main Transect in 2007 and were revisited in August of 2018 using a DGPS (~1 cm accuracy). In 2011, peat thickness was measured at 28 locations along the MOEref transect, 12 of these locations were revisited in 2018 using the same methods as above.

3.4.4 Yearly and Net Changes in Surface Elevation

The stickup (distance between pipe top and a marked point at the ground surface) increased and decreased as peat above the screened depth shrank and swelled and was thus used to determine the change in peat surface elevation. This assumes that individual pipes/ERs only moved due to the shrinking and swelling of peat and not independently due to frost heave and moss growth. To determine the change in surface elevation for each year, the range (i.e., difference between the maximum and minimum stickup) at each peatland was determined using ERs where present, or otherwise in the deepest piezometers, which were anchored into the underlying MS. Average ranges for each peatland for each year were tested for normality, then if data were normal ANOVA regressions and Tukey multiple comparisons (at the 95% confidence interval unless otherwise stated) were used to compare between study sites, individual peatlands (e.g., Bog 1, MOE Bog), and years.

To determine the long-term change in peat surface elevation, stickup data from each pipe/ER were regressed against time using linear, logarithmic, inverse, and polynomial fits to test for statistical significance ($p < 0.05$). Where significant relationships were found, the lines of best fit were used to calculate the net change in surface elevation from the beginning to end of the monitoring period (reducing the effects of short-term oscillations on final values). Where data were normal, elevation changes were compared between peatlands across the impacted and unimpacted sites using ANOVA regressions, and Tukey multiple comparisons. Changes in peat thickness in individual layers (i.e., between successive installation depths) were determined by subtracting the calculated change in surface elevation from the next deepest installation depth (i.e., change between 100 and 150 cm depths was calculated by subtracting the 100 cm piezometer stickup from that at the 150 cm piezometer).

To evaluate the peat surface oscillation in response to hydrological conditions, the change in surface elevation per unit change in water table depth ($\Delta z_e / \Delta WTD$) was calculated for two sub-periods

(2007-2011, 2012-2018) based on the range of years data were available for unimpacted MOEref and Bioherm Bog.

3.4.5 Total Stress, Effective Stress, and Porewater Pressure

To relate observed changes in peat thickness to the impacts of mine dewatering a force balance was conducted at each pipe/ER to determine the vertical effective stress compressing the peat. At a given measurement depth d (cm bgs) the vertical effective stress is determined as (Das, 2014):

$$\sigma_d' = \sigma_{t,d} - \mu_d \tag{3.1}$$

where σ_d' is the effective stress at d (kPa), $\sigma_{t,d}$ is the total stress (kPa) and μ_d is the porewater pressure (kPa). In a soil profile $\sigma_{t,d}$ is equal to the pressure exerted by the mass of overlying material, and can be calculated as (Das, 2014):

$$\sigma_{t,d} = \sum_{i=0}^{d} \gamma_{i,h_i} * \Delta i \tag{3.2}$$

where Δi is the interval soil thickness (m), in this case set to 0.05 m, for a variably saturated soil of unit weight $\gamma_{i,hi}$ (kN/m^3) at interval depth i (m bgs) and height above water table, h_i. The height above water table for interval depth i was calculated as:

$$h_i = WTD - i \tag{3.3}$$

where *WTD* is the water table depth (m bgs). For this analysis the unit weight of peat was determined from laboratory retention experiments analyzed in 0.05 m intervals for 12 bog and 12 fen peat cores up to 0.3 m bgs (Figure B1). Linear interpolation was used to determine unit weights of peat for pressures between to 0.25 and 1.0 m above the water table, due to a lack of data at intermediate pressures. Retention curves were only available for peat depths up to 0.3 m bgs, roughly representing the transition from acrotelm to catotelm. It was thus assumed that the peat structure in the catotelm changes minimally with depth (Ingram, 1978), and therefore retention properties

measured at the 0.25 m depth were representative for all depths below this. The porewater pressure μ at depth d can be calculated as (Das, 2014):

$$\mu_d = (-h_d + \Delta H)\gamma_w \qquad (3.4)$$

where $-h$ is the depth of measurement point d below the water table (m) and ΔH is the change in total hydraulic head between point d and the water table, which acts to increase or decrease the water pressure respectively, and γ_w is the unit weight of water (9.8 kN/m^3).

The distributions of water table depth, piezometer hydraulic head, and all components of effective stress were compared between all peatlands for overlapping monitoring years only, using ANOVA regressions and Tukey multiple comparisons for statistical significance where data were normal ($p<0.05$).

3.4.6 Field Hydraulic Conductivity

To determine horizontal saturated hydraulic conductivity (K_{sat}), bail tests were conducted in piezometers at all sites within monitoring intervals indicated in Table B1. A volume of water was removed using a Waterra™ foot valve and tubing until a minimum drawdown equal to 50% of the well volume was achieved in all tests, and monitored until a minimum of 90% recovery was achieved. The recovery data were then used to calculate K_{sat} using Hvorslev's hydrostatic time-lag method (Hvorslev, 1951). To determine the long-term change in K_{sat}, field values were regressed against time using linear, logarithmic, inverse, or polynomial fits to test for statistical significance ($p<0.05$). Where significant relationships were found in at least one nest within a peatland, distributions were generated for K_{sat} values measured at the beginning and end of the study period. Where no significant changes occurred, geometric averages were calculated over the entire study period.

3.4.7 Evaluating Changes in Hydrological Function

To evaluate subsidence related landscape-scale alterations to subsurface water flow, flow nets were generated for pre- and post-drainage conditions at the Main Transect using USGS software TopoDrive. In the absence of water table measurements prior to dewatering, water tables measured at the Main Transect early in the dewatering phase (2007) during wet fall conditions were used because the water table was predominantly within the acrotelm (rendering it possible to predict flowpaths in

all layers). The elevation of the top and bottom of each layer was altered when creating the post-subsidence flow net, to incorporate changes in individual layer thickness. The top 30 cm, representing the acrotelm, was assigned a hydraulic conductivity of 4.8×10^1 m/d with an anisotropy ratio of 2, representing the average values measured in lab samples collected from the Main Transect in 2012 (Figure B2), consistent with other studies in this area (Balliston *et al.,* 2018; McCarter & Price, 2017). Actual rates of subsidence were not measured within the acrotelm due to a lack of instrumentation in this layer. An order of magnitude decrease in hydraulic conductivity was initially introduced within the acrotelm in the post-drainage model to assess the theoretical influence of near surface subsidence, however, this was not included in the final model due to a lack of observable difference in flowpaths. K_{sat} measured at the 90, 150, and deep peat piezometers were assigned to successive depth intervals in each peatland (30-90 cm, 90-150 cm, and 150-peat bottom, respectively). Models were run with a catotelm anisotropy ratio of 5, reflecting average literature values (Beckwith *et al.,* 2003a,b; Gharedaghloo *et al.,* 2018, Morris *et al.,* 2019). Where a decline in K_{sat} occurred in the post-subsidence model, it was assumed a decline of equal magnitude also occurred in the vertical direction to maintain the same anisotropy ratio. The MS layer was assigned a hydraulic conductivity of 1.7×10^{-4} m/d, as measured in-field, and was assumed not to change. Advective flowpaths were initiated in TopoDrive at 50 m horizontal intervals along the transect for all scenarios. The average advective flowpaths within each depth interval and associated transit time (time for water originating at the surface to reach the surface downstream) were used for final figure generation. Two additional Topodrive scenarios were executed, to determine the individual influences of subsidence and K_{sat} on flowpaths. Pre-subsidence values were used for the non-targeted parameter in each of these two additional scenarios.

3.5 Results

3.5.1 Site Conditions

The average daily temperature, total precipitation (P), and total evapotranspiration (ET) over the months in which monitoring occurred (May to October, 2007-2018) was 10±1°C, 390 ±100 mm and 280 ±30 mm, respectively. There was a net water surplus (P-ET) all years except 2013 (-80 mm), which was greater on average in the first half of the monitoring period (average of +167 mm between 2007-2012) than the latter (average of +50 mm between 2013-2018). Surplus was largest in 2009

(290 mm) due to large amounts of rainfall. A more detailed hydrometeorological analysis can be found in Chapter 2. Mine dewatering began in January 2007 and increased from an average of 19,000 m^3/day in 2007 to a maximum of 86,000 m^3/day in 2012, before decreasing slightly to an average of 76,000 m^3/day between 2013 (Whittington & Price, 2013) and mine decommissioning in early 2019.

3.5.2 Porewater Pressure, Total Stress and Effective Stress

For overlapping monitoring periods, WTD (Figures 3.3, B3) and hydraulic head (Figure B4) did not differ significantly between any of the unimpacted peatlands, nor were there any significant changes from study period start to end. In contrast, in impacted peatlands WTD increased (Figure B3), and hydraulic head declined significantly ($p<0.01$; Figure B4) at all depths in the peat profile between 2007-2018. The two least hydrologically impacted peatlands along the Main Transect were Fen 1 and Bog 2, which are near the center of the Main Transect where the MS is at its thickest (Figure 3.1). In Fen 1 the WTD (Figures 3.3, B4) and hydraulic heads (Figure B4) were not significantly different from those in unimpacted peatlands, while in Bog 2 hydraulic heads in the top 150 cm were significantly lower but comparable to the unimpacted sites in the deep peat. In contrast, in Bogs 1 and 3 (the closest and furthest bogs to the mine, where MS is thinnest; Figure 3.1), hydraulic head distributions (Figure B4) were significantly lower and WTD (Figures 3.3, B3) significantly deeper than those at all unimpacted peatlands. In Fen 2, hydraulic head distributions were significantly lower than all unimpacted peatlands while WTD was significantly deeper than MOEref but not Bioherm Bog. The water table dropped below the well-screen in Fen 2 during numerous monitoring events, thus the differences between Fen 2 and Bioherm Bog may not be fully captured in this analysis.
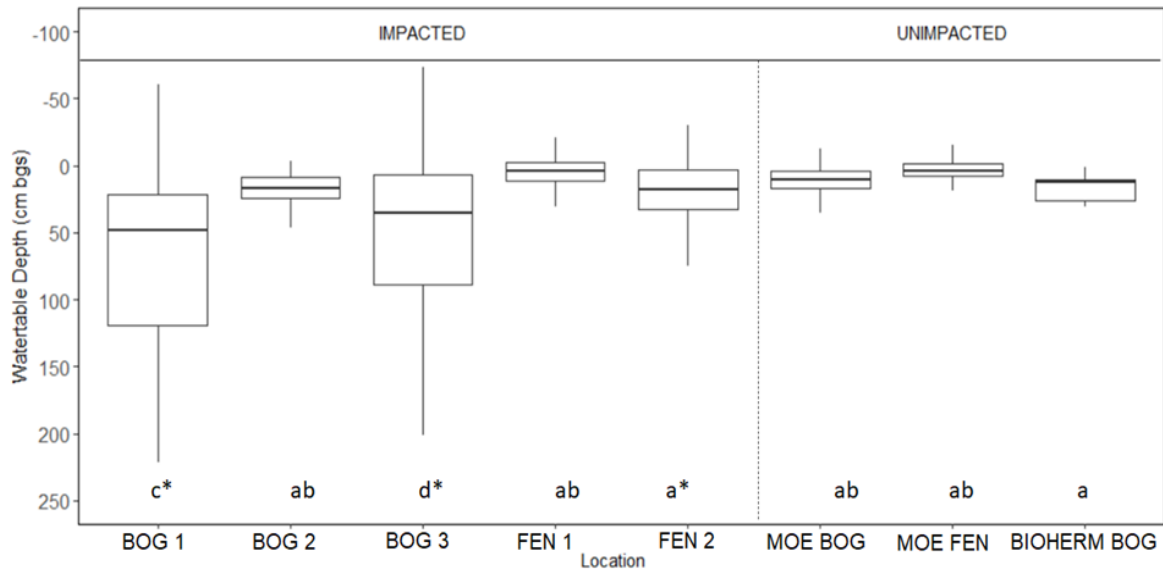
Figure 3.3. Water table depth (WTD) distributions for both impacted and unimpacted peatlands over the entire study period (2007-2018). Shared letters indicate distributions not statistically different over overlapping monitoring periods, and * indicates at least one instance where water table dropped below the well screen.

Within the unimpacted peatlands, effective stress, σ_d' (Figure 3.4), was not significantly different between MOE Bog and MOE Fen, while both σ_d' and σ'_{max} were lower in Bioherm Bog than at MOEref for all depths because of the smaller σ_t near the surface and larger μ in the deep peat. The σ' were significantly higher at all layers in Bogs 1 and 3 and Fen 2, compared to that in the unimpacted peatlands, whereas no significant difference occurred at any depth for Bog 2 and Fen 1. The differences in σ_d' between the most (Bogs 1 and 3, Fen 2) and least (Bog 2 and Fen 1) impacted peatlands became more apparent with increasing depth due to smaller porewater pressures in the former. Except for Bog 2, the difference between impacted and unimpacted peatlands σ'_{max} (red points in Figure 3.4), also increased with depth, ranging from 5-8 kPa greater in impacted peatlands at the 100 cm depth, and up to 25 kPa higher in the deep peat. Data within the MS were limited; however, trends were consistent with shallower layers, with the greatest σ' in Bog 3 and greater σ'_{max} in impacted peatlands.
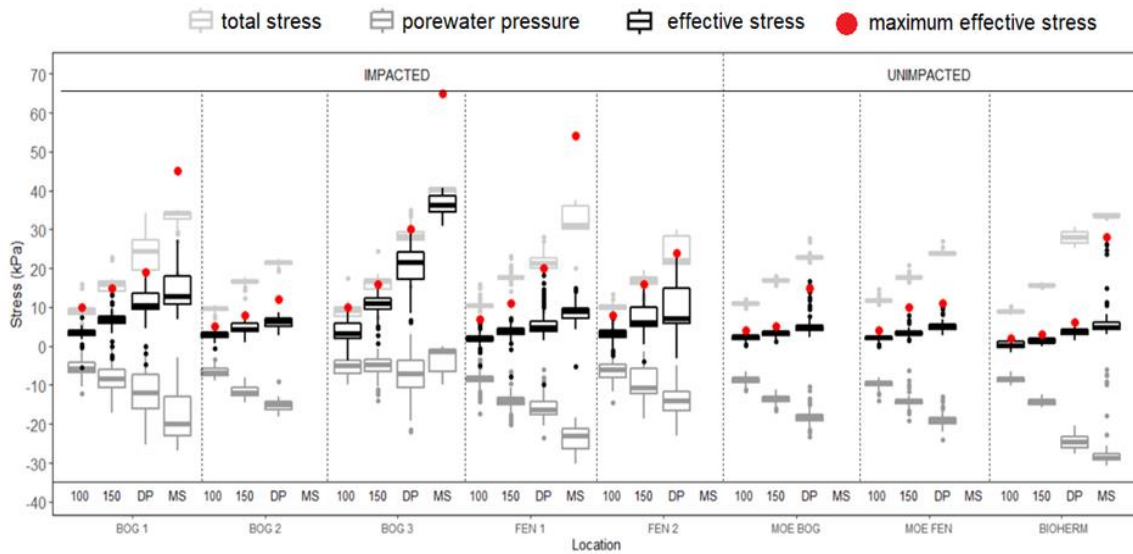
Figure 3.4. Total stress (σ_t), porewater pressure (μ) and effective stress (σ') at each installation depth (100 cm, 150 cm, deep peat (DP) and marine sediment (MS)) averaged for each peatland over the respective monitoring periods as well as maximum effective stress over the study period (red points). Here positive values correspond to pressures acting in the downwards direction.

3.5.3 Net change and variability in surface elevation

The average range in surface elevation within individual years at each peatland (Figure 3.5) was generally similar between all peatlands (~4-6 cm). Surface elevation range was highest in 2010 or 2011 for all peatlands except MOE Bog, in whose range was highest in 2012. The 2011 monitoring period was the only year in which the range was statistically different between peatlands. Here, Fen 2 and Bog 3 had significantly higher ranges than both MOE Bog and MOE Fen, though they did not differ statistically from the Bioherm Bog.
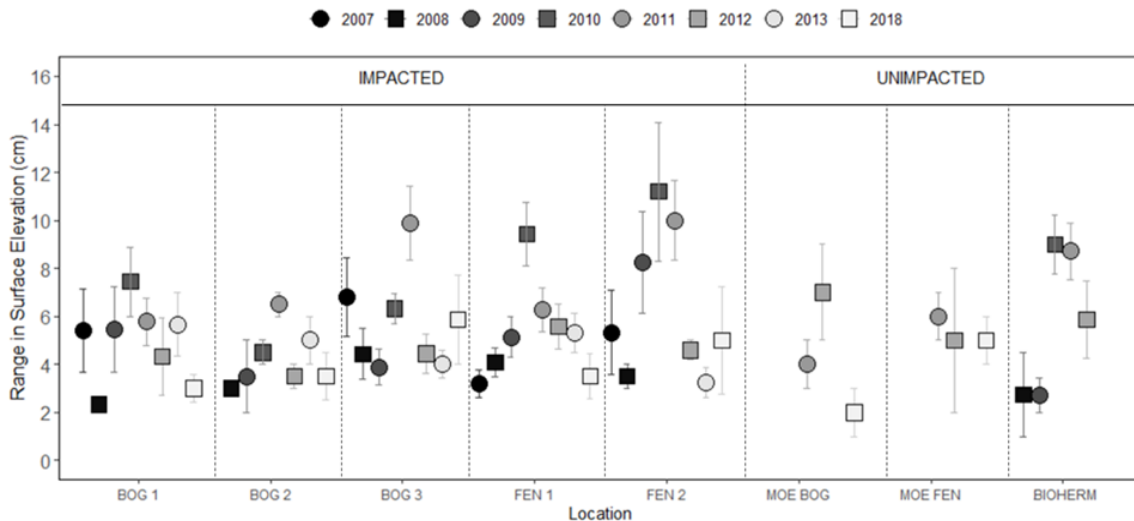
Figure 3.5. Annual range of surface elevation for each monitoring year measured using stickup values in the deep peat piezometers (symbol shows average within each peatland, whiskers show maximum and minimum).

Statistically significant net changes in measured stickup over the monitoring period were observed at most pipes/ERs within both impacted and unimpacted peatlands (Figure B5- for lines of best fit and associated r^2 values at each individual pipe/ER see Table B2). When translated to a change in thickness within individual layers at each peatland (Table 3.1) there was generally a small apparent increase in near surface thickness in MOE Bog and MOE Fen (likely the growth of vegetation at the surface). The measured increase in thickness was largest at the MOE Bog (~5 cm), however there was no significant difference between any unimpacted peatlands for any installation depth ($p>0.05$).

At the impacted peatlands, layer thickness decreased for most or all depth intervals, representing subsidence. The total peat subsidence (that measured in deep peat pipes) was similar between impacted peatlands (11-15 cm) except for Bog 2 (4 cm). Bog 2 was the only impacted peatland in which the overall change in surface elevation was not significantly different from that in unimpacted peatlands. Variability was high for the measurements of total change in peat thickness (measured via changes in peat depth; Table 3.1, Figure B5). Subsidence measured through this method was highest in Bog 3 and lowest in the unimpacted peatlands, consistent with pipe/ER measurements.

Subsidence within individual layers at the Main Transect (Table 3.1) was highly variable between peatlands. Where subsidence occurred, the decrease in layer thickness was generally between 5-10%,

and was higher near the surface (0-100 cm) in the fens and below this depth in the bogs. Though subsidence was smallest in Bog 2 it occurred exclusively in the deep peat which was thin at this peatland, resulting in the largest decrease in layer thickness of 20%. MS layers were not included because installations only penetrated the uppermost portion of this layer, thus would not represent its total subsidence.

Table 3.1. Change in thickness at individual layers, and over the entire peat profile between 2007 and 2018 at impacted and unimpacted peatlands as projected with linear or polynomial relations (Table B2). Manual change in peat depth was determined using augered manual peat depths.

		Layer Interval (cm)	Change in Layer Thickness (cm)	Change in Layer Thickness (%)	Change in peat profile thickness (%)	Manual change in peat depth (%)
IMPACTED	Bog 1	0-100	4	-4	5	6
		100-150	1	-2		
		150-~225	6	-8		
	Bog 2	0-100	0	0	2	4
		100-150	0	0		
		150-~170	4	-20		
	Bog 3	0-100	2	-2	5	13
		100-150	5	-10		
		150-~260	5	-5		
	Fen 1	0-100	9	-9	5	8
		100-150	0	0		
		150-~170	2	-10		
	Fen 2	0-100	9	-9	6	11
		100-150	3	-6		
		150-~190	0	0		
UNIMPACTED	MOE Bog	0-100	-5	5	-2	2
		100-150	0	0		
		150-~215	0	0		
	MOE Fen	0-100	-2	1	-1	3
		100-150	0	0		
		150-~190	0	0		
	Bioherm Bog	0-100	2	-2	1	-
		100-150	0	0		
		150-~250	0	0		

In the unimpacted peatlands, the change in surface elevation per unit change in water table depth ($\Delta z_e/\Delta WTD$; Table 3.2) was twice as large in MOE Fen (0.54) as in MOE Bog (0.25), corresponding to a shallower range in WTD in MOE Fen. The $\Delta z_e/\Delta WTD$ in Bioherm Bog (0.33) fell between that of MOE Fen and MOE Bog, but the water table range and distribution (Figure 3.3) was deeper although not statistically significant from that in other unimpacted sites.

Within all impacted peatlands $\Delta z_e/\Delta WTD$ decreased between the first and second monitoring periods, most notably in Bog 2 and Fen 2, which decreased by 60 and 80%, respectively and dropped below the range measured in the unimpacted peatlands. By the second monitoring period, $\Delta z_e/\Delta WTD$ was lowest in Bog 1, Bog 3, and Fen 2, corresponding to deeper water table ranges there (Table 3.2).

Table 3.2. Average change in surface elevation per unit change in water table depth ($\Delta z_e/\Delta WTD$; cm/cm) for impacted and unimpacted peatlands for overlapping monitoring intervals.

		Impacted					Unimpacted		
		Bog 1	Bog 2	Bog 3	Fen 1	Fen 2	MOE Bog	MOE Fen	Bioherm Bog
2007-2011	($\Delta z_e/\Delta WTD$) (cm/cm)	0.09	0.38	0.14	0.27	0.35	-	-	0.33
	WTD range (cm)	30 to >260 *	5 to 35	-1 to >200 *	-15 to 25	0 to >190 *	-	-	0 to 30
2011-2018	($\Delta z_e/\Delta WTD$) (cm/cm)	0.07	0.15	0.07	0.23	0.07	0.25	0.54	-
	WTD range (cm)	65 to >260 *	20 to 40	60 to >200 *	5 to 25	30 to ->190 *	-5 to 30	-15 to 20	-

* water table dropped below well bottom

3.5.4 Changes in Saturated Hydraulic Conductivity

K_{sat} was consistent with depth in MOE Bog and Bioherm Bog and above the deep peat in MOE Fen, on average ranging between 10^{-1} to 10^{-2} m/day (Figure 3.6, Table B3). The low K_{sat} in MOE Fen in the deep peat was unusual, though consistent within all piezometers screened in the deep peat at this location and observed within individual deep peat piezometers at both MOE Bog and Bioherm Bog. This could be attributed to MS present

within the screened intervals. No statistically significant differences in K_{sat} occurred at any depth at the unimpacted peatlands over time.

Within the impacted peatlands, initial K_{sat} was generally within the range of unimpacted values, except for the deep peat at Bog 2 in which the average K_{sat} was an order of magnitude lower. Mean K_{sat} declined by up to an order of magnitude at numerous depths in all three impacted bogs, most notably in Bog 3 in which declines occurred at all three depth intervals. Unlike the bog distributions, K_{sat} increased by an order of magnitude at both Fen 1 and Fen 2 at the 100 cm layer, and in the 150 cm layer in Fen 1. Where a decrease in K_{sat} did occur (i.e., in Fen 2) final distributions were still within the range of unimpacted peatlands.
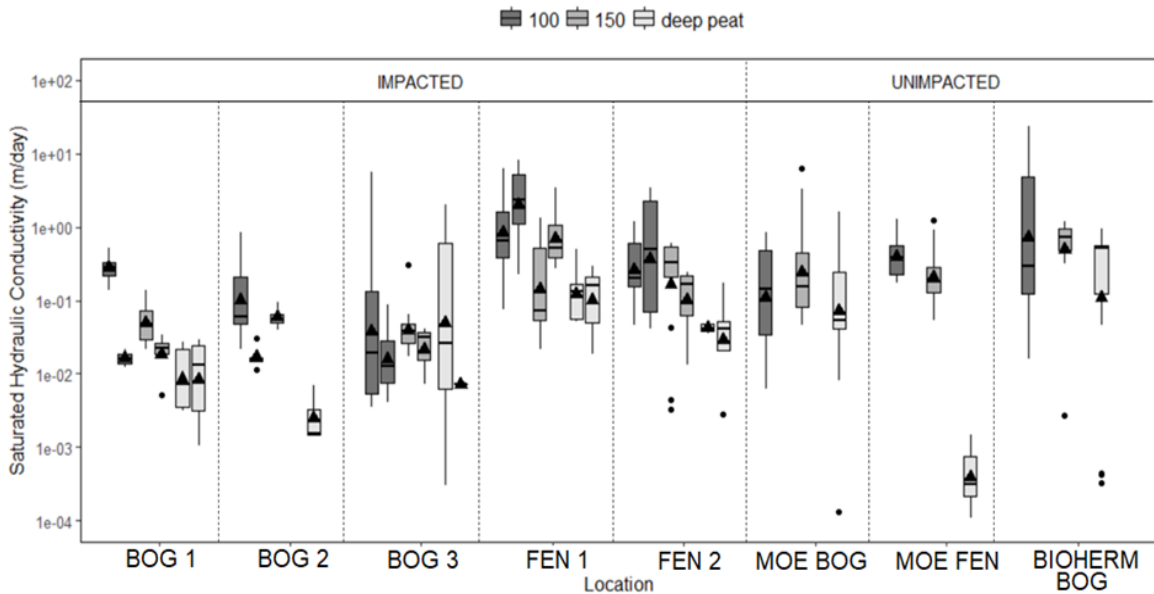
Figure 3.6. Geometric average (dots) median (line) and distributions of saturated hydraulic conductivity (K_{sat}) for each peatland by installation depth. For peatlands in which K_{sat} values changed significantly over time, start and end values are shown. Otherwise, a single distribution is shown.

3.5.5 Evaluating Changes in Hydrological Function

In flownets generated in the first and 10th years of dewatering (Figure 3.7; Topodrive discretization in Figure B6 and exports in Figure B7), advective flowpaths originated in the topographic highs

(crests of Bogs 1, 2, and 3), flowed through Fens 1 and 2, and terminated at one of two tributaries (NSGC and NNGC). Early in the study period (Figure 3.7a), the time taken for a particle of water to travel along an advective flowpath from the bog crests to tributaries increased exponentially with depth, from <10 years in the top 30 cm to >10^3 years at the bottom of the peat profile. Notable inflection points occurred where there was a change in K_{sat}, and to a smaller degree where there was a change in land slope (e.g., where Bog 1 transitions to Fen 1). The degree of inflection was more exaggerated in the intermediate and deep peat layers (i.e., below 30 cm) compared to the near surface. Ten years after mine dewatering (Figure 3.7b), there was a general deepening of flowpaths and an increase in flowpath travel time compared to the same depth intervals early in the study period, particularly within the intermediate depth (30-150 cm) in all bogs and fens. The exception occurred at the 100-150 cm depth interval in Fen 1 where intermediate flowpaths were shortened, coinciding with the increase in K_{sat} there (Figure 3.7b). The flownets generated to assess the individual impacts of dewatering-induced changes of either a) peat thickness (Figure B8a) or b) K_{sat} (Figure B8b) on flowpaths demonstrated a much greater influence of the latter. Specifically, flowpaths under the impacted peat thicknesses scenario (Figure B8a) closely matched those in the in the first year of dewatering (Figure 3.7a), whereas flowpaths in the altered K_{sat} scenario (Figure B8b) exhibited the deeper flowpaths and longer transit times observed the 10 year dewatered transect (Figure 3.7b).
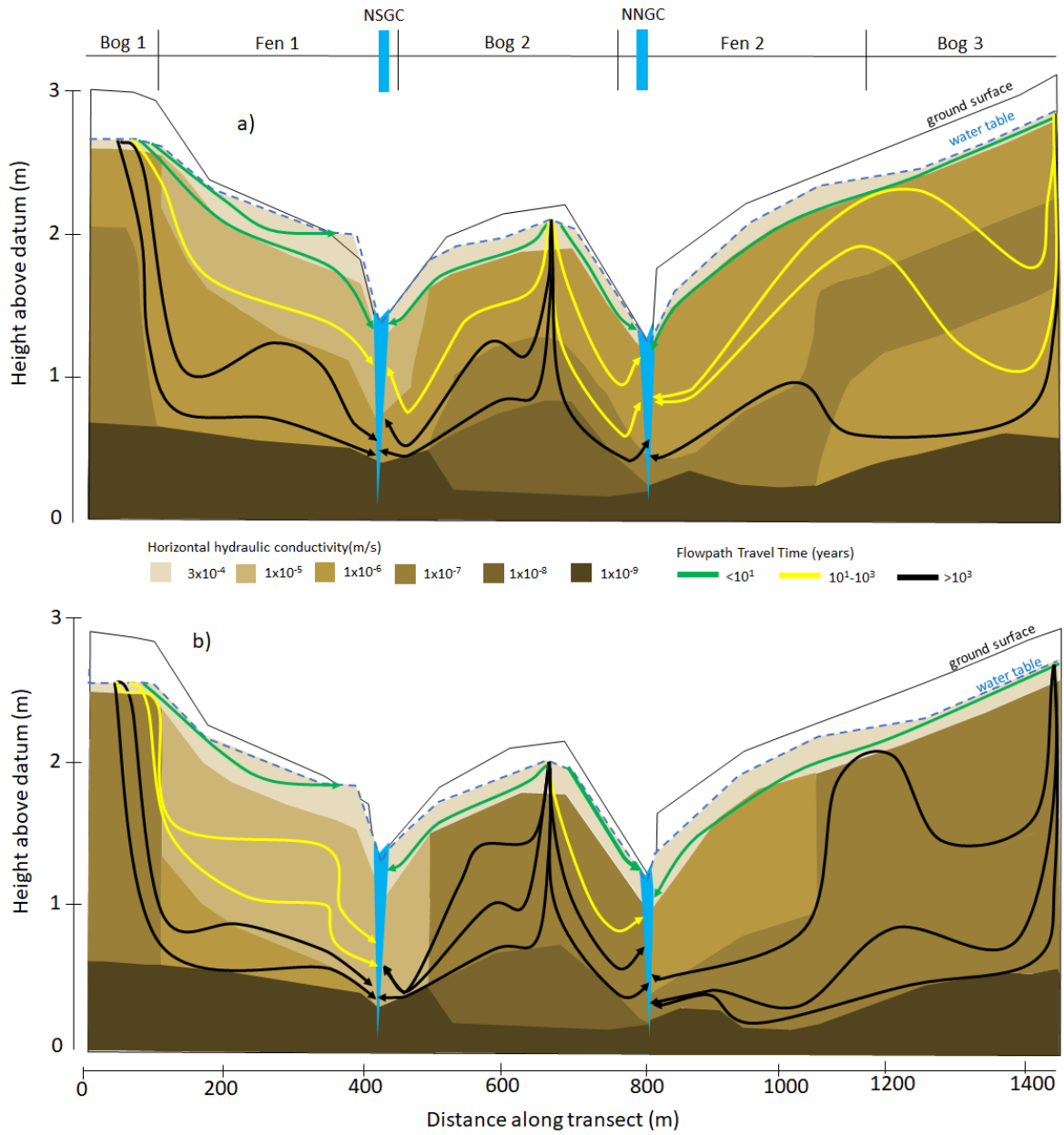
Figure 3.7. Flowpath direction (arrows) and duration (colors) a) in the first year of dewatering and b) after ten years of mine dewatering, generalized from Figure B7.

3.6 Discussion

3.6.1 Dewatering Impacts on Hydrophysical Structure

Within the unimpacted peatlands, water tables were maintained near the surface (i.e., top 30 cm) in all years (Figure 3.3) in spite of the large range of water availability observed over the study period. This was facilitated by the ability of the highly compressible peat to rise and fall with the water table (Figure 3.5), thus maintaining the water table within the higher transmissivity acrotelm and facilitating landscape connectivity (Ingram, 1983; Kellner & Halldin, 2002). Vertical gradients were also small (i.e., hydraulic heads changed little with depth; Figure B4), and effective stress was low (Figure 3.4) at the unimpacted sites. This is consistent with the absence of long-term subsidence at unimpacted sites (Table 3.1, Figure B5) or significant decreases in K_{sat} (Figure 3.6), and suggests that these systems were operating within relative hydrological equilibrium for the duration of the monitoring period.

In contrast to the unimpacted peatlands, mine dewatering and subsequent increased deep seepage (Whittington & Price, 2013; Leclair *et al.,* 2015) at the Main Transect induced a state of hydrological and geophysical disequilibrium in the peatlands there. Within the impacted peatlands the short-term fluctuations in surface elevation (Figure 3.5) were not able to effectively compensate for water losses caused by the enhanced downwards vertical gradients (large decreases in hydraulic head with depth; Figure B4; Whittington & Price, 2013). As a result, the water table fell below the acrotelm (~10-30 cm bgs) and into what was previously defined as the catotelm (i.e., perpetually saturated; Ingram, 1978), for at least a portion of the monitoring period in all impacted bogs and fens (Figures 3.3 and B3), decreasing the porewater pressure thus increasing the effective stress compared to unimpacted values (Figure 3.4). As catotelm peat is more decomposed, less fibric, and has a lower capacity for reversible consolidation (Howie & Hebda, 2018), increased stress within this layer (Figure 3.4) caused the measurable long-term subsidence present in all impacted peatlands (Table 3.1). The subsidence was likely exacerbated by peat decomposition associated with aeration of the previously saturated peat, collapsing pore structure (Teatini *et al.,* 2004; Whittington & Price, 2006; Zeitz & Velty, 2002).

The average transect-wide rate of subsidence decreased slightly from 1.2 cm/year in the first five years of dewatering (Whittington & Price, 2013), to 0.9 cm/year between 2011 and 2018. This is consistent with past studies, which observed a decline in subsidence over time due to the collapse of

increasingly small pore spaces (Kennedy & Price, 2005). The decrease in subsidence also coincides with the rate of mine dewatering, which increased leading up to 2012 then declined by 12% in the consecutive years. This subsidence rate is slower than reported values in peatlands dewatered for agriculture and peat extraction, which were 1.8-2.7 cm/year in a drained and afforested blanket bog (Anderson *et al.*, 1992), 1.3-5 cm/year in a *Sphagnum* dominated string fen drained to 20 cm bgs (Whittington & Price, 2006), and 1-2 cm/year in a drained cultivated Italian peatland of unspecified type (Teatini *et al.,* 2004). Values were likely higher in the aforementioned studies due to the presence of active drainage ditches within meters of the measurement points, and the removal of the acrotelm, which increases water table variability and the aeration of what was catotelm peat (Price, 1996).

   The hydrological changes above were most readily observed at Bogs 1 and 3, consistent with past studies that highlighted these peatlands as being at higher risk to seepage losses due to their thinner underlying MS (Figure 3.1; Whittington & Price, 2013), and the lack of upgradient water sources due to their ombrotrophic nature (Leclair *et al.,* 2015). Because the least hydrologically impacted peatland was Bog 2, which also had the thickest underlying MS, it is likely that MS thickness and not peatland type was the primary control on the observed response. Of note, Bogs 1 and 3 were on opposite end of the Main Transect (thus Bog 3 was furthest from the point of dewatering), however impacts were comparable. Though hydrological impacts were less apparent in Fens 1 and 2, they both underwent consolidation comparable to that in Bogs 1 and 3. The similar consolidation response in these fens is likely due to the initially wetter and less variable hydrological conditions of the fens (Whittington & Price, 2013; Leclair, 2015), which would impart a lower pre-consolidation pressure. Therefore, fens subject to water table lowering beyond the pre-consolidation pressure experienced a higher consolidation rate than bogs for an equivalent water table change. Given that undisturbed bogs initially had a slightly larger range of water table variability (Figure 3.3), thus a higher pre-consolidation pressure, early stages of subsidence in bogs would have been at a lower consolidation rate (recompression rate; see Kennedy & Price, 2005). Additionally, while average water table depth and effective stress were not significantly different to that in MOE Fen, both impacted fens had a higher maximum effective stress and larger maximum water table depths (Figures 3.4, B3). It has been shown at the lab scale that short, repeated periods of increased stress can result in appreciable irreversible consolidation (Ng & Eichens, 1983); thus, the subsidence here may be controlled by the deepest water tables rather than average conditions.

The decline in K_{sat} within Bogs 1 and 3 (Figure 3.6) occurred within the depth intervals that experienced the most consolidation (Table 3.1), likely attributable to the collapse of larger pores under the increased effective stress (Liu *et al.,* 2020). The magnitude of the K_{sat} decline in these layers is consistent with other studies conducted in drained peatlands (Price, 2003; Zeitz, 1991; Zeitz & Velty, 2002; Whittington & Price, 2006; Moore *et al.,* 2015). In Bog 2, however, an order of magnitude decline in K_{sat} occurred at the 100 cm depth in the absence of significantly higher effective stress (Figure 3.4) or consolidation in this layer (Table 3.1). Pressures and stress here were determined based on manual measurements that did not capture the full range of water tables experienced at these sites - there is evidence in Bog 2 that the water table is lowering over time (i.e., reaches depths of ~100 cm bgs during the lowest point of 2011; Figure B3), and thus there may be periods of increased stress that consolidate the peat at 100 cm bgs. The increase in K_{sat} within an order of magnitude at the 100 and 150 cm depths at Fen 1, and the 100 cm depth in Fen 2 is unusual (Figure 3.6) and inconsistent with consolidation and the increase of water table depth over time (Figure B3) that occurred at these locations. This increase in K_{sat} was observed in three of four nests within Fen 1 and the two nests with available data in Fen 2 (Table B3) and is thus not likely sampling error. It is possible that the lower water tables here, or the installation of the piezometers themselves, may have released trapped methane, which can reduce apparent K_{sat} (Mathur & Levesque, 1985). Fen peatlands have also been shown to generate more methane than bogs attributed largely to the higher water tables found there (Moore & Knowles, 1990), which may explain the absence of this phenomena in the three impacted bogs. However, given the uncertainties associated with methane solubility and its implications for soil-water pressure (Kellner *et al.*, 2004) and hydraulic conductivity (Beckwith & Baird, 2001), and the installation of piezometers themselves which can release trapped methane from organic soils (Mathur & Levesque, 1985), explaining the increase in K_{sat} is speculative.

Changes to the peat hydrophysical structure observed within the Main Transect will have lasting effects in the post dewatering landscape. Peat in layers that subsided and where K_{sat} decreased are likely to have lower average pore sizes, lower drainable porosity, and higher water retention for a given pressure if desaturated (Moore *et al.,* 2015; Liu *et al.,* 2020). This could act as a water preservation mechanism in times of limited water availability if this denser peat became desaturated. Conversely, the lower porosity of this peat reduces the overall water storage capacity of the peatlands (Liu *et al.,* 2020), resulting in flashier water tables during precipitation events (Whittington & Price,

2006), higher and faster peaks in downgradient streamflow, and a faster increase in water table depth during dry periods.

3.6.2 Dewatering Impacts on Hydrophysical Function

In the three unimpacted peatlands, and at the lesser impacted Fen 1 and Bog 2, the water table fluctuation zone remained within the acrotelm for the duration of the study period (i.e., the top ~30 cm bgs), which comprises poorly decomposed, highly porous peat that readily releases water during water table decline (Price, 2003; Kennedy & Price, 2005). Correspondingly, the $\Delta z_e/\Delta WTD$ ratio (an indirect measure of the peat's compressibility in the zone of water table fluctuation; Table 3.2), was within the range reported for other undisturbed bogs (0.14-0.4 cm/cm; Price, 2003 and Howie & Hebda, 2018) and fens (0.1-0.8; Lafleur & Roulet, 1992; Roulet, 1991; Waddington *et al.,* 2010). The $\Delta z_e/\Delta WTD$ was higher in MOE Fen than in MOE Bog and Bioherm Bog likely due to the shallower water table ranges in the fen (Table 3.2), which typically contains peat with highest compressibility due to lower pre-consolidation pressures there (Kellner & Haldin, 2002). Contrastingly, the water table fluctuation zone at the three most impacted locations at the Main Transect (Bogs 1 and 3 and Fen 2) fell entirely within what initially was the catotelm (Table 3.2, Figure B3), comprising highly decomposed, lower porosity peat than that in the acrotelm, which releases less water from storage during water table decline (Price, 2003; Kennedy & Price, 2005). The low $\Delta z_e/\Delta WTD$ here was also likely further exacerbated by the subsidence that occurred at these locations, which can lower porosity and drainable porosity.

The shape of advective flowpaths in the pre-subsidence scenario (Figure 3.7a) are consistent with other studies characterizing flow in bog-fen systems, where advection was predominately downwards underneath bog mounds, then redirected first upwards then laterally where there is a decline in surface slope towards fens (Glaser *et al.,* 1997; Reeve *et al.,* 2000). These flow patterns enhance the transport of solute rich water to the surface of fens, due to the intersection of advective pathways with the upwards diffusion of calcium, magnesium and other ions from the MS layer below (Price & Woo, 1988; Reeve *et al.,* 2000; Reeve *et al.,* 2001; Orlova & Branfireun, 2014). The deeper flowpaths in the post-subsidence scenario (Figure 3.7b), driven downwards by the declining K_{sat} in Bogs 1-3, likely reduced the amount of upwards transport of solute rich water. A reduction of solute rich water at the surface was likely exacerbated by the deep water tables and large downward vertical gradients present in the impacted peatlands here during dewatering (Figures 3.3, B3, B4), favouring the

downwards movement of precipitation-derived solute-poor waters (Perras, 2016). Over the long term, deeper flowpaths would reduce vertical mixing of solutes within the peat profile, which may reduce the concentrations of ecologically important chemical species such as calcium at the surface of the fens. This has the potential to shift already poor fens into bogs. The deeper intersection of flowpaths at the two tributaries may also increase the amount of MS derived ions reaching these tributaries, however, the extremely slow rate of advection is likely to render this process minimal.

When compared individually, subsidence-induced changes in K_{sat} (Figure B8b) elicited a much greater change in flowpaths when compared to subsidence-induced changes in layer thickness (Figure B8a). Because the amount of subsidence that occurred at bogs and the adjacent fens at either end of the Main Transect were similar (i.e., Bog 1 to Fen 1, and Bog 3 to Fen 2), the slope between these adjacent peatlands would not be affected, thus the lack of change in flowpaths due to subsidence is not surprising at these locations. Further, both tributaries (NNGC and NSGC) cut through the peat layer and incise into the underlying MS, and thus would not be impacted by peat subsidence. Therefore, changes to flowpaths between Bog 2, Fen 1 and Fen 2 and the adjacent tributaries would be dependent on changing water table depths and less on the ground surface elevations, the former of which was kept constant for the scope of this model.

3.7 Limitations

During the field study, the true range in water table depth and of extent of surface elevation variation in each monitoring season could not be captured due to the reliance on manual measurements, which in turn was biased towards the late spring and early summer season and was not measured at equal intervals each year. Therefore, the range in these variables is likely larger than numbers reported here. The data available were collected over a wide range of water table depths each season and are comparable to published literature, and therefore likely represent relatively broad hydrological conditions. The calculation of net change in surface elevation also assumes that the pipes/ ERs are stationary and that the change in stickup reflects consolidation. Shifts may occur due to installation in low density peat which has insufficient friction against the pipe to allow it to remain in place, and frost heave up or down (Nelson *et al.*, 1985; Chapuis & Sabourin, 1989). The former two process is unlikely to be occurring here; the shallowest installations are ~100 cm bgs, which allows for a large area of contact in higher density peat to anchor the pipe in place. Though frost heave (the upwards movement of soil and installations due to frost formation) here is possible, this

59

process occurs near the surface and is more prevalent in mined cutover peatlands (Rochefort & Lode, 2006), thus likely impacting the installations here minimally.

A large amount of variability, particularly within the K_{sat} measurements, made the analysis of these data difficult. Future studies would benefit from the collection of additional hydrophysical properties along impacted transects to pair with in-field measurements to confirm changes to peat structure at depths of changing hydraulic conductivity.

In generating the post-subsidence flownets, it was assumed that the magnitude in decrease in vertical and horizontal K_{sat} was equal at a given point. This assumption should be tested in the future, since if there were a decrease in the anisotropic ratio flowpaths would become elongated, which may reduce vertical mixing. In contrast, an increase in the anisotropy would favour downward flow which may increase flowpath travel time (Beckwith *et al.,* 2003b). Changes in MS K_{sat} were not included in this model due to a lack of long-term data in this layer. MS subsidence may further alter the landscape slopes between peatlands, further altering flow pathways. Despite these limitations, the flownets generated here provide insight in determining the general changes in flowpath direction.

3.8 Conclusions

This research has demonstrated that peat within the catotelm can consolidate rapidly and experience alterations to its hydrological structure when subjected to increasing effective stress. High volume groundwater extraction due to mine dewatering resulted in enhanced deep seepage within the peatlands, lowering hydraulic head and increasing water table depth. As a result, effective stress increased and the peat underwent consolidation, possibly irreversibly. On average, a net subsidence rate of 1 cm/year was observed across the impacted transect over the 12-year observation period, while rates were negligible or negative in unimpacted sites. The deepest water table, lowest hydraulic heads, lowest porewater pressure and highest subsidence rates were observed in Bogs 1 and 3 due to the thin underlying MS, combined with their ombrotrophic nature (i.e., lack of upgradient groundwater connection); distance from the point of dewatering did not have a measurable effect at these locations. In spite of overall higher water tables and lower average effective stress in fens along the transect, compared to bogs, subsidence was still comparable in fens and bogs. This was likely due to the higher compressibility (i.e. higher $\Delta z_e/\Delta WTD$) in fen peat due to lower pre-consolidation pressures, as well as an elevated maximum effective stress when compared to unimpacted fens during the low water table conditions observed at Fen 2. At the impacted sites, layers that experienced

subsidence generally experienced the largest decrease in K_{sat} (up to an order of magnitude), suggesting a reduction in size of flow conducting pores. However, an unexpected significant increase in K_{sat} occurred within intermediate peat at Fen 2 in spite of measured subsidence, potentially due to the release of methane, which when present can decrease apparent K_{sat}. In a post-dewatered landscape, areas that experienced subsidence, and/or a reduction in K_{sat} would have lower water losses if desaturated, due to lower porosities and specific yield and higher water retentions. During saturated conditions however, this lower specific yield would result in flashier water tables and a lower water storage capacity, lowering peatland resilience to changes in water availability.

At the most impacted peatlands (Bogs 1 and 3, and Fen 2) $\Delta z_e/\Delta WTD$ rates were an order of magnitude lower than unimpacted peatlands, attributed to consolidation as well as the deeper water tables there, which reside in low porosity, less compressible peat. Decreases in K_{sat} within the impacted bogs drove flowpaths deeper into the peat profile, which then did not deflect back up to shallow layers, as those found under fens in the pre-subsidence scenario. This would likely reduce the mixing of ion-poor surficial waters with ions diffusing upwards from the marine sediment, potentially reducing the concentration of these ions at groundwater discharge locations (i.e. fens), which may favour a shift towards bogs. Deeper flowpaths may also increase solute concentrations in the downgradient streams due to the deeper advective pathways.

This study demonstrates the complexity of dewatering related impacts within a peatland dominated landscape. Within this mine impacted radius, the most impacted peatlands were related to thin underlying MS rather than the distance from the point of dewatering, suggesting the need for environmental risk assessments and monitoring programs that incorporate factors such as peatland type and aquitard thickness, and not just proximity to disturbance. Cumulative effects of dewatering and drought may also push effective stress well above pre-consolidation limits, demonstrating a need for cumulative effects assessment and dewatering plans that are sensitive to changes in water availability. Where subsidence did occur, the resulting alterations to the landscape will have long term implications on peatland form and function after dewatering ceases, speaking to the sensitivity of these systems once consolidation limits have been reached.

3.9 Acknowledgments

Chapter 4

Hydrological and geochemical changes in disturbed sub-arctic patterned peatlands induced by mine dewatering

4.1 Summary

Patterned bog and fen peatlands of the Hudson Bay Lowlands, which form one of the largest continuous peatland complexes in the world, are globally significant stores of carbon and important water conveyance and storage features in the landscape. There is, however, increasing pressure for resource extraction operations in this region. Combined with warmer temperatures associated with climate change, this may result in reduced water availability to these peatland complexes, potentially disrupting peatland hydrological connectivity and hydrogeochemical cycling. A case study on the effects of reduced water availability on peatland hydrological and hydrogeochemical function was presented at the De Beers Victor Diamond Mine, located 90 km west of Attawapiskat. Active dewatering occurred here over a 12-year period (2007-2019) during which a 1.5 km transect was monitored within the mine impacted radius. Hydrological (i.e. streamflow and groundwater levels) and chemical (i.e. porewater and surface water samples) data were collected at the impacted transect as well as two unimpacted study sites. Results show that impacted peatlands had depleted water storage and spent an average of $50\pm20\%$ less time hydrologically connected when compared to the unimpacted sites. Where storage was depleted in downgradient fens, large lateral bog-fen gradients fluxes occurred until bog storage could no longer sustain lateral water transfer. Where storage was insufficient to maintain fluxes, tributary-fen gradient reversals were observed as well as lowered normalized streamflow compared to unimpacted systems. Depleted water storage further allowed solute-poor precipitation to reach greater depths within the peat profile, while stronger downwards gradients repressed upward advection underneath fens, limiting the amount of solute rich water reaching the surface. The recovery of fen solute concentrations will be a prolonged process (i.e., decade to centuries) due to the slow process of upwards diffusion, which may result in the transition of these systems towards ombrotrophic bogs. Further studies should focus on the susceptibility of these impacted systems to further reductions in water availability due to climatic changes.

4.2 Introduction

Patterned bog and fen peatlands cover 90% of the landscape in Canada's Hudson Bay Lowlands (HBL) region, representing one of the largest continuous peatland complexes in the world (Rouse *et al.,* 1992). A cool, wet climate, low topographic relief (Glaser *et al.* 2004), and a layer of low-permeability marine sediment (Price & Woo, 1988 a,b,c) deposited during the last glacial recession (Lee, 1960) has resulted in shallow water tables ideal for peat accumulation and a high degree of landscape connectivity. Given the absence of mineral uplands in the HBL, water is transferred from upgradient ombrotrophic bogs, towards downgradient minerotrophic fens and surface water features (Glaser, 1989; Price & Maloney, 1994). Peatland discharge contributes a significant portion of tributary flow (Orlova & Branfireun, 2014), and influences water chemistry in both lower order tributaries and major river systems draining into James and Hudson Bay (Richardson *et al.* 2012; Rouse *et al.,* 1992). Recently, increasing pressure for resource extraction operations in this area combined with warmer temperatures associated with climate change threatens long-term water availability, casting uncertainty on the ability of peatlands to sustain hydrological connectivity and maintain current hydrogeochemical cycling.

The quantity and quality of water transported within sub-arctic patterned peatland complexes has been related to a number of factors, the most common of which are peatland morphology, aquitard geochemistry, and seasonal and annual variation in weather (Price & Maloney, 1994; Quinton & Roulet, 1998; Quinton *et al.,* 2003; McCarter & Price, 2017). The vertical patterns of peat hydrophysical properties are one of the most crucial aspects of peatland morphology, typically exhibiting two distinct zones. During high water table conditions, the high transmissivity near-surface acrotelm (Ingram, 1978) becomes saturated and the landscape becomes hydrologically well-connected; shuttling water quickly from bogs towards the downgradient tributaries (McCarter & Price, 2017; Oosterwoud *et al.,* 2017). Conversely, during periods of low water availability the water table declines into the lower transmissivity catotelm (Ingram, 1978), lateral water transport occurs more slowly, and the landscape essentially becomes hydrologically disconnected (Siegel & Glaser, 1987; Oosterwoud *et al.,* 2017; Reeve *et al.*, 2000).

The geochemical composition of porewater is related to mixing processes along these bog-fen-tributary flowpaths. At the surface, bogs receive only nutrient- and ion-depleted water from precipitation (Sjors, 1963). Due to the topographic and hydraulic gradient, water flows downwards and

away from the bogs and is directed horizontally and upwards to downgradient fens. As it moves, the groundwater mixes with peat decomposition products and ions diffusing upwards from the underlying solute-rich marine sediment deposits (Glaser *et al.,* 2004, Reeve *et al.,* 2000, 200; Orlova & Branfireun, 2014). The resulting porewater composition at the surface of the fens and in the downgradient tributaries is dependent on the proportion of solute-depleted water (derived from precipitation) at the surface, and the comparatively solute-rich groundwater flowing upwards from deeper peat. The addition of minerals and nutrients to fen groundwater is crucial to maintaining fen vegetation, whereas the presence of these constituents near the surface of bogs would be detrimental to their ecological function since vegetation there are adapted to low pH and nutrient poor conditions (Zoltai & Vitt, 1995; Riley, 2011). Therefore, changes to the patterns and magnitude of groundwater flow can have cascading impacts on the geochemical conditions and ecology of bogs and fens. Disturbances associated with climate change, such as shifting temperature and precipitation regimes (IPCC, 2022), or resource extraction, such as mine dewatering and road construction, could compromise hydrologic function. Thus, these disturbances could alter water availability, flow patterns, and hydrogeochemical cycling within peatlands and downgradient tributaries.

The De Beers Victor Diamond Mine (hereafter referred to as the Victor Mine), located 90 km west of Attawapiskat, Ontario in the James Bay Lowland, provides an opportunity to characterize the effects of groundwater extraction and associated aquifer depressurization on peatland hydrological connectivity and hydrogeochemistry. Active dewatering occurred at the Victor Mine over a 12-year period (Itasca Denver, 2017). Over the first five years of dewatering, areas of thin or higher permeability MS were identified as enhanced recharge zones due to a greater susceptibility to the higher hydraulic gradients associated with aquifer depressurization (Whittington & Price, 2012a; 2012b; Leclair *et al.* 2015). Compared to pre-extraction conditions, average water table depths within the radius of depressurization increased by up to 100 cm, and deep seepage losses to the underlying mineral aquifer increased by an order of magnitude from <0.1 mm/day pre-impact (HCl, 2004) to 1-4 mm/day after five years of dewatering (Whittington & Price, 2012a, b; Leclair *et al.,* 2015). Because of the lower water tables, available water storage capacity increased in both fens and bogs, though bogs were more sensitive and exhibited a more rapid response to depressurization (Leclair *et al.*, 2015), likely due to their exclusive reliance on precipitation and potentially stronger downward hydraulic gradients (Whittington & Price, 2012b). The effects of increased water storage capacity on lateral peatland connectivity has not been assessed, nor have the effects on groundwater fluxes or porewater

geochemistry. In this area, isotopic enrichment of stable oxygen and hydrogen isotopes was observed at impacted bogs and fens, suggesting evaporatively enriched surface water was being transported to greater depths over time, though this analysis was not statistically significant nor were the changes associated with other chemical constituents (Perras, 2016). The results of these studies were further confounded by a large amount of climatic variability, which was determined to be a significant control on observed hydrology, in addition to the impacts of dewatering (Whittington & Price, 2012b; Leclair *et al.*, 2015).

Further analysis is required of a larger, longer-term dataset to properly infer the changes in water storage and fluxes between and within landscape units and along the peat profile due to mine dewatering. It would also be beneficial to conduct a detailed analysis of the hydrological connectivity of individual peatlands instrumented within the zone of influence, and to perform further geochemical analysis to relate observed hydrological impacts to changes in peat porewater chemistry. Therefore, the goal of this study is to assess the changes in water storage and transmission within and between peatlands in a mine impacted landscape and the resulting changes to peatland hydrogeochemistry. The specific objectives are to: 1) compare water table depths and lateral fluxes between bog, fens and tributaries in both unimpacted and impacted peatland complexes and assess associated differences in landscape hydrological connectivity; 2) determine the change in vertical flow patterns from both a hydrological and geochemical perspective; and 3) assess differences in porewater chemistry with depth, peatland type and degree of disturbance, and the time taken to re-establish porewater chemistry post dewatering within the disturbed peatlands.

4.3 Study Sites

Research was conducted at one impacted site (Main Transect; Figure 4.1b) and two unimpacted sites (Bioherm Bog and MOEref; Figure 4.1a and c). The impacted site is a 1.5 km transect located within 1 km of the Victor Mine (52°49'15''N, 83°53'00''W). This transect was instrumented in 2007 and intersects a sequence of five adjoining peatlands, herein referred to as Bogs 1–3 and Fens 1–2. Bogs 1–3 are of the domed form, Fen 1 transitions from a floating riparian fen subform to a stream riparian fen subform, and Fen 2 is of the stream riparian fen subform (National Wetlands Working Group, 1997; Whittington, 2013). Topographic slopes decrease from bog to fen (0.006, 0.003 and 0.003 in Bogs 1–3, respectively, and 0.003 and 0.002 in Fens 1–2). Two tributaries of the North Granny Creek stream, South North Granny Creek (NSGC) and North North Granny Creek (NNGC), are located between Bog

2 and Fens 1 and 2, respectively with catchment areas of 21 and 9 km² respectively. Slopes from fens to adjacent tributaries increase locally to ~0.020 at Fen 1/ NSGS and 0.016 in Fen 2/ NNGC. Peat thickness is variable in the region, however on average is 2.1 m in the bogs and 1.9 m in the fens. The peatlands are underlain by a glaciomarine sediment aquitard deposited during the Quaternary period composed of primarily low hydraulic conductivity clay sized particles (Canadian Environmental Assessment Agency, 2005), herein referred to as marine sediment (MS). The thickness of the MS is maximal at Bog 1 (>16 m) and decreases to <4 m at Bogs 1 and 3 (Figure 4.1b). At the southern and northern ends of the transect the MS layer is absent and the mid-Silurian Ekwan and Attawapiskat limestones form outcroppings, known as bioherms, above the surface (Singer & Cheng, 2002; Whittington & Price, 2012a). Dewatering is actively causing uneven subsidence across the landscape, continuously altering land slopes and peat and MS thickness (Chapter 3; Whittington & Price, 2012a,b).
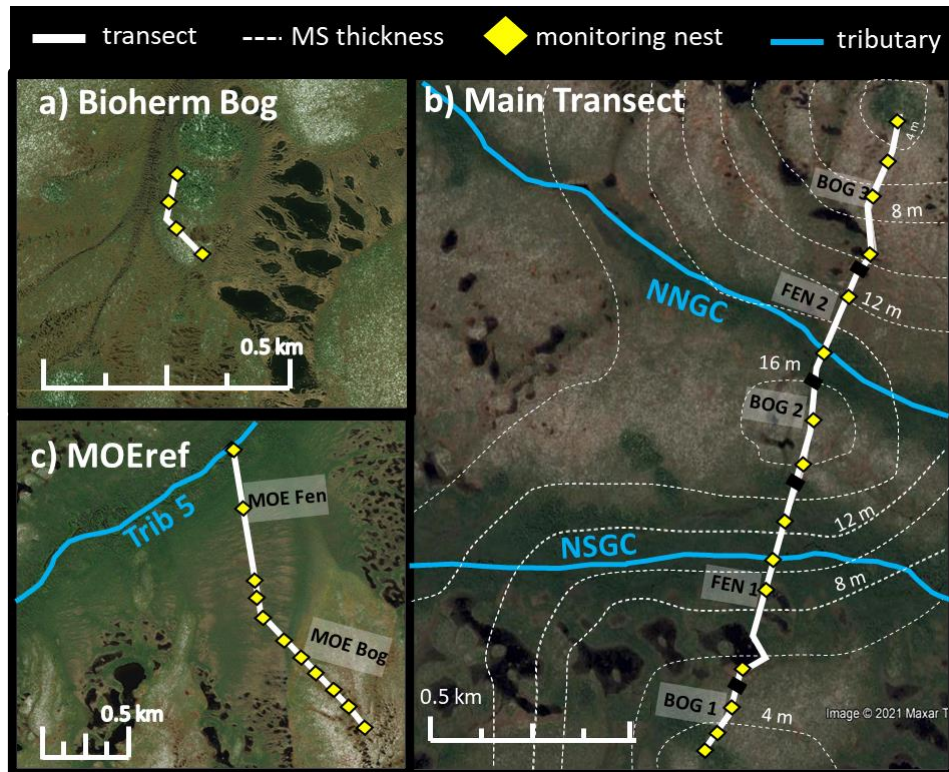
Figure 4.1. Research transects and instrumentation within the impacted a) Main Transect and unimpacted b) Bioherm Bog, and c) MOEref. Individual peatlands designated using the Canadian Wetland Classification System (NWWG, 1997) are labelled where multiple peatland

types are present. Marine sediment (MS) thickness contours are shown along the Main Transect which increase in thickness towards the center of the transect (dashed white lines).

The MOEref site is a 4.9 km^2 sub-watershed hosting a 1.5 km transect instrumented in 2010, 14 km south-southwest of the Main Transect and outside the mine cone of depression. MOEref consists of two peatlands, a domed bog (MOE Bog) with an open stunted *picea mariana* (black spruce) canopy, and a moderate-rich ribbed fen (MOE Fen). Downgradient of MOE Fen is a 2nd order segment of the Trib 5 tributary (Orlova & Branfireun, 2014; Ulanowski, 2014). Peat thickness at MOEref ranges from 2.0 to 2.3 m in the bog and decreases from bog to fen to a minimum of <0.5 m at the northern extent of the fen (Ulanowski, 2014). The average slope is 0.003 in MOE Bog and 0.002 in MOE fen (locally up to 0.01 where the fen meets Trib 5). The Bioherm Bog site comprises a single domed bog outside the zone of dewatering; instrumented along a 150 m transect starting 25 m away from a bioherm and extending outwards, with a peat thickness from 2.3 to 2.7 m (Leclair *et al.,* 2015) and an average slope of 0.003. Marine sediment (MS) thickness was not measured in the unimpacted peatlands.

4.4 Methods

4.4.1 Meteorological Parameters

Meteorological parameters, including air temperature, net radiation, wind speed and precipitation were collected hourly and summarized daily at the Victor Mine station, located 2 km from the Main Transect. Actual evapotranspiration (*AET*) was measured at two eddy covariance towers at MOEref (Table 4.1) and then fit to equilibrium *ET* using data collected at the Victor Station via the Priestley-Taylor method for data outside the MOEref measurement period (Priestley & Taylor, 1972). For more detailed description of the methodology on the *AET*/*PET* regression see Chapter 2. Only data from the non-frozen period were used due to the confounding effects of frost formation and thaw on peatland water flow and connectivity Chapter 2.

4.4.2 Site Instrumentation and Monitoring

In 2007, 18 monitoring nests were installed along the Main Transect, with 2–4 nests in each peatland (installation details in Whittington & Price, 2013). Each monitoring nest comprised wells and piezometers constructed from 2.5 cm inner-diameter PVC pipe installations including a fully screened well, and 20 cm screened piezometers installed 90 cm below ground surface (bgs), 150 cm bgs, and at a variable depth directly above the MS layer (herein referred to as deep peat). Shallow (300–350 cm

bgs) and deep (450–550 cm bgs) MS steel drivepoint piezometers (2.5 cm inner-diameter) were installed in seven nests within Bog 1, Fen 1 and Bog 3. Water level depths were measured at all pipes during monitoring events, which varied in timing and frequency between years (Table 4.1). Water level depths were corrected for fluctuations in ground surface elevation to obtain a relative depth as the peat surface rose and fell.

A total of 11 monitoring nests were instrumented along the MOEref transect in 2011, six of which were installed into MOE Bog and five in MOE Fen. Each monitoring nest included a 2.5 cm diameter PVC fully screened well and 20 cm screen length piezometers with the center of the screen at 100, 150 and 200 cm bgs. Both MOE Bog and MOE Fen were monitored intensively between 2011–2012 and revisited again in 2018 (Table 4.1). The second reference site (Bioherm Bog) was instrumented in 2008, with four bog nests that included 100 cm, 150 cm, deep peat and MS piezometers (for installation details see Leclair *et al.,* 2015). Wells were not installed in this transect and thus water levels were taken from a nearby domed bog, which was instrumented as part of the Victor Mine groundwater monitoring network, located <1 km west. Monitoring events at Bioherm Bog took place between 2008 and 2012 (Table 4.1).

Table 4.1. Monitoring period and number of monitoring events each year at the Main Transect, MOEref and Bioherm Bog Sites

	Variables	**Data Collection Period**
Main Transect high-intensity data collection	ground water elevation	2007–2008 2010– 2012, 2017– 2018
	NNGC,NSGC stage	2008– 2012
	water sampling	2010–2012
De Beers Victor Mine Meteorological Station and Monitoring Data	meteorological variables	2007–2018
	groundwater elevation	2007–2015
	NGC confluence stage	2007–2018
MOEref Bog and Fen transect	groundwater elevation	2011–2012, 2018
	evapotranspiration (AET)	2011–2015
	water sampling	2011–2012
	Trib 5A stage	2011–2012, 2018
Bioherm Bog transect	groundwater elevation	2008-2012

4.4.3 Groundwater and Surface Water Date

A subset of nests at the Main Transect and MOEref were fitted with Solinst^{TM} Levelogger pressure transducers and logged hourly over the data collection period (Table 4.1). Each well was developed after installation and prior to monitoring, to ensure screens were not blocked. Wells were re-instrumented between August 2017- August 2018, using Van Essen mini Divers (DI501) to collect hourly water table elevation data. Data were compensated for atmospheric pressure during both monitoring periods using Solinst^{TM} Barologgers and validated with manual measurements.

Gaps in data outside the high-intensity monitoring periods at the Main Transect were filled using four monitoring wells instrumented in 2007 as part of the Victor Mine environmental monitoring program (Table 4.1) and logged hourly between 2007-2015 using Solinst^{TM} Levelogger pressure transducers. Wells used for regressions were of matching peatland types and were located within 500 m of the Main Transect. To assess the accuracy of measurements outside the high-intensity monitoring period, linear regressions were conducted and compared to manual water level elevations collected at the Main Transect. Only regressions with a coefficient of determination (r^2) above 0.7 and $p<0.01$ were used for the creation of water table distribution curves (Table C1). A similar fitting process was used for MOEref data, as outlined in Chapter 2.

For establishing groundwater connectivity, water table connectivity thresholds for bogs and fens were taken from previous analysis at MOEref (Chapter 2). In that analysis, hydrological connectivity was defined as a state in which water was readily transferred across the landscape towards downgradient surface water features. This was measured via streamflow response, in which hydrological disconnection occurred when there was little to no change in streamflow over a 24-hour period. Water table connectivity thresholds were established as the average water table depth during non-frozen periods when the downgradient tributary was connected. The connectivity thresholds used here are averages from the bog (20 cm bgs) and fen (8 cm bgs).

Stage-discharge curves were generated for both NNGC and NSGC using a minimum of 70 manual measurements collected using a flow meter (Leclair *et al.,* 2015) within both tributaries between 2008-2012 (r^2=0.87, $p<0.01$ and r^2=0.86, $p<0.01$ for NNGC and NSGC, respectively). Pressure transducers were installed into both branches of North Granny Creek during the high intensity data collection period (Table 4.1). Outside of this period, stage data were regressed against a monitoring

station located ~ 2 km downgradient at the confluence of NNGC and NSGC (r^2=0.77, p<0.01 and r^2=0.83, p<0.01 respectively). Flow data from a tributary downgradient of MOEref (Trib 5A) instrumented as part of the De Beers monitoring program was used to represent unimpacted conditions, as it is a first order tributary with comparable catchment size (30 km^2) to NNGC and NSGC and is highly correlated to MOEref (Chapter 2).

4.4.4 Water Sampling

At each of the monitoring sites, water samples were collected for the analysis of stable isotopes (δ^2H and δ^{18}O), major anions and cations, pH, and DOC over the monitoring intervals in Table 4.1. Only samples from the non-frozen period were used for this analysis. A total of 20 and 17sampling events were conducted at the Main Transect and MOEref, respectively. Samples were collected using low-flow peristaltic pumps from each piezometer and along the top 5 cm of the peat profile (herein referred to as near surface) using PTFE pore water sippers inserted into undisturbed peat near each monitoring nest (Ulanowski, 2014). To characterize the isotopic and geochemical composition of atmospheric water sources, rain samples were collected during 13 rain events with a bulk rain gauge along the Main Transect (Perras, 2016) and via funnels and a storage container at the Victor Mine station rain gauge (Ulanowski, 2014). Snowpack samples were collected adjacent to monitoring nests at the Main Transect in 2012, over 8 monitoring events between April 13 and May 4. Eight additional water sampling events were conducted to assess the composition of deeper (below peat) waters, at the MS piezometers at the Main Transect and monitoring wells screened in MS and bedrock within 20 km of the study sites. Additional details of the sampling procedure and data validation can be found in Whittington (2013), Orlova & Branfireun (2014), Ulanowski (2014), and Perras (2016).

4.4.5 Lateral and Vertical Gradients and Fluxes

The amount of water that is transferred across the landscape towards the tributaries was quantified by estimating the water fluxes within the top 140 cm (approximately the minimum peat depth). These calculations were conducted at the bog-fen interface and at the fen outlet just upgradient of the tributaries. Calculations were completed at the Main Transect and MOEref over the 2007-2015 period (where continuous water table measurements were available). The flux (m^2/ unit width) was calculated each day as:

$$q = iK_{sat}d = iK_{sat}(1.4 - WTD) \tag{4.1}$$

where q is the daily flux (m²/day), i is the lateral hydraulic gradient (m/m), K_{sat} is the saturated hydraulic conductivity of the peat (m/day), d is the saturated thickness of the peat profile, and WTD is the water table depth (m bgs).

The lateral hydraulic gradient i at each interface was calculated as:

$$i = \frac{dh}{L} \tag{4.2}$$

where dh is the difference in water table elevation between the two measurement points (m), and L is the lateral distance between those points (m).

The saturated hydraulic conductivity was not constant with depth, thus a vertically-integrated hydraulic conductivity ($K_{sat,e}$) was used in determining flux, calculated as:

$$K_{sat,e} = \frac{\sum K_{sat,a} d_a}{\sum d_a} \tag{4.3}$$

where $K_{sat,a}$ (m/day) is the hydraulic conductivity measured in layer a, and d_a is the thickness of layer a. Layers used for this calculation were 5 cm thick over the saturated portion of the peat profile. Hydraulic conductivity values for each layer were taken from cores measured in the laboratory using a Darcy permeameter in the top 30 cm and interpolated from single-well response tests conducted in the field from depths below. Due to the changes in permeability arising from subsidence along the Main Transect, $K_{sat,e}$ was calculated at each nest for each given year. The average $K_{sat,e}$ for each peatland for each year is shown in Figure C1. Due to instrumentation locations hydraulic gradietns for bog/ fen fluxes were calculated over distances of ~ 100-150 m, while gradients for fen outlet fluxes were calculated over distances of 5-15 m (the streambanks are approximately 1-2 m of this). These gradients are consistent with the changes in topography across the landscape, which are low and gradual between bogs and fens and locally high where fens meet tributaries.

Due to the reliance on manual piezometer head data, monthly vertical fluxes could not be calculated, and thus only vertical hydraulic gradient was calculated when available as:

$$i_v = \frac{\Delta h}{\Delta d} = \frac{h_{dp} - h_{wt}}{d_{dp} - d_{wt}} \tag{4.4}$$

where h_{dp} and h_{wt} are total hydraulic head in the deep peat piezometer and at the water table respectively (m asl), and d_{dp} and d_{wt} are the centre screen depth of the deep peat piezometer and of the water table, respectively (m). Distributions of vertical gradients were tested for normality and, where

normal, compared statistically between peatlands for overlapping monitoring intervals using a) ANOVA regressions and Tukey pairwise comparisons if normal, or b) Kruskal Wallace test and Dunn test posthoc analysis if not normal.

4.4.6 Hydrogeochemical Analysis

In the absence of continuous vertical flux data, changes in groundwater chemistry within the peat profile were used to infer changes in vertical groundwater movement. This approach was selected due to the low hydraulic conductivity at depth (i.e., below the zone of water table fluctuation) in peatlands which results in slow advection and long travel times (Chapter 3) and thus relatively small temporal variability of solute concentrations (Reeve *et al.,* 1996; Sjors & Gunnarsson, 2002). For this analysis, at any given point in the peat profile water chemistry was assumed to be a mixture of solute-depleted precipitation from above (spring rain, summer rain, fall rain and snow) and MS derived solute-rich waters from below. To determine the geochemical parameters best representing this process, radar plots were first developed for each of these five sources, and chemical species that varied insufficiently or inconsistently were eliminated. A PCA was then conducted on the remaining chemical constituents to determine the parameter that best represented variability along the unimpacted peat profile. Concentration distributions of the selected geochemical species were then tested for normality and compared between sources using a) ANOVA regressions and Tukey pairwise comparisons if normally distributed, or b) Kruskal Wallace test and Dunn test post hoc analysis if not normally distributed. Only chemical species that were significantly different between MS and precipitation-based sources were used for further analysis. Once one or more chemical species was selected as representative, distributions at each sample depth (near surface, 100 cm bgs, 150 cm bgs and deep peat) for each peatland were tested for normality, and distributions between peatlands at a given sample depth compared statistically using a) ANOVA regressions and Tukey pairwise comparisons if normal, or b) Kruskal Wallace test and Dunn test posthoc analysis if not normal.

To assess the potential long-term implications of changes in porewater chemistry, a one-dimensional diffusion model was executed to provide an estimate of the timeline associated with the reestablishment of pre-disturbance geochemical conditions along the peat profile once dewatering has ceased. Detailed methodology for this model is located in Appendix C.

4.5 Results

4.5.1 Site Conditions

The average and standard deviation of daily temperature, total precipitation (P) and actual evapotranspiration (AET) over non-frozen months in this study period (May to October, 2007-2018) was 10 ±1°C, 390 ±100 mm and 280 ± 30 mm, respectively. There was a net water surplus (P-AET>0; Figure 4.2) all years except 2013 (-80 mm), although the surplus was greater in the first half of the monitoring period (2007-2012) than the latter (2013-2018). The largest surplus occurred in 2009 (290 mm) due to large amounts of rainfall in this year. A more detailed hydrometerological analysis can be found in Chapter 2.

Mine dewatering began in January 2007 and increased from an average of 19,000 m³/day in 2007 to a maximum of 86,000 m³/day in 2012, before decreasing slightly to an average of 76,000 m³/day between 2013 and mine decommissioning in early 2019 (unpublished data; Whittington & Price, 2013).
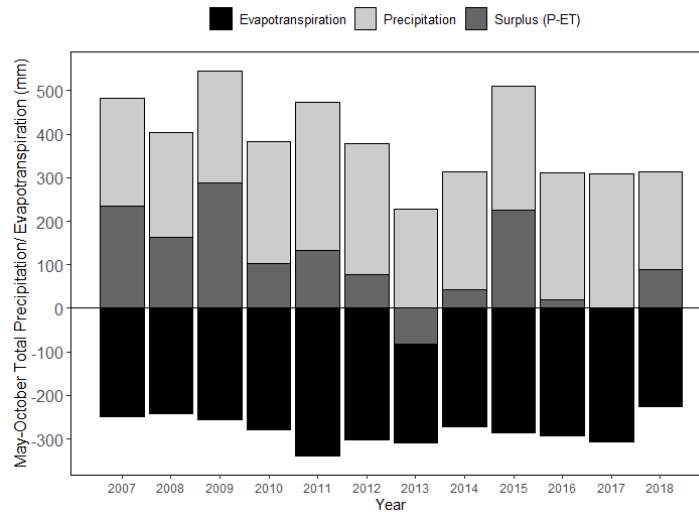
Figure 4.2. Total precipitation (light gray), actual evapotranspiration (black), and net water surplus (dark gray) for the May to October period between 2007 and 2018

4.5.2 Hydrology

In the undisturbed Bioherm Bog, MOE Bog and MOE Fen, median water table depth (WTD) was 12, 11, and -5 cm bgs, respectively (50th percentile in Figure 4.3a, b). Water tables at these sites were

above connectivity thresholds 95% of the time, and there were no statistically significant changes in yearly connection frequency for any of the unimpacted peatlands between 2007-2015 (Figures 4.3a, b, Table C2). Conversely, connectivity was less frequent and declined significantly between 2007 and 2015 at all impacted peatlands except Bog 3 (which exhibited lower connectivity prior to site instrumentation) at the 95% confidence interval (Table C2). WTD exceedance curves were most like unimpacted peatlands in Bog 2 and Fen 1 (average WTD of 14 and 7 cm bgs, respectively), however water tables only exceeded connectivity thresholds ~75% and 55% of the time, respectively, which is ~20 and 40% lower, respectively, compared to the undisturbed bogs and fen. Average water tables were deepest at Bog 3 and Fen 2 (62 and 23 cm bgs on average, respectively), falling below connectivity thresholds >75% of the time.
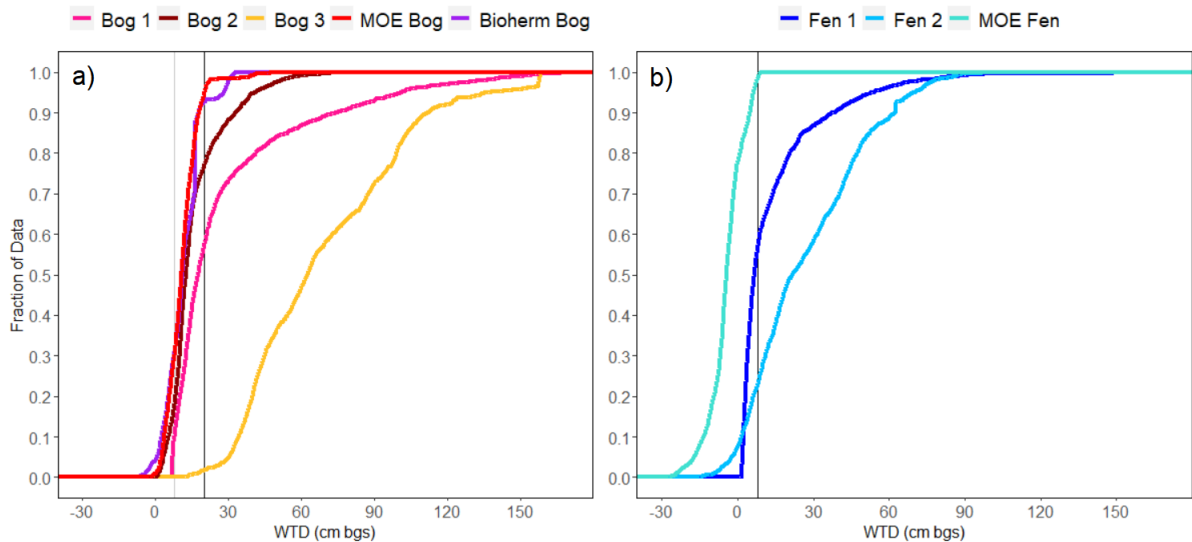
Figure 4.3. a) bog and b) fen water table depth probability exceedance curves along the impacted Main Transect, MOEref and Bioherm Bog (solid curves. Distributions were generated using data collected between 2007-2015. The thresholds for connectivity in bog and fen peatlands are 20 and 8 cm bgs, respectively (black vertical lines).

Groundwater flux from from MOE Bog to MOE Fen, and Bog 3 to Fen 2 during the non-frozen season (Figure 4.4a) did not change significantly over the monitorng period, and was an order of magnitude larger on average between Bog 3/Fen 2 than MOE Bog/MOE Fen (4.99 and 0.18 m^2/month, respectively). Groundwater flux between Bog 1/ Fen 1 was intermedate (2.7 m/month on average), however monthly fluxes dropped below MOEref values in 2013 and 2014.

Compared to the bog-to-fen fluxes, fluxes at the fen outlets were 1-2 orders of magnitude larger during most months (Figure 4.4b), which corresponded with steeper hydraulic gradients (Figure C2). At the unimpacted MOEref, fen outlet fluxes were generally largest early in the season (May totals in Figure 4.4b) and lowest mid summer, though there was a large variability between years particularly during the latter half of the monitoring period. Patterns of groundwater flow at the impacted fens of the Main Transect were each distinct. Fluxes to NSGC from Fen 1 were generally highest, though flux reversals (i.e. flow from NSGC to Fen 1) occurred in five out of nine years. While in Fen 2/ NNGC fluxes were smallest, flux reversals only occurred during May of 2014 and 2015.
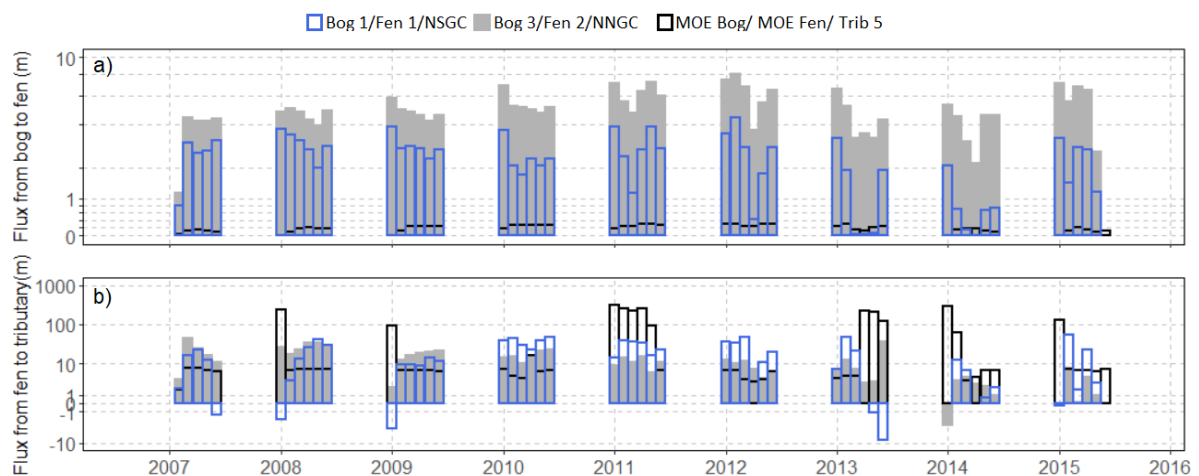
Figure 4.4. Non frozen (May-October) lateral fluxes (m/month) calculated over the top 140 cm of the peat profile over the 2007 to 2015 monitoring period. Fluxes were calculated from a) bog to fen and b) at the fen outlet directly upgradient of the tributary. Note difference in vertical axis scales.

Patterns of monthly streamflow, which were normalized by catchment area (herein referred to as runoff- Figure 4.5), were similar between NSGC and NNGC, with NSGC approximately 20% higher than NNGC for any given month. The temporal trends in Trib 5A, however, were unique. Generally, at Trib 5A there was a definite runoff peak in May, with the exception of 2016. In contrast, at both NNGC and NSGC notable May runoff peaks were delayed (e.g., 2017) or absent (e.g., 2010) in half of the study years, particularly during the latter half of the monitoring period.

There was no statistically significant change in monthly runoff over the study period (2007-2018), in part due to the high inter- and intra-annual variability. In most years, by the end of the monitoring

season, Trib 5A had the largest cumulative runoff of all three tributaries (Table 4.2), with notable exceptions in 2011 and 2012. The difference in cumulative runoff between Trib 5A and the two impacted tributaries increased between the beginning and end of the study period. On average, between 2007 and 2012 Trib 5A cumulative runoff was only 8 and 35 mm larger than NSGC and NNGC, while between 2013-2018 Trib 5A was 68 and 92 mm larger on average, respectively. These differences can be attributed mainly to runoff totals for the months of May and June. When regressed against time, the difference in May and June runoff between Trib 5A and the impacted tributaries increased significantly from the start to the end of the study period ($r^2=0.53$, $p<0.01$ and $r^2=0.67$, $p<0.01$ for May, and $r^2=0.52$, $p<0.01$ and $r^2=0.51$, $p<0.01$ for June runoff values, in NSGC and NNGC respectively).
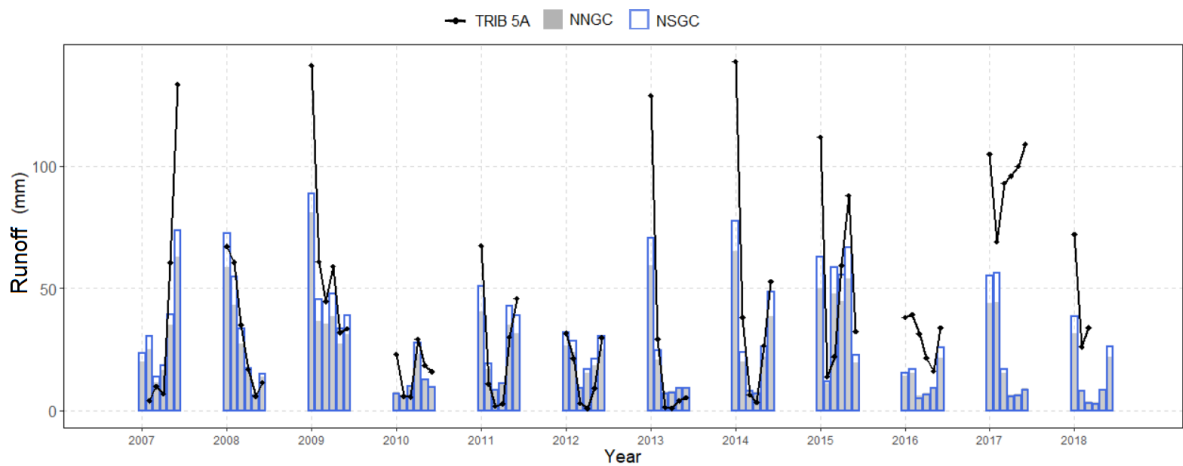
Figure 4.5. Monthly runoff over the May-October period for the unimpacted Trib 5A (near MOEref) and impacted NNGC and NSGC (Main Transect) tributaries.

Table 4.2: Cumulative runoff in the three instrumented tributaries normalized by catchment area, over the unfrozen season (May-October). The tributary with the largest cumulative runoff for each year is italicized.

	Cumulative May-October Runoff (mm)		
	TRIB 5A	**NSGC**	**NNGC**
2007	-	199	171
2008	197	*199*	165
2009	*371*	299	250
2010	*98*	73	69
2011	159	*172*	144
2012	96	*138*	119
2013	*170*	128	115
2014	*270*	191	162
2015	*328*	278	228
2016	*180*	78	74
2017	*215*	148	126
2018	-	86	78

For overlapping monitoring periods, there was no significant difference in vertical hydraulic gradients between any of the unimpacted peatlands (Figure 4.6), with average vertical gradients of -0.08, -0.05 and -0.02 cm/cm in MOE Bog, MOE Fen and Bioherm Bog respectively. Gradients were largest at the impacted Main Transect in Bog 3, and gradients at Bogs 1 and 3 and Fen 2 and were significantly different from unimpacted sites (reaching values in excess of -1 m/m). In contrast, gradients at Bog 2 and Fen 1 were not significantly different from those at the unimpacted peatlands, with the maximum annual gradients also within the range observed at MOE Bog and MOE Fen.
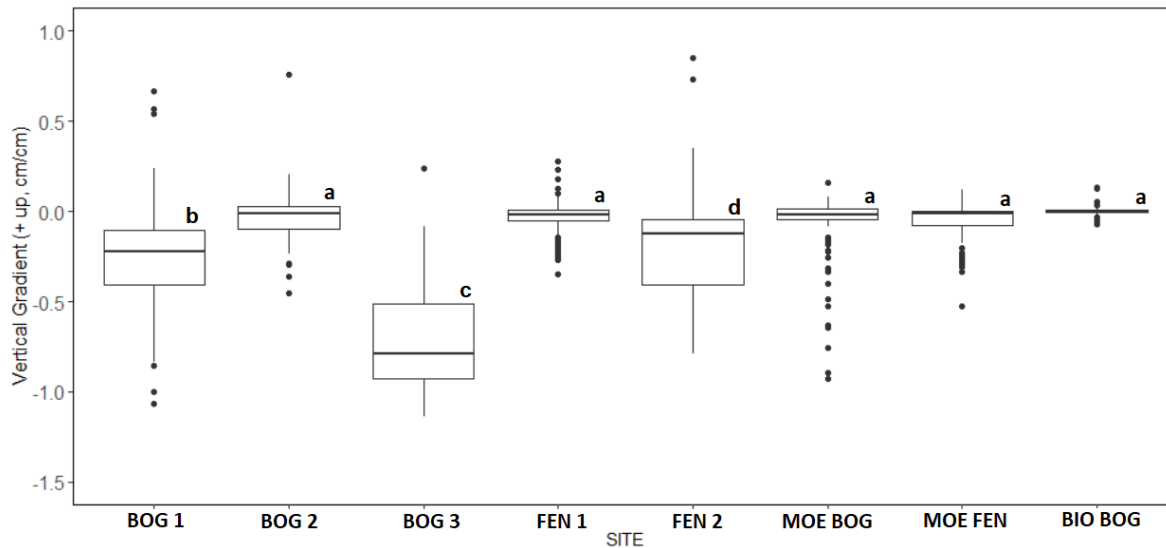
Figure 4.6. Distribution (boxes) and outliers (points) of vertical gradients between the watertable and deep peat measured between May-October, 2007-2015. Letters denote distributions which are not significantly different (p>0.05) for overlapping monitoring periods.

4.5.3 Hydrogeochemistry

The majority of analyzed chemical species (Ca^{2+}, K^-, Mg^{2+}, F^-, Na^+, SO_4^{2-}, Cl^-, δ^2H and $\delta^{18}O$) showed a distinct separation between the MS and precipitation sourced waters (Figure C3) and were used in the PCA analysis. Elevated concentrations in precipitation sources were observed for DOC, NO_3^{2-}, NH_4^+, and Li^- and were thus eliminated from further analysis.

Of the total variance, 93% was represented by the primary and secondary principal components of the PCA (80% and 13% respectively, Figure C4 axis), therefore these two dimensions were considered sufficient. The primary component was mainly represented by Ca^{2+} (96% of primary component, 77% overall variance) The second component was mainly represented by Cl^- (79% of secondary component, 10% overall variance). The next most influential component (SO_4^{2-}) represented only 4% of the total variance, therefore only Ca^{2+} and Cl^- were selected for further analysis. Source waters showed a significant difference in Ca^{2+} concentration between MS-derived water and precipitation (Figure C5). In contrast, Cl^- concentrations were not significantly different between MS derived water, fall rain and spring rain, and there were several outliers which were orders of magnitude larger than median concentrations, thus Cl^- was removed from further analysis. No significant differences in Ca^{2+} concentrations between seasons or years were determined for each

peatland depth (Table C3), therefore a single distribution was used for all data over the period of sampling availability.

In the unimpacted bogs and fens, Ca^{2+} concentrations increased consistently with depth and reached median MS source concentrations by 150 cm in MOE Fen and the deep peat in MOE bog (Figure 4.7). Generally, Ca^{2+}concentrations in the top 150 cm were lower within the impacted peatlands compared to the unimpacted sites for a given depth and peatland type (i.e., bog or fen). However, concentrations converged below 150 cm at all locations (Figure 4.7). This was statistically significant for Fen 2 at all depths, Bog 1 and 3 below the near surface (samples taken from the top five cm), and Fen 1 in the top 100 cm. Bog 2 was the only peatland in the Main Transect where Ca^{2+} concentrations were not statistically different to MOE Bog at any depth. Of note Ca^{2+} concentrations in near surface samples are less certain due to the higher temporal variability of chemistry there.
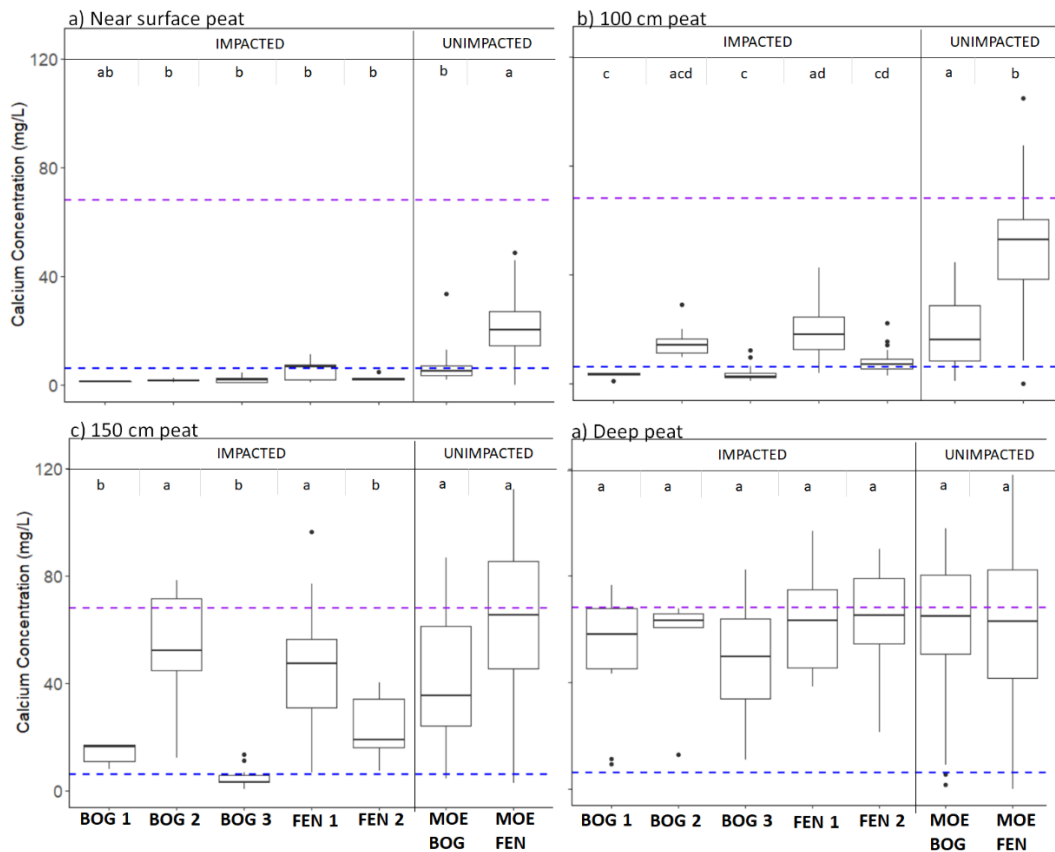
Figure 4.7. Ca^{2+} concentrations of porewater a) near surface, b) 100 cm bgs, c) 150 cm bgs, and d) deep peat. The purple dashed line is the median Ca^{2+}concentration in the MS porewater, and the blue dashed line is the median Ca^{2+}concentration in the averaged precipitation.

In addition to Ca^{2+}, two chemical parameters (pH and DOC) showed significant differences between impacted and unimpacted fens and bogs (Figures 4.8a, b). These parameters could not be used to directly infer the mixing of MS and precipitation derived waters due to low sample size (pH) or elevated concentrations in precipitation sourced waters (DOC; Figure C3) but may be still illustrative of differing geochemical processes in impacted and unimpacted peat profiles. At the impacted peatlands pH was generally lower and DOC higher at a given depth compared with unimpacted porewaters. In the fens, differences in DOC were statistically significant for all depths, and pH differences were statistically significant in the top 100 cm. Below the 100 cm depth values approached those of the unimpacted peatlands.
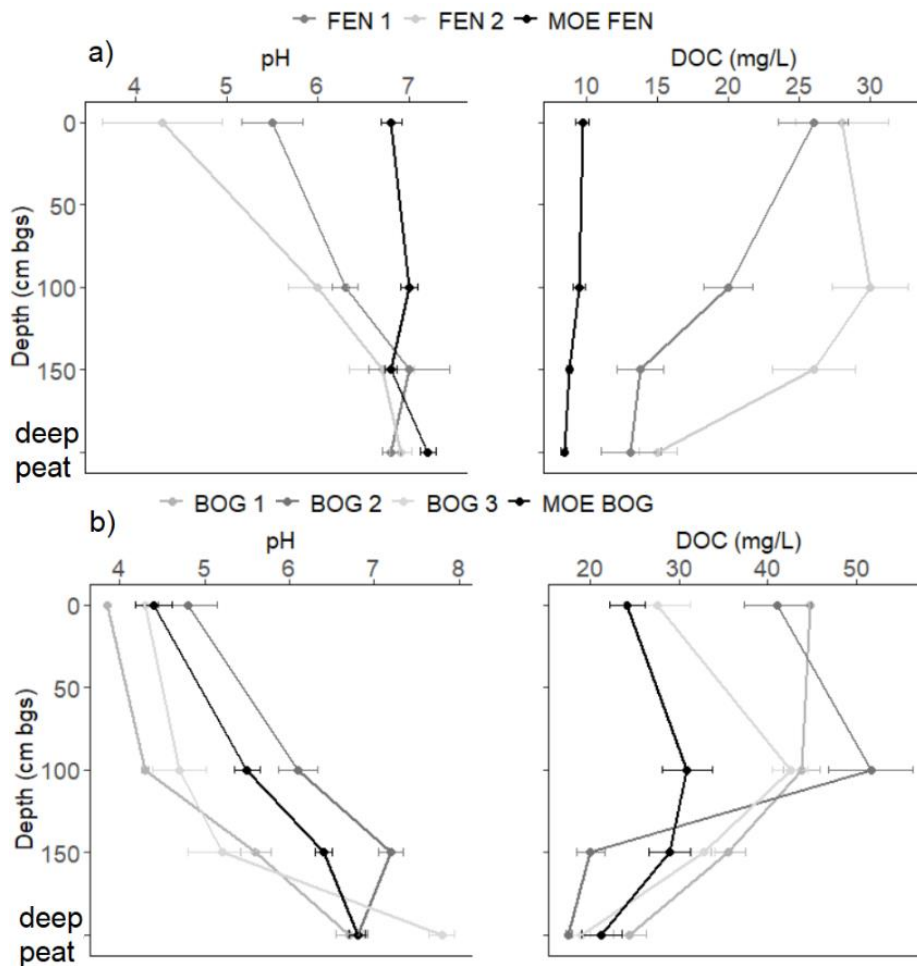
Figure 4.8. Average (points) and standard error (error bars) for pH, and DOC concentration along the peat profile at the impacted and unimpacted a) fen and b) bog.

81

4.6 Discussion

4.6.1 Hydrological Connectivity and Flux

The unimpacted peatlands studied here generally maintained a high degree of connectivity during the unfrozen season (Figure 4.3, Table C2), even in years that experienced a net water deficit, such as 2013 (Figure 4.2). Water tables were consistently shallower in MOE Fen than in the unimpacted bogs (Figure 4.3), and lateral fluxes at the outlet of the MOE Fen were 1–2 order of magnitude higher (though more variable) compared to fluxes between MOE Bog and MOE Fen (Figures 4.4, C2). This is consistent with past studies that identified the role of patterned fens as effective conveyors of water during high water table conditions, and bogs as water storage mechanisms that release smaller, albeit more consistent fluxes (Price & Maloney, 1994; Quinton *et al.,* 2003). Periods of high lateral fluxes from the MOE Fen towards Trib 5 (peaks in Figure 4.4b) occurred in May after storage was replenished by the spring freshet (Chapter 2), consistent with other studies in other northern peatland-dominated catchments (Quinton *et al.,* 2003; Oosterwoud *et al.,* 2017), and in mid-summer during years that experienced a water deficit but connectivity in the fen was maintained (Figure 4.2, Table C2). Lateral fluxes from bog to fen and fen to tributary at the MOEref are likely underestimated, as the estimates of K_{sat} used for these fluxes fail to capture the preferential flow paths that form in microtopographical lows during high water table conditions (Price & Maloney, 1994; McCarter & Price, 2017; Balliston *et al.,* 2018). Vertical gradients within the unimpacted peatlands (Figure 4.6) were small (<0.01), typically downwards, and larger in the bogs than MOE Fen. The magnitude of the vertical gradients at unimpacted sites were within the range of other reported patterned fens (Price & Maloney, 1994), and bogs (Reeve *et al.,* 2000; Fraser *et al.,* 2001).

At the impacted Main Transect, water tables in both bogs and fens were deeper, and more frequently below the connectivity thresholds (Figure 4.3, Table C2), compared to the unimpacted peatlands, suggesting pervasive deficits in peatland water storage, and desaturation of the high hydraulic conductivity acrotelm (Figure C1). The deeper water tables at Bog 1 and Bog 3 (compared to Bog 2) and Fen 2 (compared to Fen 1), are consistent with thinner underlying MS (contours in Figure 4.1a), being in close proximity to bioherms; both conditions have been identified as higher risk in past studies to increased deep seepage (Chapter 3, Whittington & Price, 2012a,b; Leclair *et al.,* 2015). Differences in vertical hydraulic gradients between impacted peatlands largely matched patterns in water table distribution. Vertical gradient distributions were not significantly different in

Bog 2 and Fen 1 compared to the unimpacted sites (Figure 4.6). In contrast, downwards gradients dominated at the most impacted sites, Bogs 1 and 3 and Fen 2, suggesting that dewatering below the peat profile is responsible for the deeper water tables. The extremely large vertical gradients measured in Bogs 1 and 3 ($\leq$ -1m/m) is likely in due to the pronounced decrease in hydraulic conductivity with depth (Hart *et al.,* 2008), which spanned 3 orders of magnitude between the surface and deep peat, in addition to underlying depressurization due to mine dewatering.

When compared to MOEref, steeper horizontal hydraulic gradients between Bog 1/Fen 1 and Bog 3/Fen 2 (Figure C.2a) within the impacted peatlands typically resulted in larger lateral groundwater fluxes (Figure 4.4), in spite of the desaturation of the high transmissivity upper layer. Non-negligible lateral fluxes were also maintained in all years between Bog 3 and Fen 2 (Figure 4.4a) despite water tables residing primarily in the lower conductivity catotelm (Figures 4.3, C1). This could be aided by localized low-lying areas within Bog 3 such as fen water tracks, which were able to maintain higher connectivity in an otherwise disconnected landscape. At the interface between Bog 1 and Fen 2, during the two driest monitoring seasons (2013 and 2014; Figure 4.2) lateral gradients reversed and groundwater exchange became negligible (Figures 4.4a C2a), demonstrating landscape disconnection.

During most of the frost-free season, impacted fen outlet groundwater fluxes were within an order of magnitude of MOEref due to the larger lateral gradients driving flow in the former, and higher water tables intersecting the high conductivity acrotelm in the latter (Figures 4.4b, C2b). The lateral gradient and flow reversals (flux from tributary to fen) observed in the impacted fens during spring high flow periods (i.e., 2008, 2009 and 2014) and dry summers (i.e., 2013, 2014) was unusual, and has not been observed in unimpacted patterned peatlands. Since the majority of NSGC and NNGC watersheds are outside the area of impact (Leclair *et al.,* 2015) the streams could have contributed water to the depleted storage within impacted fens, which normally supply water to the streams.

The seasonal trends in runoff in all three instrumented tributaries, which generally peaked in May and occasionally again in October (Figure 4.5), is consistent with other rivers in this region, as is the large interannual variability in flow (Déry *et al.,* 2005). There was a disproportionally larger increase in flow with an increase in catchment size; NSGC and NNGC have 50 and 20% of Trib 5A flow with 70% and 30% catchment area. In previous studies on catchments in HBL this has been attributed to more and larger channel fen systems present in larger catchments, which more effectively convey flow compared to smaller watersheds (Richardson *et al.* 2012; Quinton *et al.,* 2003). This is likely the

case during times high water availability; however, during low flow periods bog connectivity is maintained during lower water tables (Chapter 2). The more similar flows during lower flow years (i.e., 2011 and 2012) is likely due to the higher similarity of bog "baseflow" between catchments compared to the higher flows derived from surficial connectivity (Richardson *et al.,* 2012). The increasing disparity of flow between the impacted tributaries and Trib 5A from the beginning to end of the study period is likely due to a depletion of storage due to mine dewatering, which, when combined with overwinter drainage that occurs in these systems (Chapter 2), results in a lower proportion of snowmelt contributing to streamflow in the early summer months (statistically significant differences in May and June flow).

Theoretically, the depleted storage, lower connectivity, and lateral flux reversals in the impacted peatlands at the Main Transect should result in less water entering the portions of NSGC and NNGC within the radius of impact, particularly during traditionally wet periods such as spring freshet when fluxes are normally disproportionally high (Quinton *et al,* 2003). Prior to dewatering, it was predicted that flow losses of ~24,600 m^3 would occur at the confluence of NSGC and NNGC (Granny Creek), representing 24% of the total flow (AMEC, 2008). A landscape scale flow model would greatly aid in the determination of peatland response to locally lowered watertables on runoff and flow distribution, particularly due to the non-linear nature of impact (i.e., deeper water tables further from the point of dewatering), and the large portion of watersheds outside of the impact radius feeding NSGC and NNGC (Leclair *et al.,* 2015).

4.6.2 Chemical Analysis

The results of the radial plot, PCA, and concentration distribution analysis (Figures C3–C5), which identified Ca^{2+} as the dominant contributor to variability in porewater chemistry, agrees with cluster analysis on samples from the HBL performed in Reeve *et al.,* (1996) and by piper plot and PCA analysis by Orlova & Branfireun (2014). The secondary grouping of $Cl^-/Na^+/SO_4^{2-}$ here is likely associated with salts trapped within the underling MS from connate seawater (Price & Woo, 1988c). The high variability of Cl^- within the MS and unimpacted peatlands (Figure C5b) is consistent with past studies in the area (Reeve *et al.,* 1996; Orlova & Branfireun, 2014), and may be due to long-term flushing of this relatively conservative ion downgradient from bog to fen and tributary, as observed closer to the coast in HBL (Price & Woo, 1988b, c). The elevated Ca^{2+} concentrations in fall precipitation is unexpected, and is hypothesized to be from contamination of dust from gravel roads at

the Victor Mine, as both fall rainfall events used for the analysis were collected in 2012 (an abnormally dry fall- Chapter Two) when the mine was still active.

4.6.3 Impacts of Dewatering on Hydrogeochemistry

Ca^{2+} concentrations (Figure 4.7), and higher pH (Figure 4.8) were observed in MOE Fen compared to MOE Bog at all depths. This is consistent with the enrichment of water in carbonate-derived minerals along the presumed groundwater flowpaths between bog and fen (Reeve *et al.,* 2001). DOC concentrations increased from the surface to mid-peat (~100–150 cm; Figure 4.8) and were higher in both bogs than MOE Fen. The elevated DOC concentrations in the bogs compared to MOE Fen, is likely attributable to lower water tables and thicker zone of water table fluctuation in the former (Figure 4.3a), which results in greater aerobic decomposition and less DOC dilution (Urban *et al.*, 1989; Chanton *et al.,* 1995; Tfaily *et al.,* 2018). For all depths, pH, Ca^{2+}, and DOC concentrations were within the range reported in other bogs and poor to moderate-rich fens in the HBL (Reeve *et al.,* 1996) and abroad (Gorham *et al.,* 1985; Quinton & Roulet, 1998; Sjörs, 2002; Bourbonniere, 2009).

Conceptual patterns in groundwater flow at the impacted Main Transect (flowpaths in Figure 4.9) were previously generated in Chapter 3, and derived from vertical and lateral hydraulic gradients (Figures 4.6 & C2) and hydraulic conductivity values (Figure C1). Locations with Ca^{2+} depleted waters relative to unimpacted peatlands (depicted as dark grey shaded areas in Figure 4.9, derived from data in Figure 4.7), occurred in all impacted peatlands except Bog 2. Locations that had the most depleted waters at depth were those with the strongest downward vertical gradients (Figure 4.6) and deepest water tables (Figure 4.3, Figure 4.9 blue lines), and corresponded to locations with thin or absent MS (i.e., bioherm adjacent locations at the north and south limits). These also coincide with locations of lower pH, and elevated DOC concentrations (Figure 4.8) compared to unimpacted sites and the lesser impacted peatlands at the Main Transect (i.e., Bog 2 and Fen 1).

The processes illustrated in Figure 4.9 suggest that the large downwards gradients and low water tables are introducing acidic, solute-depleted water downwards in the peat profile to depths not typically seen in natural systems in this study, or in other patterned bogs and fens (Roulet, 1991; Lafleur & Roulet, 1992), and peatlands at large (Batzer & Baldwin, 2012). This both diluted and displaced the carbonate-based ions (i.e., Ca^{2+}) held within the porewater, and counteracted upwards diffusion. As a result, porewater acid neutralization capacities were reduced, and porewater pH decreased (Shotyk, 1988; Urban *et al.,* 1989; Rippy & Nelson, 2007). The decreased upwards

mobility of carbonate-based ions is best demonstrated in Fen 2, where flow paths were deepest (Figure 4.9). Here, surficial pH (4.2±0.1), Ca^{2+} within the top 150 cm, and DOC at all depths of the peat profile were within ranges more typical for bogs than poor fens (Bourbonniere, 2009; Shotyk, 1988; Sjörs, 2002; Gorham *et al*, 1985; Reeve *et al.,* 1996). However, pH, Ca^{2+} and DOC concentrations within the impacted bogs (Figure 4.8b) were at the upper end of literature ranges in natural bogs (Blodau, 2002; Reeve *et al.,* 1996; Bourbonniere, 2009). Sampling occurred only halfway through the mine lifespan, but over time, the abnormally deep and variable water tables relative to the unimpacted peatlands (Figure 4.3), is expected to increase oxygen availability at depth. This would increase aerobic decomposition, and in conjunction with the large downward gradients (Figure 4.6), may facilitate downwards migration of labile carbon from the near-surface. The effect of both would increase DOC production (Chanton *et al.,* 1995; Tfaily *et al.,* 2018).
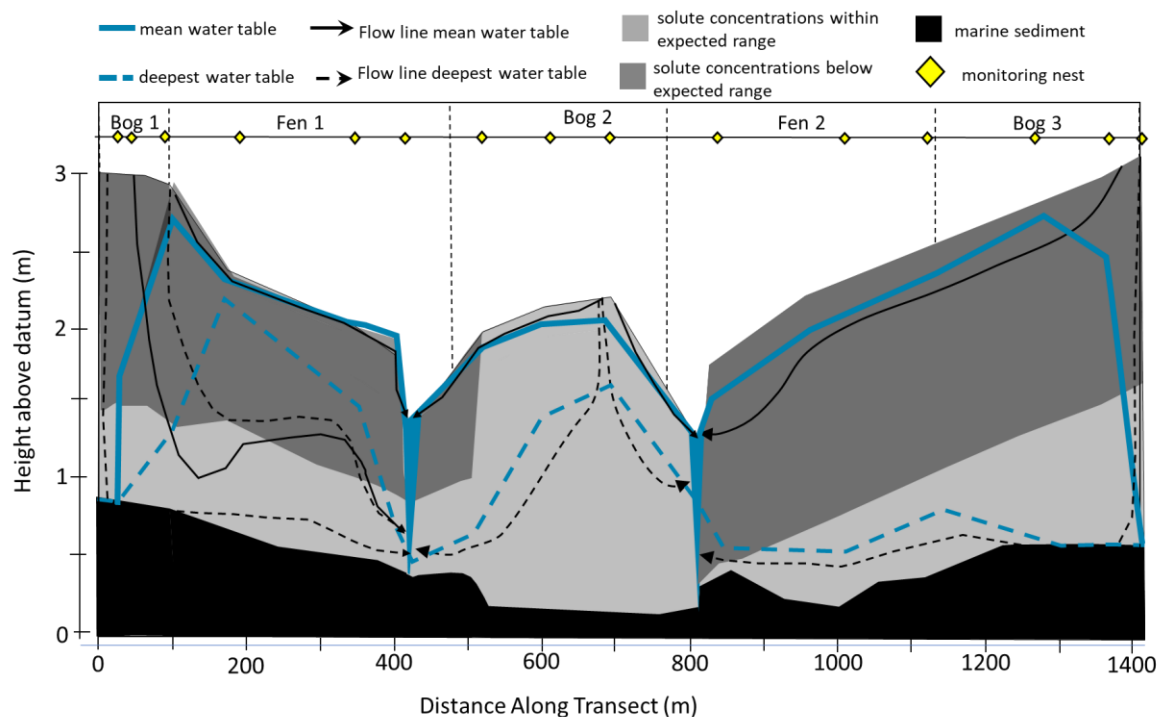
Figure 4.9. Cross-section of the Main Transect showing the average (solid blue line) and maximum (dashed blue line) water table depths as well as the conceptual flow paths (black arrows). Shaded areas indicate depth intervals in which Ca^{2+} concentrations were significantly lower than unimpacted peatlands of matching peatland class (i.e., bog or fen) for a given depth.

If depleted concentrations were measured at the 100 cm depth, shaded areas were extended to the surface where porewaters are depleted in calcium for all locations.

4.6.4 Long-term and Large-scale Implications

Over the first 6 years of dewatering, the lower water tables at the Main Transect decreased the influence of MS-derived water, as shown by significantly lower Ca^{2+} concentrations. This reduced the abundance of carbonate ions and thus the acid-neutralization capability of the near-surface porewater, creating bog-like conditions at Fen 2. In the long-term this could reduce the number of calcium-dependent species and increase the competitive advantage for calcium-intolerant *Sphagnum* mosses (Vicherová *et al.,* 2015), potentially shifting the mine-impacted landscape from fen to bog. Bogs are conceptualized as water storage features on the landscape, so the shift from fen to bog that accompanies mine dewatering may reduce lateral connectivity between adjacent peatlands and to surface water features. This could be exacerbated when combined with subsidence from dewatering, and generally lower water tables, both of which act to reduce topographical variability (Whittington & Price, 2012b, Chapter 3). Lower water tables can lead to enhanced decomposition as a consequence of the expansion of the aerobic zone. This has the potential to increase DOC production and thus carbon export, and potentially mobilize metals such as aluminum and iron which are commonly bound to the peat (Blodau, 2002; Helmer *et al.,* 1990; Moore, 1988). Long-term depletion of water storage will reduce connectivity and potentially eliminate the large areas of ponded water currently found in patterned bogs and fens. This is consistent with visual observations of dry ponds, or exposed sections of bare peat where ponds once existed within the area of mine dewatering. Downgradient, reduced connectivity may result in lower runoff, or increase water fluxes from unimpacted areas, which will lower the amount of water in storage and exacerbate peatland vulnerability to drought. Given that streamflow across the HBL has declined over the past 37 years, the combined effects of mine dewatering may have implications on long-term water availability in the region (Dery *et al.,* 2005).

The analysis here addresses an actively dewatered system, and thus represents conditions not in chemical equilibrium. In the absence of dewatering (i.e., following mine closure) it is expected that vertical gradients will gradually return to a pre-disturbance state (apart from the influence of irreversible consolidation- Chapter 3). In this case, once water tables have recovered, flowpaths between bog, fen, and tributary will re-establish, notwithstanding the irreversible consolidation, and

87

approximate undisturbed sites. The timeline associated with the return to equilibrium geochemical conditions was assessed with a one-dimensional analytical solution to the groundwater flow and transport equation (Ogata & Banks, 1961; results in Appendix C). Based exclusively on diffusion from the MS, it would take approximately 75 years for the Ca^{2+} concentrations in the impacted bogs (Bog 1 and 3) to reflect pre-disturbance conditions along the depth profile (Figure C6). However, Bog 2 did not exhibit a pronounced difference in Ca^{2+} concentration from the reference location (MOE Bog), as is expected at this location (Figure 4.9). The modelling indicates that Fen 1 and 2 would require hundreds of years to return to pre-disturbance conditions (Figure C6). Yet, unlike bogs, fens have other transport mechanisms that could bring an influx of Ca^{2+} and hasten the return to an equilibrium geochemical profile. Since lateral groundwater advection from upgradient bogs or fens is not represented in the model, the estimated time for fen Ca^{2+} concentrations to re-equilibrate may be overestimated. Nonetheless, decades or perhaps centuries will be required for pre-disturbance geochemical conditions to be re-established at peatland systems that were impacted by mine dewatering. Consequently, the duration for which the surface of fens experiences depleted nutrient conditions may be long enough to trigger (or accelerate) the transition of fens towards ombrotrophy (Hargen *et al.,* 2014). Future mining operations, such as the proposed Ring of Fire, will operate for decades and may impact larger proportions of watersheds. Thus, peatlands within the impacted area will likely be at greater risk of these long-term effects, particularly when paired with the effects of projected climate change, specifically, higher temperatures, longer summers and changing precipitation patterns in this region (IPCC, 2022).

4.7 Limitations

Due to the confounding effects of frost formation and thaw on water table depth and connectivity, only the non-frozen season was used in the analysis. In past studies, it has been shown that active drainage can occur at both bog and fen peatlands underneath the frost table, which can then influence spring and summer connectivity, when overwinter deficits are not filled (Chapter 2; Price & FitzGibbon, 1987). This will likely exacerbate the already depleted storage in the most impacted systems. Furthermore, deeper water tables resulted in lower water contents deeper in the peat profile, which is a known positive feedback mechanism for deeper frost table formation. This has the potential to alter the dynamics of seasonal ground ice formation, thaw, and the partitioning of

snowmelt across the landscape. Given the implications of seasonal ground ice on peatland storage and runoff, this should be studied further.

Due to an absence of continuous water level data directly upgradient of the fen outlets, the calculation of flux at the fen outlet was determined using hydraulic gradients between the fen and the tributary. This assumes a constant lateral hydraulic gradient between the fen outlet and the stream, which may be inaccurate. Though this may result in an overestimation of lateral fluxes the direction of flux and the relative magnitudes between the three locations are believed to be accurate for the analysis presented in this paper.

The selection of Ca^{2+} as a proxy for vertical groundwater movement, and the assessment of equilibrium post-mining must be used with caution due to the non-conservative nature of this ion. Specifically, due to the high cation exchange capacity of peat, large proportions of Ca^{2+} can bind to the surface of the peat (Sjörs, 2002; Rippy & Nelson, 2007). The presence of adsorption sites within the peat matrix may further slow the process of Ca^{2+} re-equilibration as Ca^{2+} is pulled out of solution.

Water samples in this analysis were only available until 2012, which fails to capture the long-term effects of dewatering on near-surface geochemistry. Aquifer depressurization increased from 2007-2012, so the main impacts attributable to dewatering was likely captured, however the interaction with drier seasons such as 2013 likely exacerbated the effects identified here. Groundwater sampling events were limited to the non-frozen season, however in natural peatland systems, chemistry changes little below the zone of water table fluctuation (Ulanowski, 2014; Orlova & Branfireun, 2014) due to the low gradients and hydraulic conductivity at depth. Thus, except for the solute concentration in porewater samples, the geochemical conditions reported in this study are representative of overall patterns.

4.8 Conclusions

This study has shown that over the 12 years of mine dewatering, aquifer depressurization and subsequent increases in deep seepage has disrupted both the hydrological and hydrogeochemical feedbacks within the bog and fen peatlands studied here. When compared to unimpacted bogs and fens, lateral and vertical gradients were generally steeper and water tables lower in impacted peatlands. The degree of hydrological impact was variable, and a function of both large scale (i.e., climatic variability and dewatering volume) and peatland scale (i.e., peatland type, landscape position, thickness of the underlying aquitard) processes. Bogs and fens located in areas of thin

underlying marine sediment (Bog 1, Bog 3 and Fen 2) experienced the deepest water tables and largest increases in downwards vertical gradients. This resulted in disruptions to lateral flowpaths between upgradient bogs and downgradient fens and tributaries. Bog-to-fen fluxes were elevated when compared to the unimpacted site due to the depleted water storage in impacted fens which increased lateral hydraulic gradients. In spite of this, impacted fen-to-tributary fluxes were smaller, suggesting the increased delivery of water from upgradient bogs was not sufficient to increase water tables above thresholds required for landscape connectivity. At the extreme, this resulted in the reversal of gradients between tributaries and upgradient fens, which was unobserved at the unimpacted peatland complex. An increasing disparity was observed in cumulative runoff between NNGC/NSGC and an unimpacted tributary, when normalized by catchment area, particularly during spring and early summer (May-June) where more water was entering storage in the impacted peatlands rather than being shuttled downstream.

The lowering of water tables and disruption of fluxes within impacted peatlands instigated changes to peatland geochemistry. The proportion of water derived from the underlying solute-rich marine sediment was significantly lower in impacted peatlands, as demonstrated by depleted concentrations of Ca^{2+} compared to unimpacted peatlands. Solute-depleted water from precipitation reached 150 cm bgs at the locations, which experienced the deepest water tables and most disrupted fluxes (Bog 1, Bog 3 and Fen 2). Notable decreases in pH and elevated concentrations of DOC were observed at depth, which was correlated with deeper water tables and a decreased proportion of MS derived waters. This has implications on the future development of these systems, favouring calcium-intolerant bog vegetation such as *Sphagnum* mosses, over calcium tolerant fen species.

There are a number of long-term implications on the future functioning of these systems, even when dewatering is no longer active in the mine. The deeper watertables increased oxygen availability at depth, leading to enhanced decomposition, which may have increased DOC production, carbon export, and may have mobilized metals typical bound to the peat matrix. Upon rewetting this may result in a flux of liberated compounds through the peatlands and to downgradient surface water features. As vertical gradients return to a pre-disturbance state flowpaths between bog, fen and tributary may re-establish, however due to the slow processes of upwards diffusion it may take decades or centuries for calcium concentrations to reach those previous to dewatering within the most impacted locations. This may be a long enough period to alter the ecological trajectory of these systems. Future mining operations, such as the proposed Ring of Fire, which will have a far larger

90

footprint, require greater dewatering, and are expected to operate over a longer time period could influence a much greater area of peatlands in the HBL. Peatlands within the impacted area will likely be at greater risk of long-term effects, this will only be exacerbated by the higher temperatures, longer summers and changing precipitation patterns associated with projected climate change in this region (IPCC, 2022).

4.9 Acknowledgments

Chapter 5
Conclusions

Peatlands are resilient systems, evidenced by the numerous complex hydrological and geochemical feedbacks that allow them to adapt and persist under a wide range of environmental conditions. In the peatland-dominated Hudson Bay Lowlands (HBL), water availability is highly variable across seasons and years. A series of autogenic feedbacks are thus necessary to maintain the shallow water tables required for landscape connectivity, continued peat accumulation and prevention of moisture stress in mosses at the surface. This dissertation has characterized a number of these feedbacks and their thresholds in both undisturbed and mine-dewatered (i.e., Main Transect) peatlands near the De Beers Victor Diamond Mine to gain a better understanding of the large-scale responses of these systems to anthropogenic disturbance expected in the future.

Autogenic responses to water availability were highly related to the fluctuation of the water table, which declined due to reduced water inputs (i.e., where precipitation was low or where frost prevented water from entering storage) and/or increased water losses (i.e., during high summer *ET* or where dewatering increased downwards seepage). If water availability was high, water tables were maintained above a connectivity threshold ranging from 5 to 25 cm bgs across the landscape (approximately the high transmissivity acrotelm) and excess water was shuttled downgradient and exported from the systems via the tributaries. Where water tables fell below the connectivity threshold into the lower transmissivity deeper peat, lateral water fluxes downgradient were reduced, thus limiting water losses. Where disconnection was non-uniform across the landscape (i.e., during partially frozen conditions in the spring or areas of differing MS thickness in mine impacted peatlands), lateral hydraulic gradients increased, and non-negligible fluxes were observed at depth. This acted to replenish the areas of disproportionally depleted storage until hydraulic gradients were reduced.

As water tables dropped below the near surface, an additional water preservation mechanism was initiated through the reversible consolidation of near surface peat (mire breathing), which was observed as average seasonal surface fluctuations of ~5 ±2 cm in both impacted and unimpacted peatlands. In the unimpacted peatlands, water tables were maintained at or above previously experienced depths (i.e., the effective stress remained below the pre-consolidation pressure) and the surface rebounded once water tables increased, resulting in no long-term changes in hydraulic

conductivity. Where water tables dropped below pre-consolidation thresholds, the system instead entered a period of disequilibrium. Here, consolidation continued as irreversible subsidence within the peat profile, which lowered the surface of the impacted peatlands ~15 cm and decreased saturated hydraulic conductivity at depth up to an order of magnitude. This was non-uniform across the landscape (e.g., was greater in bogs with thin underlying MS layers and in fens due to lower pre-consolidation pressures). Where hydraulic conductivity decreased, flowpaths were driven deeper into the peat profile, increasing hydraulic transit times and in some cases eliminating intermediate flowpaths which originally advected downwards and laterally under bogs and upwelled at adjacent fens, instead upwelling further downgradient at the tributaries.

Where autogenic feedbacks prevented large water table drops (i.e., at the unimpacted peatlands and where MS was thick at the Main Transect), porewater geochemistry measured at depth ($\geq$100 cm bgs) did not vary significantly across seasons or years. The concentration of Ca^{2+} at these unimpacted sites was a function of position along the bog-fen-tributary flowpaths. Solute poor precipitation-sourced waters advected downwards under the bogs, mixed with decomposition products and solute rich waters at depth from MS derived solutes, then upwelled at downgradient fens. In areas of consistently depleted water storage (i.e., at the north and south portions of the Main Transect), Ca^{2+} concentrations were comparatively diluted at depth. This was due to the increased downwards migration of solute poor precipitation-sourced waters, and the repressed upwards advection of solute-rich waters due to strong downwards hydraulic gradients and altered flowpaths. Both acted to reduce the amount of solute rich water reaching the downgradient fens, and resultantly bog-like surface Ca^{2+} concentrations and pH were observed in the most impacted fen at the Main Transect. Increased concentrations of DOC were also observed within the areas of deepest water tables, likely due to the increased presence of oxygen in the typically anoxic zone, which can enhance decomposition.

It is clear in most of the mine-impacted peatlands that water losses related to dewatering prompted long term feedbacks which resulted in irreversible changes to peat structure, reduction of lateral water transfer along the bog-fen-tributary pathway, depleted water storage, and alterations to peatland geochemistry. It is important to note that while periodic desiccation and drying of the surface was observed in the field, large scale moss death and ecosystem collapse was not. It may be that if conditions observed here continued over a prolonged period these impacted peatlands would be driven towards a new equilibrium state. With reduced water transfer and lower water tables, there may be a reduction in microtopography as species at topographical extremes are outcompeted by

those more resilient to water table fluctuations. A general shift from fens, which require higher water tables, upgradient water inputs, and more solute rich water, to bogs, which are hydrologically disconnected and adapted to lower water tables, could be possible. Alternatively, water tables may deepen enough to accelerate decomposition within the thicker peat deposits and naturally lower water tables in bogs, favoring shallower peat systems. Post de-watering, re-establishment of peatland equilibrium would also be varied. The time for water table recovery would likely be short (1-5 years), largely due to large inflow of water during spring freshet, provided water is able to enter peatland storage (i.e., snow melt occurs after frost thaw). Water table response may be flashier where subsidence occurred, however, due to lower specific yields associated with a shift to smaller pore sizes, prompting more periods of hydrologic disconnection where water availability becomes limited. Bog-fen-tributary connectivity may also be reduced due to the deepening of flowpaths related to peat subsidence and reduced lateral conductivity. Geochemically, the deeper flowpaths within impacted peatlands combined with the slow nature of upwards solute diffusion from the underlying MS would result in a decadal to centurial timeline for the re-establishment of non-conservative solute concentrations such as Ca^{2+}. This slow recovery of Ca^{2+} may alter the ecological trajectory of these systems towards ombrotrophic bogs even in the absence of active dewatering and the maintenance of high water table conditions. Many of the same changes as those from dewatering have been projected to occur during climate warming scenarios, where water availability will be reduced due to hotter temperatures and higher evapotranspiration and may result in lesser water availability in this region in the coming decades. It is currently unknown how these systems will equilibrate; this will likely depend on the shift in precipitation patterns in this region as well as the changes in spring temperature, which have been shown to regulate entrance of snowmelt into peatland storage.

Though the lifespan of the De Beers Victor mine was relatively short, there is an increasing push to 'open the North' to resource extraction operations and development projects. The most prominent extraction operation is the Ring of Fire (RoF), a ~5000 km^2 deposit of mineable minerals, including but not limited to copper, zinc, nickel, vanadium, chromite, and gold, located at the western limits of the HBL (Ontario Chamber of Commerce, 2014). There are a number of unique challenges when attempting to apply lessons learned from this research to this potential development. Most obvious is the sheer difference in size between operations; the De Beers mine is approximately 1/1000th the size of the RoF. This discrepancy alludes to a much larger radius of impact associated with dewatering. This is of particular importance for downgradient tributaries; while only 15% of the North Granny

Creek catchment in this study was within the radius of dewatering (Leclair *et al.,* 2015), entire catchments and/or significant portions of headwaters may be within the zone of influence within RoF operations. Contrastingly, the RoF is located at the intersection of the Canadian Shield and the Hudson Bay Lowland, where the Shield may have a lower hydraulic conductivity than that in marine sediment. This difference may better protect overlying peatlands from dewatering effects than the MS layer studied here. Even so, climate change effects must be considered cumulatively with the anticipated dewatering for this much larger mining operation. Greater temperature fluctuations and longer unfrozen periods projected in the HBL region in the future will likely result in increased *AET*, more years with snowmelt and frost thaw desynchronization, and greater drainage of peatlands to the tributary during shoulder seasons. Future research should focus on applying the responses to resource extraction and climate change related disturbance here to different locations and scales of peatland complexes to better understand the cumulative effects of these anthropogenic disturbances on the trajectory of these systems. As the peatlands of the HBL represent one of the largest storages of solid carbon globally and could become large carbon sources to the atmosphere if disturbed, it is not an overstatement to suggest the collapse of these systems would have significant consequences on the trajectory the earth's climate.

References

AMEC (2008) *Request for Permits to Take Water and Certificate of Approval to allow Full Scale, Well Field Dewatering of the Bedrock Aquifer for Open Pit Mining* [report]

Anderson, A. R., Pyatt, D. G., Sayers, J. M., Blackhall, S. R., & Robinson, H. D. (1992). Volume and mass budgets of blanket peat in the north of Scotland. *Suo*, *43*, 195-198.

Balliston, N. E., McCarter, C. P. R., & Price, J. S. (2018). Microtopographical and hydrophysical controls on subsurface flow and solute transport: A continuous solute release experiment in a subarctic bog. *Hydrological Processes*, *32*(19), 2963-2975.

Balliston, N. E., & Price, J. S. (2020). Heterogeneity of the peat profile and its role in unsaturated sodium chloride rise at field and laboratory scales. *Vadose Zone Journal, 19*(1), e20015.

Batzer, D. P., & Baldwin, A. H. (Eds.). (2012). *Wetland habitats of North America: ecology and conservation concerns*. Univ of California Press.

Beckwith, C. W., & Baird, A. J. (2001). Effect of biogenic gas bubbles on water flow through poorly decomposed blanket peat. *Water Resources Research, 37*(3), 551-558.

Beckwith, C. W., Baird, A. J., & Heathwaite, A. L. (2003a). Anisotropy and depth-related heterogeneity of hydraulic conductivity in a bog peat. I: laboratory measurements. *Hydrological Processes, 17*(1), 89-101.

Beckwith, C. W., Baird, A. J., & Heathwaite, A. L. (2003b). Anisotropy and depth-related heterogeneity of hydraulic conductivity in a bog peat. II: modelling the effects on groundwater flow. *Hydrological Processes, 17*(1), 103-113.

Belyea, L. R., & Clymo, R. S. (2001). Feedback control of the rate of peat formation. Proceedings of the Royal Society of London. *Series B: Biological Sciences, 268*(1473), 1315-1321.

Berry, P. L., & Poskitt, T. J. (1972). The consolidation of peat. *Geotechnique*, *22*(1), 27-52.

Blodau, C. (2002). Carbon cycling in peatlands A review of processes and controls. *Environmental Reviews, 10*(2), 111-134.

Bourbonniere, R. A. (2009). Review of water chemistry research in natural and disturbed peatlands. *Canadian Water Resources Journal, 34*(4), 393-414.

Canadian Environmental Assessment Agency (2005). *Victor Diamond Project Comprehensive Study Report.* Ottawa, Ontario: Canadian Environmental Assessment Agency, www.ceaa. gc.ca/80C30413-docs/report_e.pdf

Chanton, J. P., Bauer, J. E., Glaser, P. A., Siegel, D. I., Kelley, C. A., Tyler, S. C., ... & Lazrus, A. (1995). Radiocarbon evidence for the substrates supporting methane formation within northern Minnesota peatlands. *Geochimica et Cosmochimica Acta, 59*(17), 3663-3668.

Chapuis, R. P., & Sabourin, L. (1989). Effects of installation of piezometers and wells on groundwater characteristics and measurements. *Canadian Geotechnical Journal, 26(*4), 604-613.

Chong (2014). *Resource Development in Canada: A Case Study on the Ring of Fire*. Library of Parliament, Economics, Resources and International Affairs Division. https://epe.lac-bac.gc.ca/100/201/301/weekly_checklist/2014/internet/w14-26-U-E.html/collections/collection_2014/bdp-lop/bp/2014-17-eng.pdf

Chow, T. L., Rees, H. W., Ghanem, I., & Cormier, R. (1992). Compactability of cultivated Sphagnum peat material and its influence on hydrologic characteristics. *Soil Science, 153*(4), 300-306.

Clymo, R. S. (1984). The limits to peat bog growth. *Philosophical Transactions of the Royal Society of London. B, Biological Sciences, 303*(1117), 605-654.

Connon, R. F., Quinton, W. L., Craig, J. R., Hanisch, J., & Sonnentag, O. (2015). The hydrology of interconnected bog complexes in discontinuous permafrost terrains. *Hydrological Processes, 29*(18), 3831-3847.

Das, B., & Sobhan, K., (2014). Principles of Geotechnical Engineering 8th Ed. Instructor, 201601. Cengage Learning.

Déry, S. J., Stieglitz, M., McKenna, E. C., & Wood, E. F. (2005). Characteristics and trends of river discharge into Hudson, James, and Ungava Bays, 1964–2000. *Journal of Climate, 18*(14), 2540-2557.

Difebo, A., Richardson, M., & Price, J. (2015). Fusion of multi-spectral imagery and LIDAR digital terrain derivatives for ecosystem mapping and morphological characterization of a northern peatland complex. *Remote Sensing of Wetlands: Applications and Advances*. CRC Press Inc, Boca Raton, FL.

Emili, L. A., & Price, J. S. (2006). Hydrological processes controlling ground and surface water flow from a hypermaritime forest–peatland complex, Diana Lake Provincial Park, British Columbia, Canada. *Hydrological Processes, 20*(13), 2819-2837.

Eppinga, M. B., Rietkerk, M., Belyea, L. R., Nilsson, M. B., Ruiter, P. C. D., & Wassen, M. J. (2010). Resource contrast in patterned peatlands increases along a climatic gradient. *Ecology, 91*(8), 2344-2355.

Environment Canada. (2020a). Canadian climate normals 1971-2010: Moosonee. Retrieved November 2, 2020 from http://www.climate.weatheroffice.gc.ca/climate_normals/

Environment Canada. (2020b). Canadian climate normals 1971-2010: Lansdowne House. Retrieved November 2, 2020 from http://www.climate.weatheroffice.gc.ca/climate_normals/

Fitzgerald, D. F., Price, J. S., & Gibson, J. J. (2003). Hillslope-swamp interactions and flow pathways in a hypermaritime rainforest, British Columbia. *Hydrological Processes, 17*(15), 3005-3022.

Foster, D. R., & King, G. A. (1984). Landscape features, vegetation and developmental history of a patterned fen in south-eastern Labrador, Canada. The Journal of Ecology, *72*, 115-143.

Fox, P. J., & Edil, T. B. (1996). Effects of stress and temperature on secondary compression of peat. *Canadian Geotechnical Journal, 33*(3), 405-415.

Fraser, C. J. D., Roulet, N. T., & Lafleur, M. (2001). Groundwater flow patterns in a large peatland. *Journal of Hydrology, 246*(1-4), 142-154.

Fritz, C. (2006). *Surface oscillation in peatlands: How variable and important is it?* [Doctoral dissertation, The University of Waikato].

Gharedaghloo, B., Price, J. S., Rezanezhad, F., & Quinton, W. L. (2018). Evaluating the hydraulic and transport properties of peat soil using pore network modeling and X-ray micro computed tomography. *Journal of Hydrology*, *561*, 494-508.

Glaser, P. H. (1989). Detecting biotic and hydrogeochemical processes in large peat basins with Landsat TM imagery. *Remote Sensing of Environment, 28*, 109-119.

Glaser, P. H., Siegel, D. I., Romanowicz, E. A., & Shen, Y. P. (1997). Regional linkages between raised bogs and the climate, groundwater, and landscape of north-western Minnesota. *Journal of Ecology,* 3-16.

Glaser, P. H., Siegel, D. I., Reeve, A. S., Janssens, J. A., & Janecky, D. R. (2004a). Tectonic drivers for vegetation patterning and landscape evolution in the Albany River region of the Hudson Bay Lowlands. *Journal of Ecology, 92*(6), 1054–1070.

Glaser, P. H., Hansen, B. C., Siegel, D. I., Reeve, A. S., & Morin, P. J. (2004b). Rates, pathways and drivers for peatland development in the Hudson Bay Lowlands, northern Ontario, Canada. J*ournal of Ecology, 92*(6), 1036-1053.

Gofar, N., & Sutejo, Y. (2007). Long term compression behavior of fibrous peat. *Malaysian Journal of Civil Engineering, 19*(2).

Goodbrand, A., Westbrook, C. J., & van der Kamp, G. (2019). Hydrological functions of a peatland in a Boreal Plains catchment. *Hydrological Processes, 33*(4), 562-574.

Harris, L. I., Roulet, N. T., & Moore, T. R. (2020). Mechanisms for the development of microform patterns in peatlands of the Hudson Bay Lowland. *Ecosystems, 23*(4), 741-767.

Gorham, E., Eisenreich, S. J., Ford, J., & Santelmann, M. V. (1985). Chemistry of bog waters. *Chemical processes in lakes* (pp. 339-362). John Wiley and Sons.

Hargan, K. E., Rühland, K. M., Paterson, A. M., Holmquist, J., MacDonald, G. M., Bunbury, J., ... & Smol, J. P. (2015). Long-term successional changes in peatlands of the Hudson Bay Lowlands, Canada inferred from the ecological dynamics of multiple proxies. *The Holocene, 25*(1), 92-107.

Hart, D. J., Bradbury, K. R., & Gotkowitz, M. B. (2008). Is one an upper limit for natural hydraulic gradients? *Groundwater, 46*(4), 518-520.

Hayward, P. M., & Clymo, R. S. (1982). Profiles of water content and pore size in Sphagnum and peat, and their relation to peat bog ecology. *Proceedings of the Royal Society of London. Series B. Biological Sciences, 215*(1200), 299-325.

HCI, (2004). *Dewatering of Victor Diamond Project Predicted Engineering, Cost, and Environmental Factors. Addendum I: Update of Ground-Water FlowModel Utilzing New Surface-Water Chemistry and Flow Data from Nayshkootayaow River and Results of Sensitivity Analysis.* [report]

Helbig, M., Humphreys, E. R., & Todd, A. (2019). Contrasting temperature sensitivity of CO2 exchange in peatlands of the Hudson Bay Lowlands, Canada. Journal of Geophysical Research: *Biogeosciences, 124*(7), 2126-2143.

Helmer, E. H., Urban, N. R., & Eisenreich, S. J. (1990). Aluminum geochemistry in peatland waters. *Biogeochemistry, 9*(3), 247-276.

Hilbert, D. W., Roulet, N., & Moore, T. (2000). Modelling and analysis of peatlands as dynamical systems. *Journal of Ecology, 88*(2), 230-242.

Hobbs, N. B. (1986). Mire morphology and the properties and behaviour of some British and foreign peats. *Quarterly Journal of Engineering Geology and Hydrogeology, 19*(1), 7-80.

Howie, S. A., & Hebda, R. J. (2018). Bog surface oscillation (mire breathing): A useful measure in raised bog restoration. *Hydrological Processes, 32*(11), 1518-1530.

Humphreys, E. R., Charron, C., Brown, M., & Jones, R. (2014). Two bogs in the Canadian Hudson Bay Lowlands and a temperate bog reveal similar annual net ecosystem exchange of CO2. *Arctic, Antarctic, and Alpine Research, 46*(1), 103-113.

Hvorslev, M. J. (1951). *Time lag and soil permeability in ground-water observations* (No. 36). Waterways Experiment Station, Corps of Engineers, US Army.

Ingram, H. A. P. (1978). Soil layers in mires: function and terminology. *Journal of Soil Science, 29*(2), 224-227.

Ingram (1983). Hydrology. *Ecosystems of the World 4A: Moores: Swamp, bog, fen and moor*, Gore AJP (ed), Elsevier Scientific, Amsterdam

International Panel on Climate Change(2013) *The Physical Science Basis. Contribution of Working Group I to the Fifth Assessment Report of the Intergovernmental Panel on Climate Change*. Edited by

Stocker TF, Qin D, Plattner G-K, Tignor M, Allen SK, Boschung J, Nauels A, Xia Y, Bex V, Midgley PM. Cambridge University Press, Cambridge, UK and New York, NY, USA, 2013. 1535.

IPCC, (2022). *Climate Change 2022: Impacts, Adaptation, and Vulnerability. Contribution of Working Group II to the Sixth Assessment Report of the Intergovernmental Panel on Climate Change* Edited by Pörtner, H.O.,. Roberts D.C, Tignor, M., Poloczanska E.S, Mintenbeck K., Alegría A., Craig M., Langsdorf S.,. Löschke S, Möller V., Okem A., Rama B.. Cambridge University Press. In Press.

Itasca Denver. (2016) *De Beers Group of Companies Inc. Victor Update of the Victor Integrated Groundwater Flow Model as per condition 4.1.5 permit to take water* #1810-99FHAD (or amended). Department E (ed.).

Itasca Denver, Inc. (2017) *Update of the Victor Groundwater Flow Model Based on 2016 Hydrogeologic Data* [Technical Memorandum]

Kellner, E., & Halldin, S. (2002). Water budget and surface-layer water storage in a Sphagnum bog in central Sweden. *Hydrological Processes, 16*(1), 87-103.

Kennedy, G. W., & Price, J. S. (2005). A conceptual model of volume-change controls on the hydrology of cutover peats. *Journal of Hydrology, 302*(1-4), 13-27.

Keller, J. K., White, J. R., Bridgham, S. D., & Pastor, J. (2004). Climate change effects on carbon and nitrogen mineralization in peatlands through changes in soil quality. *Global Change Biology, 10*(7), 1053-1064.

Khalafzai, M. A. K., McGee, T. K., & Parlee, B. (2019). Flooding in the James Bay region of Northern Ontario, Canada: Learning from traditional knowledge of Kashechewan First Nation. *International Journal of Disaster Risk Reduction, 36*, 101100.

Lafleur, P. M., & Roulet, N. T. (1992). A comparison of evaporation rates from two fens of the Hudson Bay Lowland. Aquatic Botany, 44(1), 59-69.

Leclair, M. (2015). The hydrological interactions within a mine impacted peatland, James Bay Lowland, Canada [Master's thesis, University of Waterloo]. UWSpace.

Leclair, M., Whittington, P., & Price, J. (2015). Hydrological functions of a mine-impacted and natural peatland-dominated watershed, James Bay Lowland. *Journal of Hydrology: Regional Studies, 4*, 732-747.

Lee, H. A. (1959). *Surficial Geology of Southern District of Keewatin: And the Keewatin Ice Divide, Northwest Territories*. Queen's printer.

Liu, H., Price, J., Rezanezhad, F., & Lennartz, B. (2020). Centennial-scale shifts in hydrophysical properties of peat induced by drainage. *Water Resources Research, 56*(10), e2020WR027538.

Loisel, J., Gallego-Sala, A. V., Amesbury, M. J., Magnan, G., Anshari, G., Beilman, D. W., ... & Wu, J. (2021). Expert assessment of future vulnerability of the global peatland carbon sink. *Nature climate change, 11*(1), 70-77.

Long, A. J., & Valder, J. F. (2011). Multivariate analyses with end-member mixing to characterize groundwater flow: Wind Cave and associated aquifers. *Journal of Hydrology, 409*(1-2), 315-327.

Martini, I. P. (1981). Morphology and sediments of the emergent Ontario coast of James Bay, Canada. Geografiska Annaler: Series A, *Physical Geography, 63*(1-2), 81-94.

Mathur, S. P., & Levesque, M. (1985). Negative effect of depth on saturated hydraulic conductivity of histosols. *Soil science, 140*(6), 462-466.

McCarter, C. P., & Price, J. S. (2017). Experimental hydrological forcing to illustrate water flow processes of a subarctic ladder fen peatland. *Hydrological Processes, 31*(8), 1578-1589.

McDonald, B. C. (1969). Glacial and interglacial stratigraphy, Hudson Bay lowlands. *Geological Survey of Canada Paper, 68*(53), 78-99.

Moore, T. R. (1987). Thermal regime of peatlands in subarctic eastern Canada. *Canadian Journal of Earth Sciences, 24*(7), 1352-1359.

Moore, T. R. (1988). Dissolved iron and organic matter in northern peatlands. *Soil Science, 145*(1), 70-76.

Moore, T. R., & Knowles, R. (1990). Methane emissions from fen, bog and swamp peatlands in Quebec. *Biogeochemistry, 11*(1), 45-61.

Moore, P. A., Morris, P. J., & Waddington, J. M. (2015). Multi-decadal water table manipulation alters peatland hydraulic structure and moisture retention. *Hydrological Processes, 29*(13), 2970-2982.

Morris, P. J., Baird, A. J., Eades, P. A., & Surridge, B. W. (2019). Controls on near-surface hydraulic conductivity in a raised bog. *Water Resources Research, 55*(2), 1531-1543.

National Wetlands Working Group (1997) *The Canadian Wetland Classification System* (2nd Edition) University of Waterloo, Waterloo, ON

Nelson, F. E., Outcalt, S. I., Goodwin, C. W., & Hinkel, K. M. (1985). Diurnal thermal regime in a peat-covered palsa, Toolik Lake, Alaska. *Arctic*, *38*(4), 310-315.

Ng, S. Y., & Eischens, G. R. (1983). Repeated short-term consolidation of peats. *Testing of peats and organic soils*. ASTM International.

Ogata, A., & Banks, R. B. (1961). *A solution of the differential equation of longitudinal dispersion in porous media: fluid movement in earth materials*. US Government Printing Office.

Oleszczuk, R., Szatylowicz, J., Brandyk, T., & Gnatowski, T. (2000). An analysis of the influence of shrinkage on water retention characteristics of fen peat-moorsh soil. *Suo, 51*(3), 139-147.

Ontario Chamber of Commerce (2014). *Beneath the Surface: Uncovering the Economic Potential of Ontario's Ring of Fire.* ISBN PDF: 978-1-928052-02-9.

Oosterwoud, M., van der Ploeg, M., van der Schaaf, S., & van der Zee, S. (2017). Variation in hydrologic connectivity as a result of microtopography explained by discharge to catchment size relationship. *Hydrological Processes, 31*(15), 2683–2699.

Orlova, J., & Branfireun, B. A. (2014). Surface water and groundwater contributions to streamflow in the James Bay Lowland, Canada. *Arctic, Antarctic, and Alpine Research, 46*(1), 236-250.

Perras, E. (2016). Hydrological and geochemical implications of aquifer depressurization on expansive peatland systems in the Hudson/James Bay Lowlands [Master's thesis, University of Waterloo). UWSpace.

Price, J.S. (1987). The influence of wetland and mineral terrain types on snowmelt runoff in the subarctic. *Canadian Water Resources Journal. 2*(2), 43 52.

Price, J.S. (1994). Patterned Peatlands. *Canadian Geographer, 38*, 363-367.

Price, J. (1996). Soil moisture, water tension, and water table relationships in a managed cutover bog. *Journal of Hydrology, 202*(1-4), 21-32.

Price, J. S. (2003). Role and character of seasonal peat soil deformation on the hydrology of undisturbed and cutover peatlands. *Water Resources Research, 39*(9).

Price, J.S., and FitzGibbon, J.E., (1987). Groundwater storage and stream¬flow in a subarctic wetland, Saskatchewan. *Canadian Journal of Earth Sciences*, *24*(10), 2074 2081.

Price, J. S., Maloney, D. A., & Downey, F. G. (1991). Peatlands of the Lake Melville coastal plain, Labrador. In Northern Hydrology: Selected Perspectives *Proceedings of the Northern Hydrology Symposium* (No. 6, pp. 293-302).

Price, J., & Maloney, D. (1994). Hydrology of a patterned bog-fen complex in southeastern Labrador, *Canada. Nordic Hydrology, 25*(5), 313–330.

Price, J. S., & Schlotzhauer, S. M. (1999). Importance of shrinkage and compression in determining water storage changes in peat: the case of a mined peatland. *Hydrological Processes, 13*(16), 2591-2601.

Price, J. S., & Woo, M. K. (1988a). Origin of salt in coastal marshes of Hudson and James bays. *Canadian Journal of Earth Sciences, 25*(1), 145-147.

Price, J. S., & Woo, M. K. (1988b). Studies of a subarctic coastal marsh, I. Hydrology. *Journal of Hydrology, 103*(3-4), 275-292.

Price, J. S., & Woo, M. K. (1988c). Studies of a subarctic coastal marsh, II. Salinity. *Journal of Hydrology, 103*(3-4), 293-307.

Price, J. S., Woo, M. K., & Maxwell, B. (1989). Salinity of marshes along the James Bay coast, Ontario, Canada. *Physical Geography, 10*(1), 1-12.

Price, J. S., Cagampan, J., & Kellner, E. (2005). Assessment of peat compressibility: is there an easy way?. *Hydrological Processes, 19*(17), 3469-3475.

Priestley, C. H. B., & Taylor, R. J. (1972). On the assessment of surface heat flux and evaporation using large-scale parameters. *Monthly weather review, 100*(2), 81-92.

Quinton, W. L., Hayashi, M., & Pietroniro, A. (2003). Connectivity and storage functions of channel fens and flat bogs in northern basins. *Hydrological Processes, 17*(18), 3665–3684.

Quinton, W. L., & Roulet, N. T. (1998). Spring and summer runoff hydrology of a subarctic patterned wetland. *Arctic and Alpine Research, 30*(3), 285-294.

Reeve, A. S., Siegel, D. I., & Glaser, P. H. (1996). Geochemical controls on peatland pore water from the Hudson Bay Lowland: A multivariate statistical approach. *Journal of Hydrology, 181*(1-4), 285-304.

Reeve, A. S., Siegel, D. I., & Glaser, P. H. (2000). Simulating vertical flow in large peatlands. *Journal of Hydrology, 227*(1-4), 207-217.

Reeve, A. S., Siegel, D. I., & Glaser, P. H. (2001). Simulating dispersive mixing in large peatlands. *Journal of Hydrology, 242*(1-2), 103-114.

Rezanezhad, F., Price, J. S., Quinton, W. L., Lennartz, B., Milojevic, T., & Van Cappellen, P. (2016). Structure of peat soils and implications for water storage, flow and solute transport: A review update for geochemists. *Chemical Geology, 429*, 75-84.

Richardson, M., Ketcheson, S., Whittington, P., & Price, J. (2012). The influences of catchment geomorphology and scale on runoff generation in a northern peatland complex. *Hydrological Processes, 26*(12), 1805–1817.

Riley, J. L (2011) *Wetlands of the Hudson Bay Lowland: A Regional Overview*, Nature Conservancy of Canada, Toronto, Ontario

Rippy, J. F., & Nelson, P. V. (2007). Cation exchange capacity and base saturation variation among Alberta, Canada, moss peats. *HortScience, 42*(2), 349-352.

Rochefort, L., & Lode, E. (2006). Restoration of degraded boreal peatlands. *Boreal peatland ecosystems* (pp. 381-423). Springer, Berlin, Heidelberg.

Roulet, N. T. (1991). Surface level and water table fluctuations in a subarctic fen. *Arctic and Alpine Research, 23*(3), 303-310.

Rouse, W. R., Woo, M. K., & Price, J. S. (1992). Damming James Bay: I. Potential impacts on coastal climate and the water balance. *Canadian Geographer, 36*(1), 2-7.

Schothorst, C. J. (1977). Subsidence of low moor peat soils in the western Netherlands. *Geoderma, 17*(4), 265-291.

Shotyk, W. (1988). Review of the inorganic geochemistry of peats and peatland waters. *Earth-Science Reviews, 25*(2), 95-176.

Siegel, D. I. (1983). Ground water and the evolution of patterned mires, Glacial Lake Agassiz peatlands, northern Minnesota. *The Journal of Ecology*, 913-921.

Siegel, D. I., & Glaser, P. H. (1987). Groundwater flow in a bog-fen complex, lost river peatland, northern Minnesota. *The Journal of Ecology, 75*, 743–754.

Siegel, D. I., & Glaser, P. (2006). The hydrology of peatlands. *Boreal Peatland Ecosystems, 188*, 289–311.

Singer, S. N., and Cheng, C. K., (2002) *An assessment of the groundwater resources of northern Ontario: areas draining into Hudson Bay, James Bay and Upper Ottawa River.* Toronto: Ontario Ministry of the Environment, Environmental Monitoring and Reporting Branch, Hydrogeology of Ontario Series (Report 2).

Sjörs, H. (1963). *Bogs and fens on Attawapiskat River, northern Ontario* (pp. 45-133). Roger Duhanel, Queen's Printer.

Sjörs, H., & Gunnarsson, U. (2002). Calcium and pH in north and central Swedish mire waters. *Journal of Ecology*, *90*(4), 650-657.

Spence, C., & Woo, M. K. (2003). Hydrology of subarctic Canadian shield: Soil-filled valleys. *Journal of Hydrology, 279*(1-4), 151-166.

Spence, C., Guan, X. J., & Phillips, R. (2011). The hydrological functions of a boreal wetland. *Wetlands, 31*(1), 75-85.

Streich, S. C., & Westbrook, C. J. (2020). Hydrological function of a mountain fen at low elevation under dry conditions. *Hydrological Processes, 34*(2), 244-257.

Teatini, P., Putti, Mgambolati, G. Ferraris, S., & Camporese, M. (2004). Reversible/irreversible peat surface displacements and hydrological regime in the Zennare Basin, Venice. *Scientific Research and Safeguarding of Venice (CORILA Research Program 2001–2003, 2002 Results)*, 93-106.

Tfaily, M. M., Wilson, R. M., Cooper, W. T., Kostka, J. E., Hanson, P., & Chanton, J. P. (2018). Vertical stratification of peat pore water dissolved organic matter composition in a peat bog in northern Minnesota. *Journal of Geophysical Research: Biogeosciences, 123*(2), 479-494.

Todd, A., & Humphreys, E. (2018a). *AmeriFlux CA-ARF Attawapiskat River Fen*. Lawrence Berkeley National Lab.(LBNL), Berkeley, CA (United States). AmeriFlux; Carleton University; Ministry of Environment and Climate Change.

Todd, A., & Humphreys, E. (2018b). *AmeriFlux CA-ARB Attawapiskat River Bog*. Lawrence Berkeley National Lab.(LBNL), Berkeley, CA (United States). AmeriFlux; Carleton University; Ministry of Environment and Climate Change.

Ulanowski, T. A. (2014). *Hydrology and biogeochemistry of a bog-fen-tributary complex in the Hudson Bay Lowlands, Ontario, Canada*. [Master's Thesis: University of Western Ontario]. Electronic Thesis and Dissertation Repository.

Ulanowski, T. A., & Branfireun, B. A. (2013). Small-scale variability in peatland pore-water biogeochemistry, Hudson Bay Lowland, Canada. *Science of the Total Environment, 454*, 211-218.

Urban, N. R., Bayley, S. E., & Eisenreich, S. J. (1989). Export of dissolved organic carbon and acidity from peatlands. *Water Resources Research, 25*(7), 1619-1628.

Van Huizen, B., Sutton, O. F., Price, J. S., & Petrone, R. M. (2022). Assessing the importance of bi-directional melting when modeling boreal peatland freeze/thaw dynamics. *Journal of Hydrology, 604*, 127236.

Vicherová, E., Hájek, M., & Hájek, T. (2015). Calcium intolerance of fen mosses: physiological evidence, effects of nutrient availability and successional drivers. *Perspectives in Plant Ecology, Evolution and Systematics, 17*(5), 347-359.

Vitt, D. H. (1994). An overview of factors that influence the development of Canadian peatlands. *The Memoirs of the Entomological Society of Canada, 126*(S169), 7-20.

Vitt, D. H., Halsey, L. A., Bray, J., & Kinser, A. (2003). Patterns of bryophyte richness in a complex boreal landscape: identifying key habitats at McClelland Lake wetland. *The Bryologist, 106*(3), 372-382.

Waddington, J. M., Kellner, E., Strack, M., & Price, J. S. (2010). Differential peat deformation, compressibility, and water storage between peatland microforms: Implications for ecosystem function and development. *Water Resources Research, 46*(7).

Wells, C., Ketcheson, S., & Price, J. (2017). Hydrology of a wetland-dominated headwater basin in the Boreal Plain, Alberta, Canada. *Journal of Hydrology, 547*, 168-183.

Whittington, P., & Price, J. (2012a). Effect of mine dewatering on peatlands of the James Bay Lowland: the role of bioherms. *Hydrological Processes, 26*(12), 1818-1826.

Whittington, P., & Price, J. S. (2012b). Effect of mine dewatering on the peatlands of the James Bay Lowland: the role of marine sediments on mitigating peatland drainage. *Hydrological Processes*, *27*(13), 1845-1853.

Whittington, P. (2013). The impacts of diamond mining to Peatlands in the James Bay Lowlands. [Doctoral thesis: University of Waterloo]. UWSpace.

Whittington, P., & Price, J. S. (2013). Effect of mine dewatering on the peatlands of the James Bay Lowland: the role of marine sediments on mitigating peatland drainage. *Hydrological Processes, 27*(13), 1845-1853.

Whittington, P. N., & Price, J. S. (2006). The effects of water table draw-down (as a surrogate for climate change) on the hydrology of a fen peatland, Canada. *Hydrological Processes, 20*(17), 3589-3600.

Whittington, P., Ketcheson, S., Price, J., Richardson, M., & Di Febo, A. (2012). Areal differentiation of snow accumulation and melt between peatland types in the James Bay Lowland. *Hydrological Processes, 26*(17), 2663-2671.

Whittington, P., & Price, J. (2012). Effect of mine dewatering on peatlands of the James Bay Lowland: the role of bioherms. *Hydrological Processes, 26*(12), 1818-1826.

Whittington, P., & Price, J. S. (2013). Effect of mine dewatering on the peatlands of the James Bay Lowland: the role of marine sediments on mitigating peatland drainage. *Hydrological Processes, 27*(13), 1845-1853.

Woo, M. K. (1986). Permafrost hydrology in North America. *Atmosphere-Ocean, 24*(3), 201-234.

Wright, N., Hayashi, M., & Quinton, W. L. (2009). Spatial and temporal variations in active layer thawing and their implication on runoff generation in peat-covered permafrost terrain. *Water Resources Research, 45*(5).

Zeitz, J. (1991) Untersuchungen über Filtrationseigenshaften von Niedermoorböden mit Hilfe verschiedener Methoden unter Berücksichtigung der Bodenentwicklung Z.Kultertechnik Landetw. *32*, 227-234

Zeitz, J., & Velty, S. (2002). Soil properties of drained and rewetted fen soils. *Journal of Plant Nutrition and Soil Science, 165*(5), 618-626.

Zoltai, S. C., & Vitt, D. H. (1995). Canadian wetlands: environmental gradients and classification. *Vegetation, 118*(1), 131-137.

Appendices

Appendix A

Chapter 2 Supplementary Information
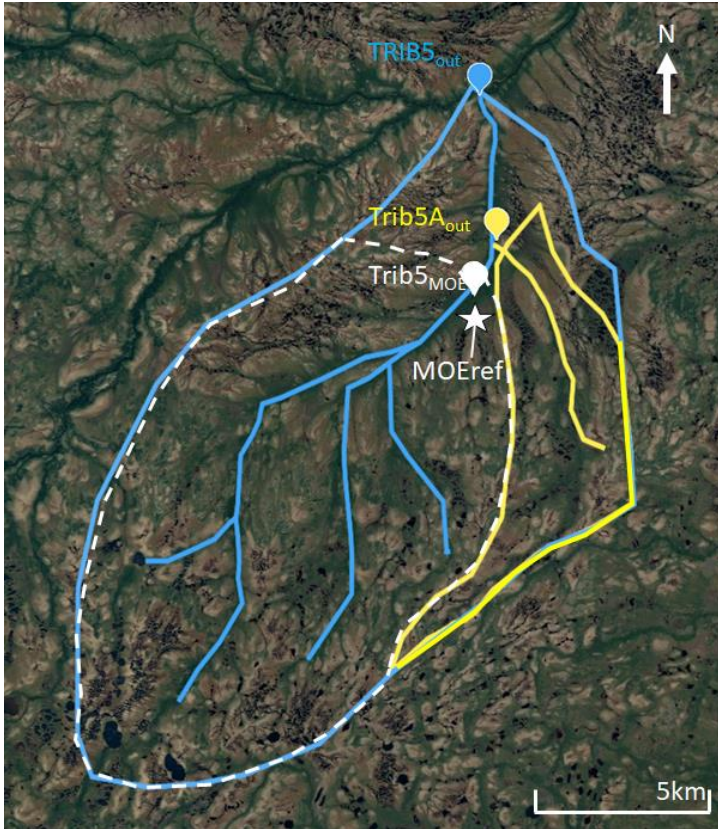
Figure A1. Stage and or/streamflow measurement gauges (balloons) and their corresponding catchment areas (dashed and solid lines of corresponding colours). The location of the MOE study site is also shown (white star).

Unused well	Closest Used well	r²	Line of best fit
B200	BD	0.78	y=1.0221x-1.44
B400	BO	0.87	y=1.5193x+9.08
F000	FI	0.92	y=1.0519x+3.7
F080S	FI	0.98	y=0.8872+10.5
F450S	FI	0.99	y=0.954x+11.1
F650S	FU	0.94	y=1.08x+7.8
F500N	FO	0.81	y=0.9029x+1.8
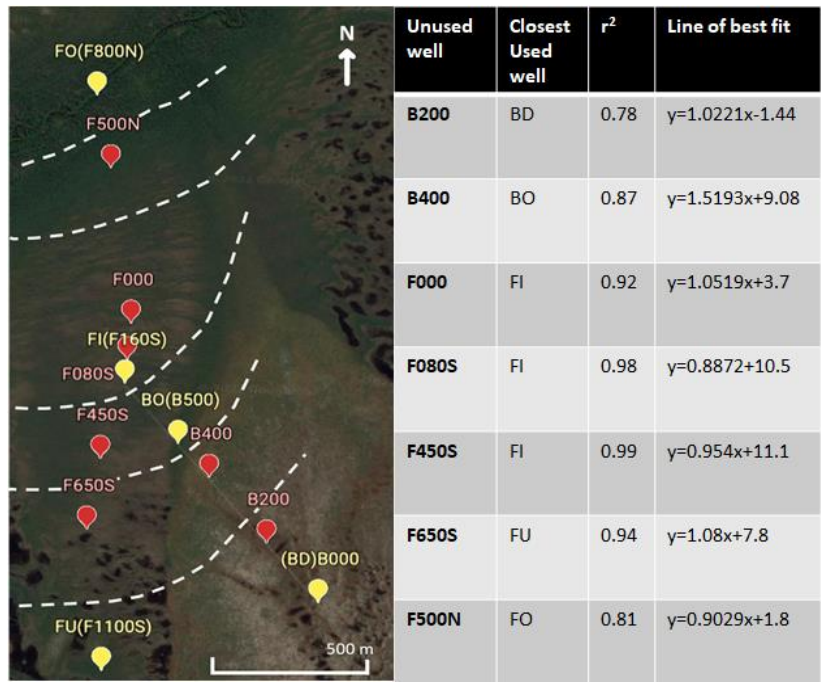
Figure A2. Location of the 13 wells instumented along the study site (left), including the five selected to reprent the main landscape units (yellow) and the eight that were not (red). Regressions were conducted between the used and unused wells to ensure selected wells adequately captured water level fluctuations across the landscape units (right).
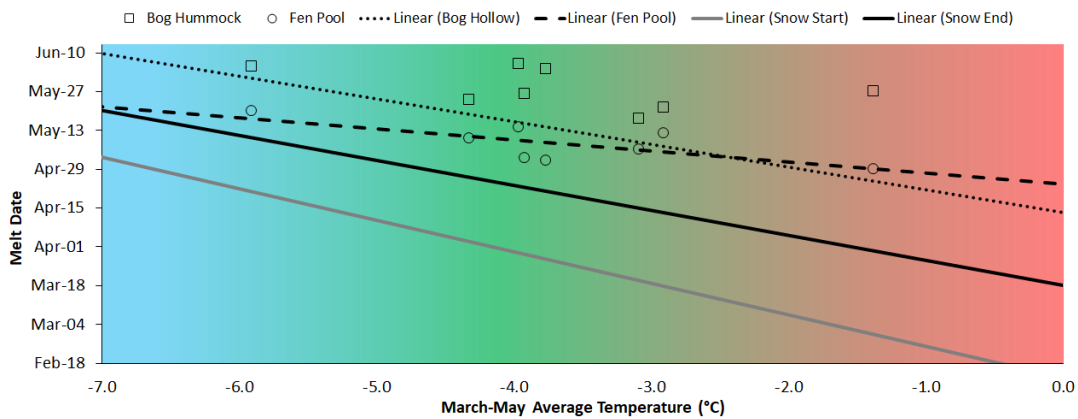
Figure A3. Regression lines of best fit (points not shown) of the relationship between March-May average temperature and bog hollow frost thaw, fen pool frost thaw, and snow melt start and end (solid and dashed lines). Data points show the bog hummock frost thaw date and fen ridge frost thaw

data, which did not have a significant correlation with temperature. The blue, green and red shaded areas indicated March-May temperatures which are below, average, and above average, respectively.
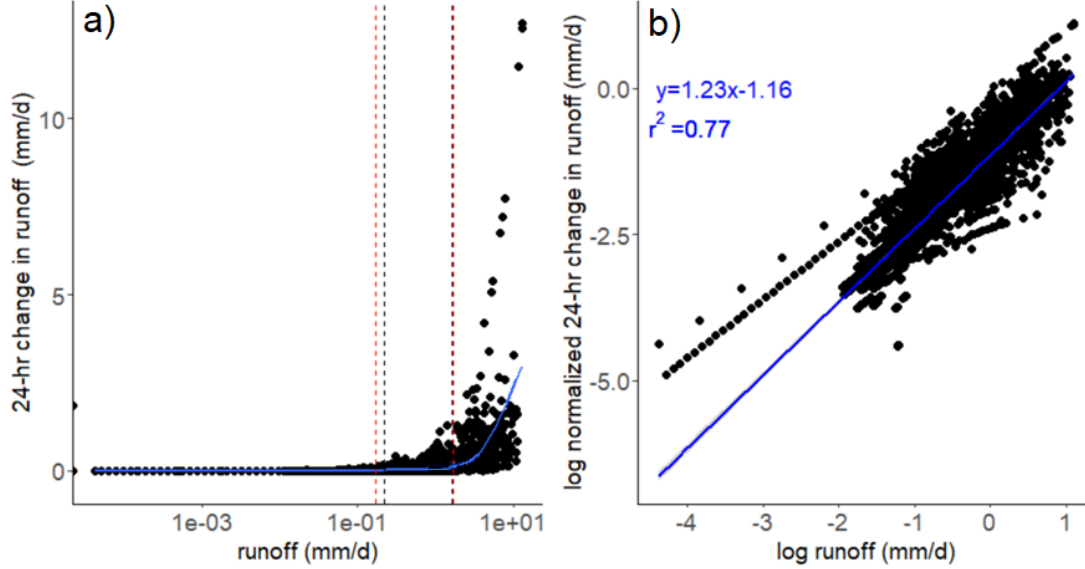
Figure A4. 24-hour runoff change at Trib5out as a function of daily runoff (a) and log-log plot of the same variables (b) fitted with a straight line representing a power function (blue) for values above the disconnection threshold. Black dashed lines indicate the disconnected/connected (0.20 mm/ day) and connected/ high activity (1.5 mm/ day) thresholds developed at this location, while red dashed lines indicate thresholds developed at Trib5MOE.

Table A1: Regression outputs for MOEref monitoring wells against Victor Mine monitoring wells (all p<0.01) The bolded r2 value represents the dataset selected for fitting.

		Victor Mine Monitoring Wells			
		Bog Dome	**Bog Outlet**	**Fen down**	**Fen upper**
MOEref Monitoring Wells	**Bog Dome**	**0.78**	0.76	-	-
	Bog Outlet	0.74	**0.76**	-	-
	Fen Inlet	-	-	**0.94**	0.85
	Fen Upper	-	-	0.85	**0.90**
	Fen Outlet	-	-	**0.87**	0.71

Appendix B

Chapter 3 Supplementary Information
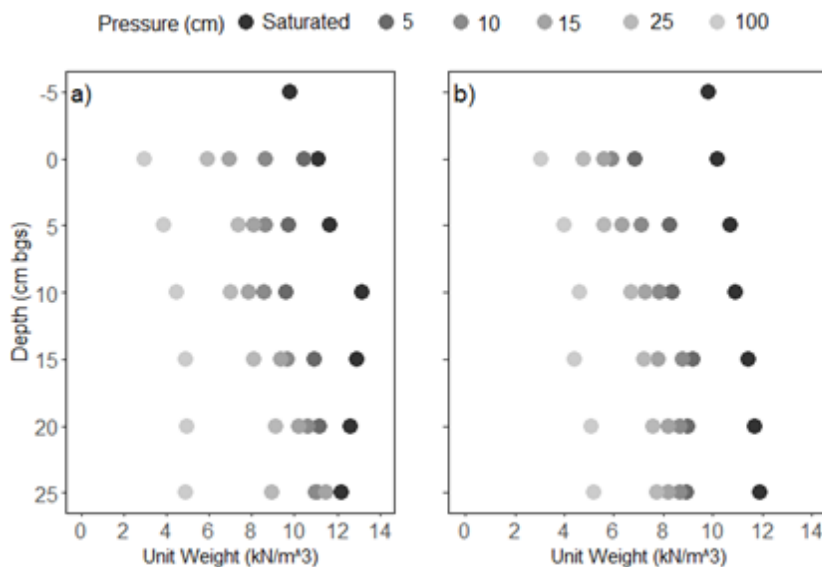
Figure B1. Unit weights for soil at varying negative pressures (i.e., heights above water table) for a) fen soil and b) bog soil. Each point represents the average of 12 (10 cm diameter, 5 cm height centered at the indicated depth) peat samples (6 from ridge/ hummock and 6 from pool/hollow). Retention analysis was used to estimate moisture content for a given pressure (i.e., equivalent height above water table (cm), which was converted to unit weight using peat particle density. given pressure (i.e. equivalent height above water table (cm)), which was converted to unit weight using peat particle density.
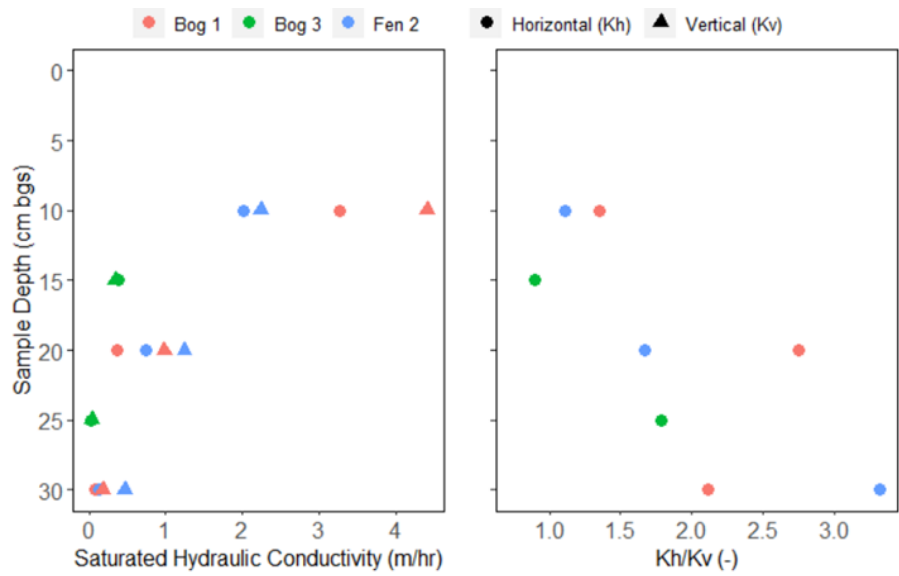
Figure B2. Laboratory measured acrotelm Ksat and anisotropy by depth and by peatland type. Samples (10 cm diameter, 5 cm height centered at the indicated depth) were collected during the summer of 2012.
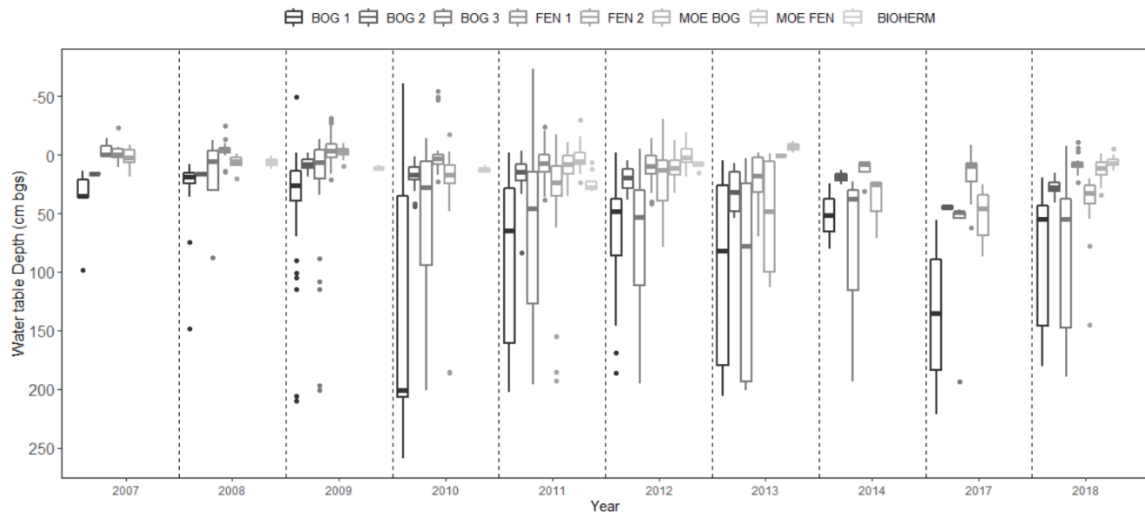
Figure B3. Water table depth (WTD) box and whisker plots for all peatlands for each year in the monitoring period (2007-2018).
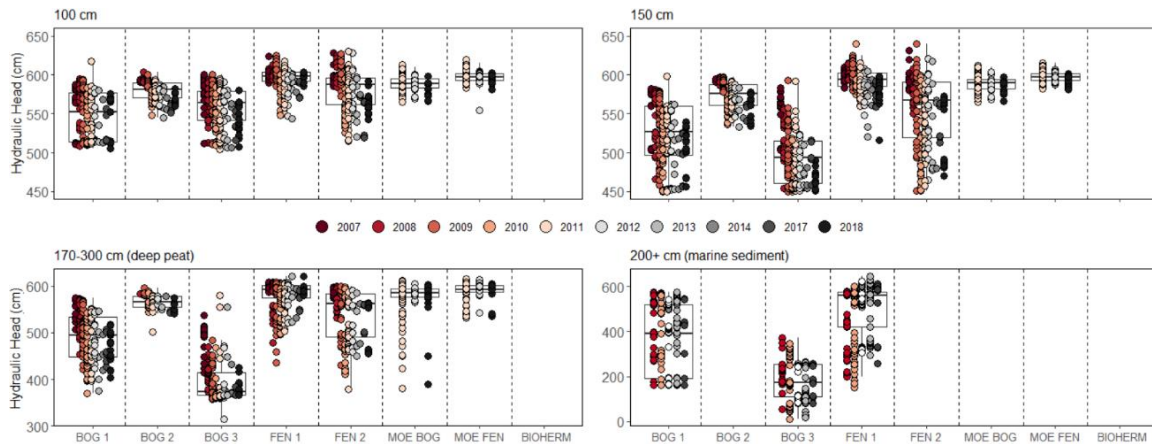
Figure B4. Piezometer hydraulic head measurements (points) and distributions (boxplots) at the a) 100 cm, b) 150 cm, c) deep peat and d) MS piezometers over site- specific monitoring periods. Letters indicate where distributions are not significantly different for overlapping monitoring periods. Note: Hydraulic head is relative to a datum at each monitoring location, and thus is used for vertical comparisons only and not lateral flow between peatlands. A datum of 600 cm bgs was used at each monitoring nest to calculate hydraulic head within each piezometer, to account for differences in screen depth along the peat profile.
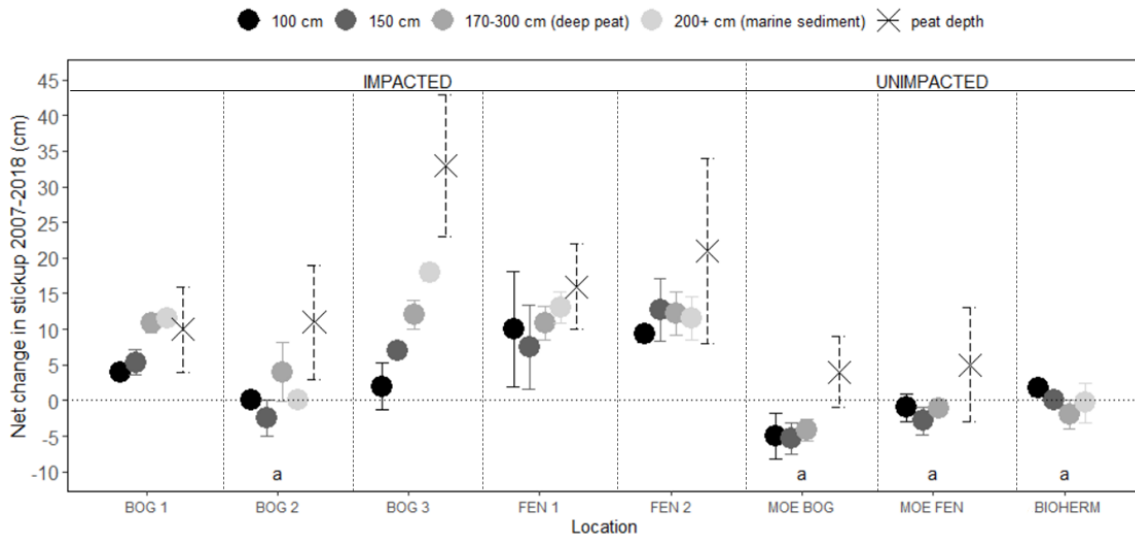
Figure B5. Net change in stickup between 2007 and 2018 by depth (circles) calculated using equations derived from lines of best fit (Table B1), and changes in peat depth (X's) measured at the

112

beginning and end of monitoring periods. The letter "a" (above peatland labels) indicates changes which are not significantly different between peatlands at any depth.

Before dewatering:
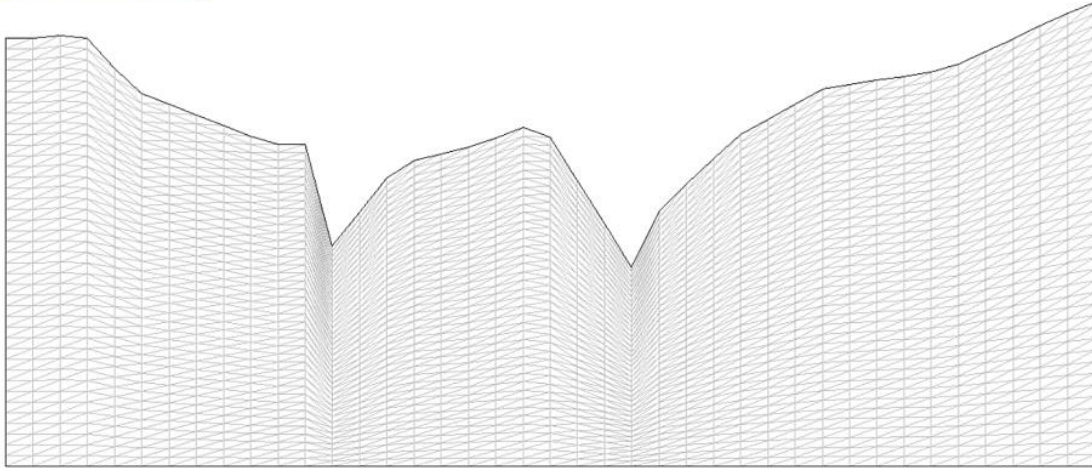
After dewatering:
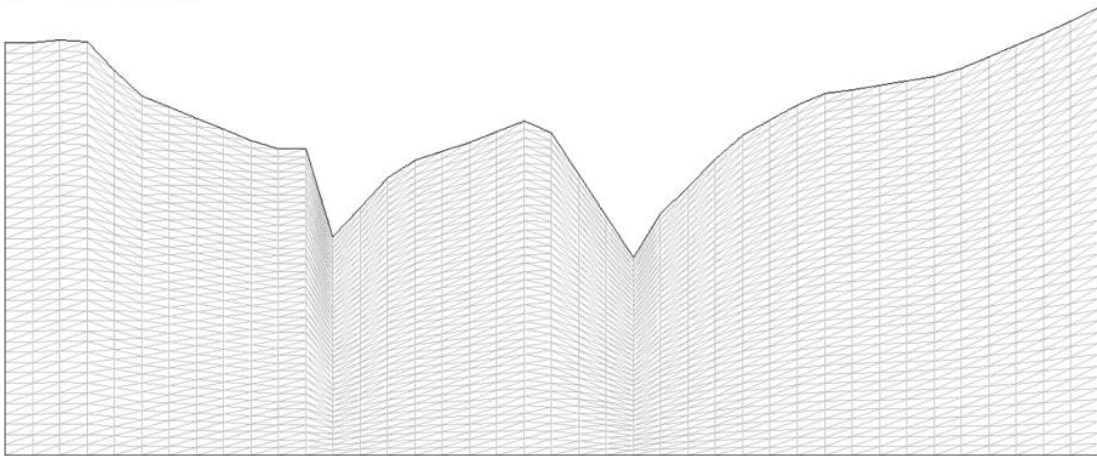
Figure B6. Model discretization for the Main Transect before (top) and after (bottom) subsidence using USGS Topodrive software.
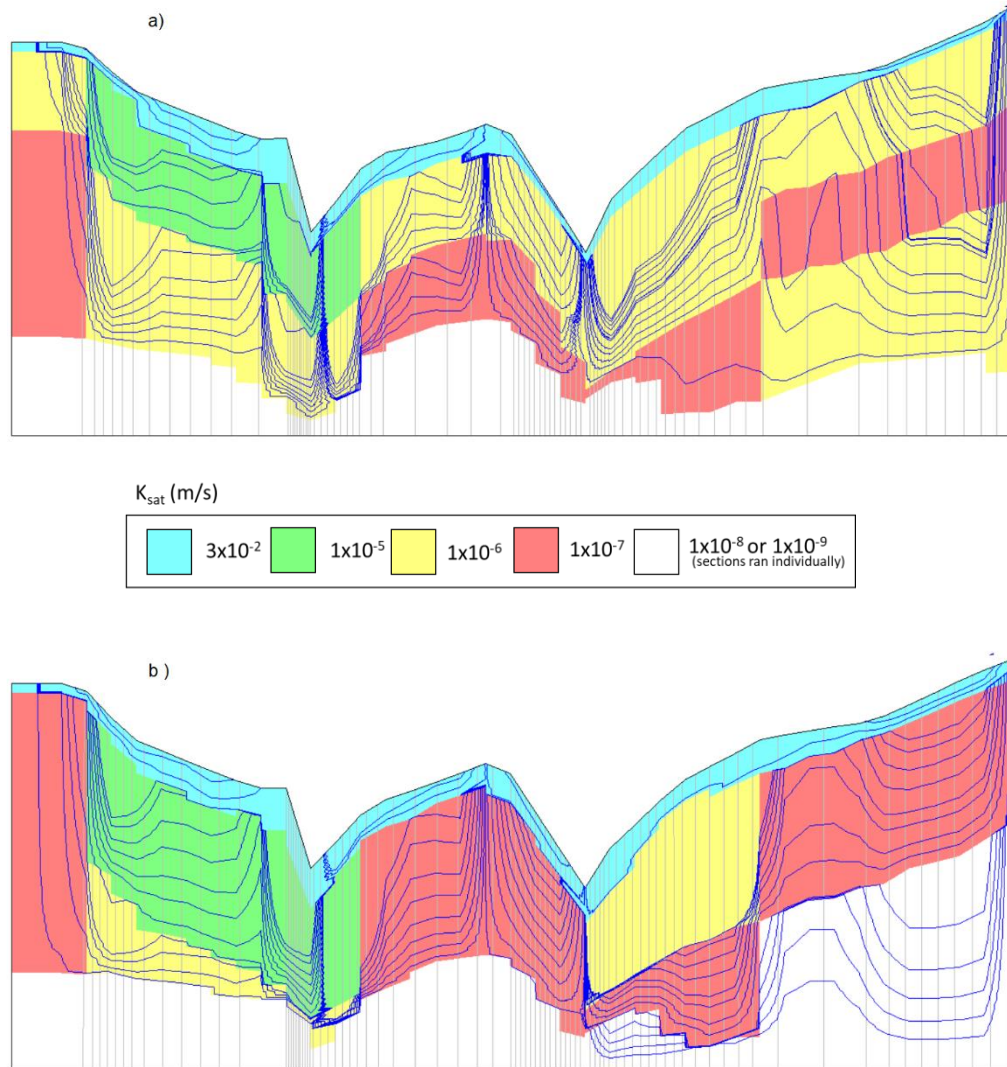
Figure B7. Topodrive model output for a) pre-subsidence and b) post-subsidence ground surface elevations and lateral hydraulic conductivity values. An anisotropic ratio of 2 was assumed for the top 30 cm and 5 below, Blue lines indicate flowpaths, while coloured bars indicate differing layers of hydraulic conductivity (m/s).
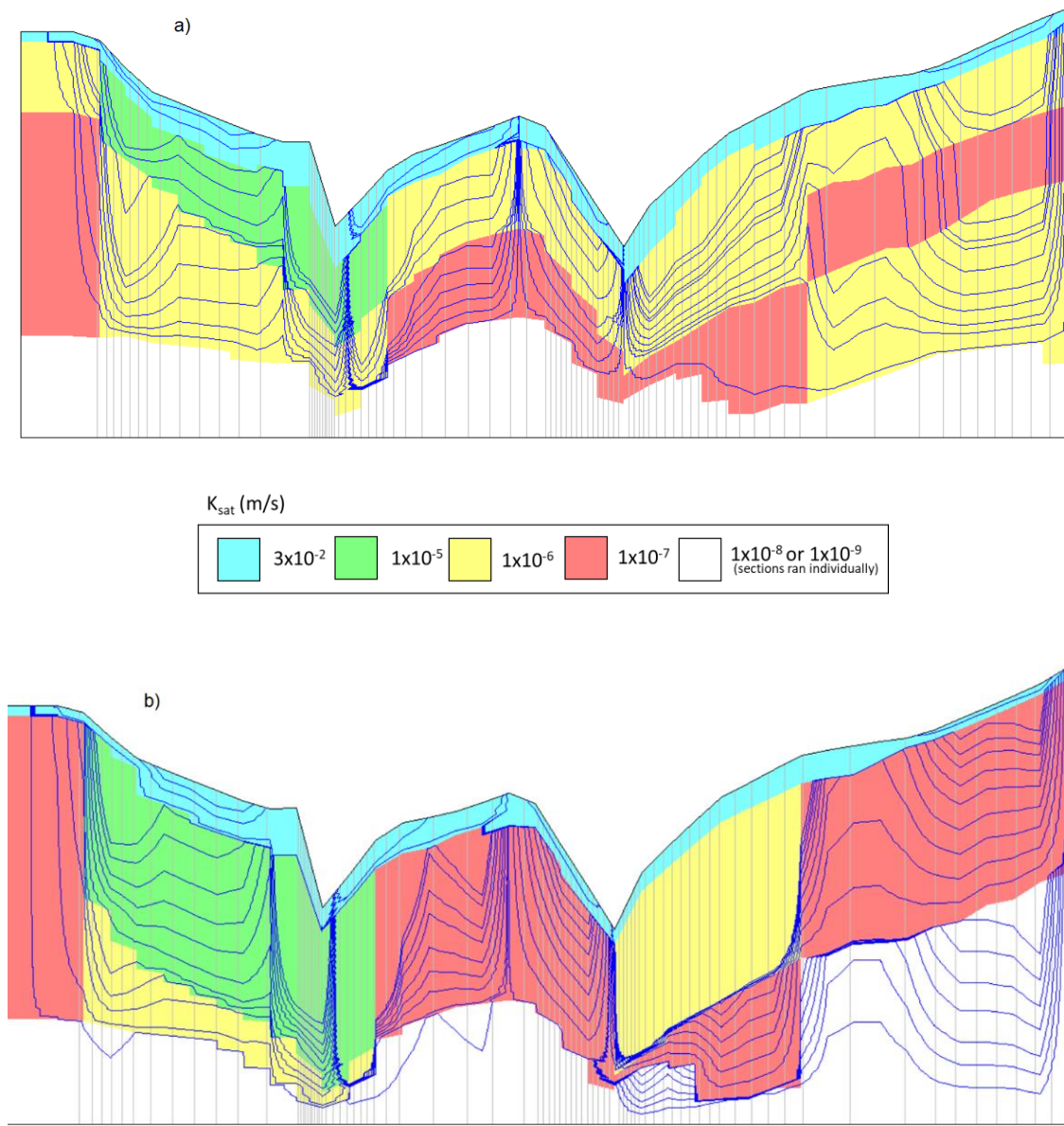
Figure B8. Topodrive model output scenarios a) post subsidence ground surface elevations and pre-subsidence lateral hydraulic conductivity values, and b) pre-subsidence ground surface elevations and post subsidence hydraulic conductivity values. An anisotropic ratio of 2 was assumed for the top 30 cm and 5 below, Blue lines indicate flowpaths, while coloured bars indicate differing layers of hydraulic conductivity (m/s).

Table B1. Monitoring period and number of monitoring events each year at the Main Transect, MOEref, and Bioherm Bog.

Year	Main Transect		MOEref		Bioherm Bog	
	Monitoring Period	Monitoring events (k tests)	Monitoring Period	Monitoring events (k tests)	Monitoring Period	Monitoring events (k tests)
2007	Aug-Oct	5(5)	-	-	-	-
2008	May-Oct	10(3)	-	-	May-Oct	3
2009	Jun- Oct	9 (3)	-	-	Jun- Oct	4(3)
2010	May -Aug	13(1)	-	-	May -Aug	9(1)
2011	May -Oct	18(1)	May -Oct	14 (2)	May -Oct	10(1)
2012	May-Aug	4 (1)	May-Aug	8	May-Aug	5
2013	Jun-Aug	2	-	-	-	-
2014	Aug	1	-	-	-	-
2017	Aug	1(1)	-	-	-	-
2018	Jun-Aug	5(2)	Jun-Aug	2 (2)	-	-

Table B2. Summary of regression results for the changes in stickup (cm; y) over time (days;x) for all monitoring nests, including the number of monitoring events (n). Where results were statistically significant for linear or polynomial regressions the r2, p value and associated equation are provided. Monitoring intervals are shown in Table B1.

Site	Nest	Depth (cm bgs)	Number of Monitoring Events (n)	r^2	p	Equation of Best Fit	Direction of Change
BOG 1	45	100	66	na	na	na	stable
BOG 1	65	100	69	0.7	<0.01	$y = -4.52 \times 10^{-7}x^2 + 3.85 \times 10^{-2}x - 7.86 \times 10^2$	increasing
BOG 1	100	100	71	0.4	<0.01	$y = -2.03 \times 10^{-7}x^2 + 1.78 \times 10^{-2}x - 3.47 \times 10^2$	increasing
BOG 1	45	150	69	0.7	<0.01	$y = 1.96 \times 10^{-3}x - 4.16 \times 10^1$	increasing
BOG 1	65	150	71	0.5	<0.01	$y = 1.41 \times 10^{-3}x - 2.56 \times 10^1$	increasing
BOG 1	100	150	71	0.2	<0.01	$y = -3.71 \times 10^{-7}x^2 + 3.12 \times 10^{-2}x - 6.2 \times 10^2$	increasing
BOG 1	45	DEEP PEAT	123	0.9	<0.01	$y = -1.25 \times 10^{-6}x^2 + 1.06 \times 10^{-1}x - 2.20 \times 10^3$	increasing

116

BOG 1	65	DEEP PEAT	201	0.7	<0.01	$y = -1.03 \times 10^{-6}x^2 + 8.77 \times 10^{-2}x - 1.83 \times 10^3$	increasing
BOG 1	100	DEEP PEAT	189	0.2	<0.01	$y = -4.59 \times 10^{-7}x^2 + 3.86 \times 10^{-2}x - 7.69 \times 10^2$	increasing
BOG 2	645	100	69	na	na	na	increasing
BOG 2	735	100	56	na	na	na	increasing
BOG 2	645	150	69	na	na	na	stable
BOG 2	735	150	56	0.8	<0.01	$y = -1.21 \times 10^{-6}x^2 + 9.84 \times 10^{-2}x - 1.99 \times 10^3$	decreasing
BOG 2	735	DEEP PEAT	112	0.3	<0.01	$y = 1.21 \times 10^{-6}x^2 - 9.80 \times 10^{-2}x + 2.04 \times 10^3$	increasing
BOG 3	1295	100	71	0.3	<0.01	$y = -4.95 \times 10^{-7}x^2 + 3.91 \times 10^{-2}x - 7.4 \times 10^2$	decreasing
BOG 3	1445	100	71	0.6	<0.01	$y = -5.31 \times 10^{-7}x^2 + 4.6 \times 10^{-2}x - 9.58 \times 10^2$	increasing
BOG 3	1485	100	71	0.2	<0.01	$y = 7.33 \times 10^{-4}x + 5.26 \times 10^0$	increasing
BOG 3	1295	150	73	na	na	na	increasing
BOG 3	1445	150	72	0.3	<0.01	$y = 1.7 \times 10^{-3}x - 3.08 \times 10^1$	increasing
BOG 3	1485	150	72	0.2	<0.01	$y = -56 \times 10^{-7}x^2 + 4.75 \times 10^{-2}x - 9.63 \times 10^2$	increasing
BOG 3	1295	DEEP PEAT	131	0.8	<0.01	$y = -1.62 \times 10^{-6}x^2 + 1.38 \times 10^{-1}x - 2.89 \times 10^3$	increasing
BOG 3	1445	DEEP PEAT	124	0.8	<0.01	$y = -1.53 \times 10^{-6}x^2 + 1.31 \times 10^{-1}x - 2.78 \times 10^3$	increasing
BOG 3	1485	DEEP PEAT	193	0.7	<0.01	$y = -1.88 \times 10^{-6}x^2 + 1.59 \times 10^{-1}x - 3.31 \times 10^3$	increasing
FEN 1	180	100	71	0.7	<0.01	$y = 3.52 \times 10^{-3}x - 1.1 \times 10^2$	increasing
FEN 1	365	100	71	0.1	0.01	$y = -8.0 \times 10^{-4}x + 4.70 \times 10^1$	decreasing
FEN 1	430	100	71	0.9	<0.01	$y = -1.44 \times 10^{-6}x^2 + 1.27 \times 10^{-1}x - 2.72 \times 10^3$	increasing
FEN 1	540	100	69	0.1	<0.01	$y = -1.30 \times 10^{-3}x + 6.95 \times 10^1$	decreasing
FEN 1	180	150	69	0.5	<0.01	$y = 3.85 \times 10^{-3}x - 1.14 \times 10^2$	increasing
FEN 1	365	150	70	0.1	0.01	$y = -5.11 \times 10^{-7}x^2 + 4.21 \times 10^{-2}x - 8.24 \times 10^2$	decreasing
FEN 1	430	150	72	0.8	<0.01	$y = 5.07 \times 10^{-3}x - 1.57 \times 10^2$	increasing
FEN 1	540	150	72	0.5	<0.01	$y = -1.30 \times 10^{-3}x + 6.95 \times 10^1$	decreasing
FEN 1	180	DEEP PEAT	189	0.5	<0.01	$y = 2.6 \times 10^{-3}x - 5.64 \times 10^1$	increasing
FEN 1	365	DEEP PEAT	194	0.6	<0.01	$y = -4.26 \times 10^{-7}x^2 + 3.73 \times 10^{-2}x - 7.52 \times 10^2$	increasing
FEN 1	430	DEEP PEAT	125	0.7	<0.01	$y = -1.19 \times 10^{-6}x^2 + 1.03 \times 10^{-1}x - 2.14 \times 10^3$	increasing
FEN 1	540	DEEP PEAT	187	0.3	<0.01	$y = 9.46 \times 10^{-7}x^2 - 7.64 \times 10^{-2}x + 1.57 \times 10^3$	increasing
FEN 2	875	100	72	0.1	<0.01	$y = -3.44 \times 10^1x + 1.73 \times 10^{-3}$	increasing
FEN 2	1005	100	72	0.4	<0.01	$y = -1.07 \times 10^{-6}x^2 + 9.05 \times 10^{-2}x - 1.88 \times 10^3$	increasing
FEN 2	1130	100	72	0.9	<0.01	$y = -7.78 \times 10^{-3}x - 2.71 \times 10^2$	increasing
FEN 2	875	150	72	0.2	<0.01	$y = -3.00 \times 10^{-7}x^2 + 2.93 \times 10^{-2}x - 5.87 \times 10^2$	increasing
FEN 2	1005	150	72	0.1	<0.01	$y = -3.33 \times 10^{-7}x^2 + 2.84 \times 10^{-2}x - 5.63 \times 10^2$	increasing
FEN 2	1130	150	72	0.5	<0.01	$y = 3.88 \times 10^{-3}x - 1.16 \times 10^2$	increasing

FEN 2	1005	DEEP PEAT	244	0.5	<0.01	$y = -1.16 \times 10^{-6}x^2 + 9.80 \times 10^{-2}x - 2.02 \times 10^3$	increasing
FEN 2	1130	DEEP PEAT	189	0.7	<0.01	$y = -2.24 \times 10^{-6}x^2 + 1.91 \times 10^{-1}x - 4.00 \times 10^3$	increasing
MOE BOG	0	100	20	na	na	na	
MOE BOG	100	100	21	0.4	<0.01	$y = -1.83 \times 10^{-3}x + 1.23 \times 10^2$	decreasing
MOE BOG	200	100	20	0.4	<0.01	$y = -1.65 \times 10^{-3}x + 1.15 \times 10^2$	decreasing
MOE BOG	300	100	20	na	na	na	stable
MOE BOG	400	100	19	0.8	<0.01	$y = -1.97 \times 10^{-3}x + 1.25 \times 10^2$	decreasing
MOE BOG	500	100	19	0.9	<0.01	$y = -7.50 \times 10^{-3}x + 3.56 \times 10^2$	decreasing
MOE BOG	0	150	20	na	na	na	
MOE BOG	100	150	21	0.6	<0.01	$y = 1.9 \times 10^{-6}x^2 - 1.63 \times 10^{-1}x + 3.56 \times 10^3$	decreasing
MOE BOG	200	150	20	0.6	<0.01	$y = -3.89 \times 10^{-3}x + 2.12 \times 10^2$	decreasing
MOE BOG	300	150	20	0.3	0.01	$y = -1.03 \times 10^{-3}x + 9.18 \times 10^2$	decreasing
MOE BOG	400	150	19	0.5	<0.01	$y = -9.77 \times 10^{-4}x + 8.74 \times 10^2$	decreasing
MOE BOG	500	150	19	0.8	<0.01	$y = -3.35 \times 10^{-3}x + 1.87 \times 10^2$	decreasing
MOE BOG	100	DEEP PEAT	48	na	na	na	decreasing
MOE BOG	200	DEEP PEAT	45	0.6	<0.01	$y = -3.45 \times 10^{-3}x + 2.00 \times 10^2$	decreasing
MOE BOG	300	DEEP PEAT	47	0.4	<0.01	$y = -7.91 \times 10^{-3}x + 8.60 \times 10^2$	decreasing
MOE BOG	400	DEEP PEAT	44	0.6	<0.01	$y = -9.49 \times 10^{-7}x^2 + 7.93 \times 10^{-2}x - 1.60 \times 10^3$	decreasing
MOE BOG	500	DEEP PEAT	50	0.9	<0.01	$y = -2.62 \times 10^{-6}x^2 + 2.17 \times 10^{-1}x - 4.44 \times 10^3$	decreasing
MOE FEN	0	100	22	na	na	na	stable
MOE FEN	80S	100	20	0.5	<0.01	$y = 1.57 \times 10^{-6}x^2 - 1.35 \times 10^{-1}x + 2.95 \times 10^3$	decreasing
MOE FEN	160S	100	20	na	na	na	stable
MOE FEN	650S	100	11	0.9	<0.01	$y = -3.36 \times 10^{-3}x + 1.85 \times 10^2$	decreasing
MOE FEN	1100S	100	10	na	na	na	stable
MOE FEN	500N	100	21	0.8	<0.01	$y = -2.61 \times 10^{-6}x^2 + 2.16 \times 10^{-1}x - 4.4 \times 10^3$	decreasing
MOE FEN	800N	100	17	na	na	na	stable
MOE FEN	0	150	21	na	na	na	stable
MOE FEN	80S	150	21	0.7	<0.01	$y = -2.16 \times 10^{-6}x^2 + 1.78 \times 10^{-1}x - 3.62 \times 10^3$	decreasing
MOE FEN	160S	150	20	na	na	na	increasing
MOE FEN	450S	150	10	0.8	<0.01	$y = -3.37 \times 10^{-3}x + 1.90 \times 10^2$	decreasing
MOE FEN	650S	150	11	na	na	na	stable
MOE FEN	1100S	150	10	na	na	na	decreasing
MOE FEN	500N	150	20	0.8	<0.01	$y = -3.45 \times 10^{-3}x + 1.84 \times 10^2$	decreasing
MOE FEN	800N	150	17	0.4	<0.01	$y = 2.17 \times 10^{-3}x - 1.65 \times 10^0$	increasing
MOE FEN	0	DEEP PEAT	41	na	na	na	stable
MOE FEN	80S	DEEP PEAT	45	na	na	na	decreasing

MOE FEN	160S	DEEP PEAT	20	na	na	na	stable
MOE FEN	650S	DEEP PEAT	24	0.3	0.01	$y= -1.11\times10^{-3}x + 1.08\times10^{2}$	decreasing
MOE FEN	500N	DEEP PEAT	42	na	na	na	decreasing
MOE FEN	800N	DEEP PEAT	20	0.2	0.02	$y= -1.25\times10^{-3}x + 1.13\times10^{2}$	decreasing
BIOHERM BOG	25	100	31	0.2	0.02	$y= -4.23\times10^{-6}x^{2} + 3.43\times10^{-1}x - 6.92\times10^{3}$	increasing
BIOHERM BOG	40	100	36	0.4	<0.01	$y= -2.70\times10^{-6}x^{2} + 2.21\times10^{-1}x - 4.5\times10^{3}$	increasing
BIOHERM BOG	80	100	34	na	na	na	stable
BIOHERM BOG	150	100	30	na	na	na	stable
BIOHERM BOG	25	150	31	na	na	na	stable
BIOHERM BOG	40	150	36	na	na	na	stable
BIOHERM BOG	80	150	34	na	na	na	stable
BIOHERM BOG	150	150	30	na	na	na	stable
BIOHERM BOG	25	150	59	0.3	<0.01	$y= 1.26\times10^{-6}x^{2} - 1.07\times10^{-1}x + 2.28\times10^{3}$	decreasing
BIOHERM BOG	40	150	73	na	na	na	stable
BIOHERM BOG	80	150	67	na	na	na	stable
BIOHERM BOG	150	150	33	na	na	na	stable

Table B3. Summary of regression results for the changes in Ksat (m/day; y) over time (day; x) for all monitoring nests, including the number of monitoring events used for the regression (n). Where results were statistically significant for linear or polynomial regressions the r2, p value and associated equation are provided. Locations where water levels were too low for Ksat testing at least 50% of the time were designated as dry. Monitoring intervals are detailed in Table B1.

Site	Nest	Depth (cm bgs)	Number of Monitoring Events (n)	r^{2}	p	Equation of Best Fit	Direction of Change
BOG 1	45	100	2	dry	dry	dry	dry
BOG 1	65	100	5	0.4	0.05	$y= -2.23\times10^{-6}x + 9.24\times10^{-2}$	decreasing
BOG 1	100	100	16	0.8	<0.01	$y= 1.26\times10^{-9}x^{2} -1.07\times10^{-4}x + 2.262\times10^{0}$	decreasing
BOG 1	45	150	5	dry	dry	dry	dry
BOG 1	65	150	10	na	na	na	decreasing
BOG 1	100	150	13	0.3	0.04	$y= -2.52\times10^{-7}x + 1.17\times10^{-2}$	decreasing
BOG 1	45	DEEP PEAT	12	0.9	0.05	$y= -5.65\times10^{-7}x + 2.36\times10^{-2}$	decreasing

BOG 1	65	DEEP PEAT	12	na	na	na	decreasing
BOG 1	100	DEEP PEAT	16	na	na	na	stable
BOG 2	645	100	14	0.4	<0.01	$y= -3.81 \times 10^{-7}x + 1.70 \times 10^{-2}$	decreasing
BOG 2	735	100	8	0.8	<0.01	$y= -6.71 \times 10^{-6}x + 2.99 \times 10^{-1}$	decreasing
BOG 2	645	150	15	na	na	na	stable
BOG 2	735	150	5	na	na	na	stable
BOG 2	735	DEEP PEAT	7	na	na	na	stable
BOG 3	1295	100	11	0.2	0.05	$y= -1.82 \times 10^{-7}x + 7.57 \times 10^{-3}$	decreasing
BOG 3	1445	100	14	0.7	<0.01	$y= 1.6 \times 10^{-9}x^2 -2.1 \times 10^{-5}x + 5.85 \times 10^{-1}$	decreasing
BOG 3	1485	100	6	dry	dry	dry	dry
BOG 3	1295	150	13	0.5	0.03	$y= 2.43 \times 10^{-10}x^2 -2.1 \times 10^{-5}x + 4.35 \times 10^{-1}$	decreasing
BOG 3	1445	150	12	na	na	na	decreasing
BOG 3	1485	150	6	dry	dry	dry	dry
BOG 3	1295	DEEP PEAT	3	dry	dry	dry	decreasing
BOG 3	1445	DEEP PEAT	9	na	na	na	decreasing
BOG 3	1485	DEEP PEAT	4	dry	dry	dry	dry
FEN 1	180	100	23	0.3	<0.01	$y= 1.36 \times 10^{-8}x^2 +1.16 \times 10^{-3}x - 2.45 \times 10^{-1}$	increasing
FEN 1	365	100	16	na	na	na	stable
FEN 1	430	100	16	0.2	0.05	$y= 1.23 \times 10^{-3}x - 4.89 \times 10^{1}$	increasing
FEN 1	540	100	13	na	na	na	stable
FEN 1	180	150	14	0.3	0.04	$y= 1.07 \times 10^{-5}x - 3.75 \times 10^{-1}$	increasing
FEN 1	365	150	14	0.2	0.05	$y= 1.97 \times 10^{-6}x - 6.08 \times 10^{-2}$	increasing
FEN 1	430	150	16	0.7	<0.01	$y= -1.03 \times 10^{-9}x^2 + 8.73 \times 10^{-5}x - 1.84 \times 10^{0}$	increasing
FEN 1	540	150	12	na	na	na	decreasing
FEN 1	180	DEEP PEAT	13	na	na	na	stable
FEN 1	365	DEEP PEAT	15	0.5	<0.01	$y= -6.16 \times 10^{-10}x^2 + 5.14 \times 10^{-5}x - 1.07 \times 10^{0}$	increasing
FEN 1	540	DEEP PEAT	14	0.6	<0.01	$y= -2.37 \times 10^{-7}x + 1.15 \times 10^{-2}$	decreasing
FEN 2	875	100	13	na	na	na	increasing
FEN 2	1005	100	17	0.3	0.02	$y= 1.32 \times 10^{-5}x - 4.86 \times 10^{-1}$	increasing
FEN 2	1130	100	16	na	na	na	na
FEN 2	875	150	13	na	na	na	na
FEN 2	1005	150	14	0.4	<0.01	$y= -4.43 \times 10^{-6}x + 2.01 \times 10^{-1}$	decreasing
FEN 2	1130	150	13	0.4	<0.01	$y= 2.54 \times 10^{-9}x^2 - 2.12 \times 10^{-4}x - 4.42 \times 10^{0}$	decreasing
FEN 2	1005	DEEP PEAT	13	na	na	na	stable

FEN 2	1130	DEEP PEAT	13	0.3	0.03	$y= -2.11 \times 10^{-7}x + 9.97 \times 10^{-3}$	decreasing
MOE BOG	0	100	2	na	na	na	stable
MOE BOG	100	100	4	na	na	na	increasing
MOE BOG	200	100	3	na	na	na	increasing
MOE BOG	300	100	3	na	na	na	increasing
MOE BOG	400	100	3	na	na	na	stable
MOE BOG	500	100	3	na	na	na	stable
MOE BOG	0	150	4	na	na	na	stable
MOE BOG	100	150	4	na	na	na	increasing
MOE BOG	200	150	4	na	na	na	stable
MOE BOG	300	150	2	na	na	na	stable
MOE BOG	400	150	3	na	na	na	stable
MOE BOG	500	150	3	na	na	na	stable
MOE BOG	100	DEEP PEAT	4	na	na	na	increasing
MOE BOG	200	DEEP PEAT	3	na	na	na	increasing
MOE BOG	300	DEEP PEAT	4	na	na	na	stable
MOE BOG	400	DEEP PEAT	4	na	na	na	increasing
MOE BOG	500	DEEP PEAT	3	na	na	na	increasing
MOE FEN	0	100	4	na	na	na	stable
MOE FEN	80S	100	4	na	na	na	stable
MOE FEN	160S	100	4	na	na	na	increasing
MOE FEN	650S	100	2	na	na	na	stable
MOE FEN	1100S	100	2	na	na	na	stable
MOE FEN	500N	100	4	na	na	na	stable
MOE FEN	800N	100	4	na	na	na	stable
MOE FEN	0	150	4	na	na	na	stable
MOE FEN	80S	150	4	na	na	na	stable
MOE FEN	160S	150	4	na	na	na	increasing
MOE FEN	450S	150	2	na	na	na	stable
MOE FEN	650S	150	2	na	na	na	stable
MOE FEN	1100S	150	2	na	na	na	stable
MOE FEN	500N	150	4	na	na	na	stable
MOE FEN	800N	150	4	na	na	na	stable
MOE FEN	0	DEEP PEAT	4	na	na	na	stable
MOE FEN	80S	DEEP PEAT	4	na	na	na	stable
MOE FEN	160S	DEEP PEAT	4	na	na	na	stable
MOE FEN	650S	DEEP PEAT	2	na	na	na	stable

121

MOE FEN	500N	DEEP PEAT	4	na	na	na	stable
MOE FEN	800N	DEEP PEAT	4	na	na	na	stable
BIOHERM BOG	25	100	5	na	na	na	stable
BIOHERM BOG	40	100	5	na	na	na	stable
BIOHERM BOG	80	100	4	na	na	na	stable
BIOHERM BOG	150	100	5	na	na	na	stable
BIOHERM BOG	25	150	5	na	na	na	stable
BIOHERM BOG	40	150	5	na	na	na	stable
BIOHERM BOG	80	150	3	na	na	na	stable
BIOHERM BOG	150	150	5	na	na	na	stable
BIOHERM BOG	25	150	5	na	na	na	stable
BIOHERM BOG	40	150	5	na	na	na	stable
BIOHERM BOG	80	150	5	na	na	na	stable
BIOHERM BOG	150	150	5	na	na	na	increasing
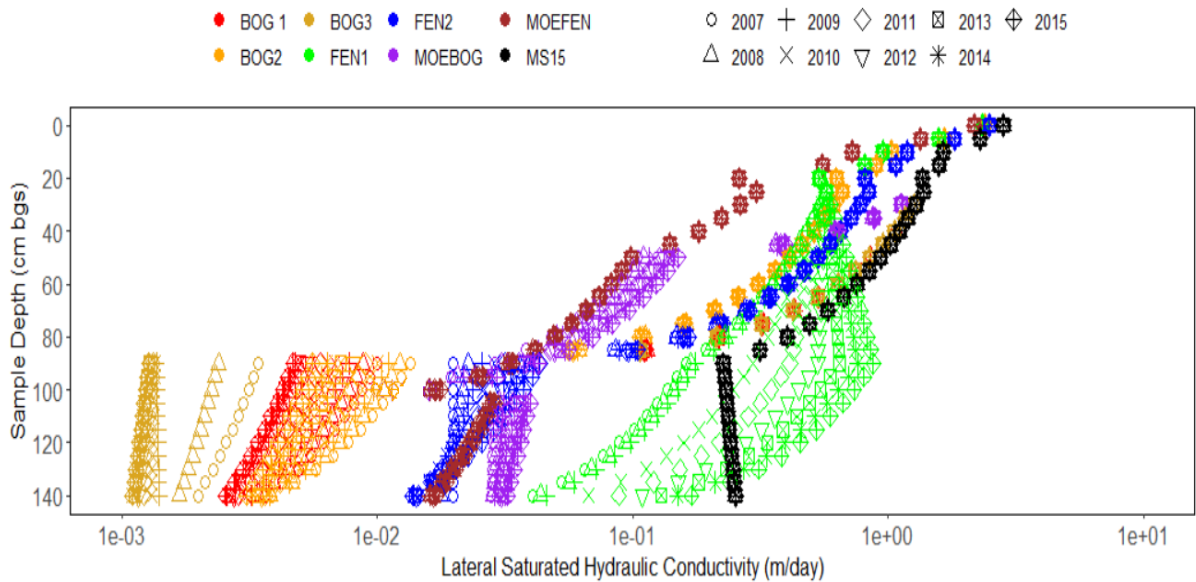
Figure C1. Lateral saturated hydraulic conductivity by depth using samples taken from bogs and fens in the Main Transect over the top 25 cm from laboratory values, and below this linearly interpolated by depth from bail tests conducted in-field in piezometers. Values were averaged for each year at each peatland due to the active effects of dewatering on peat structure.
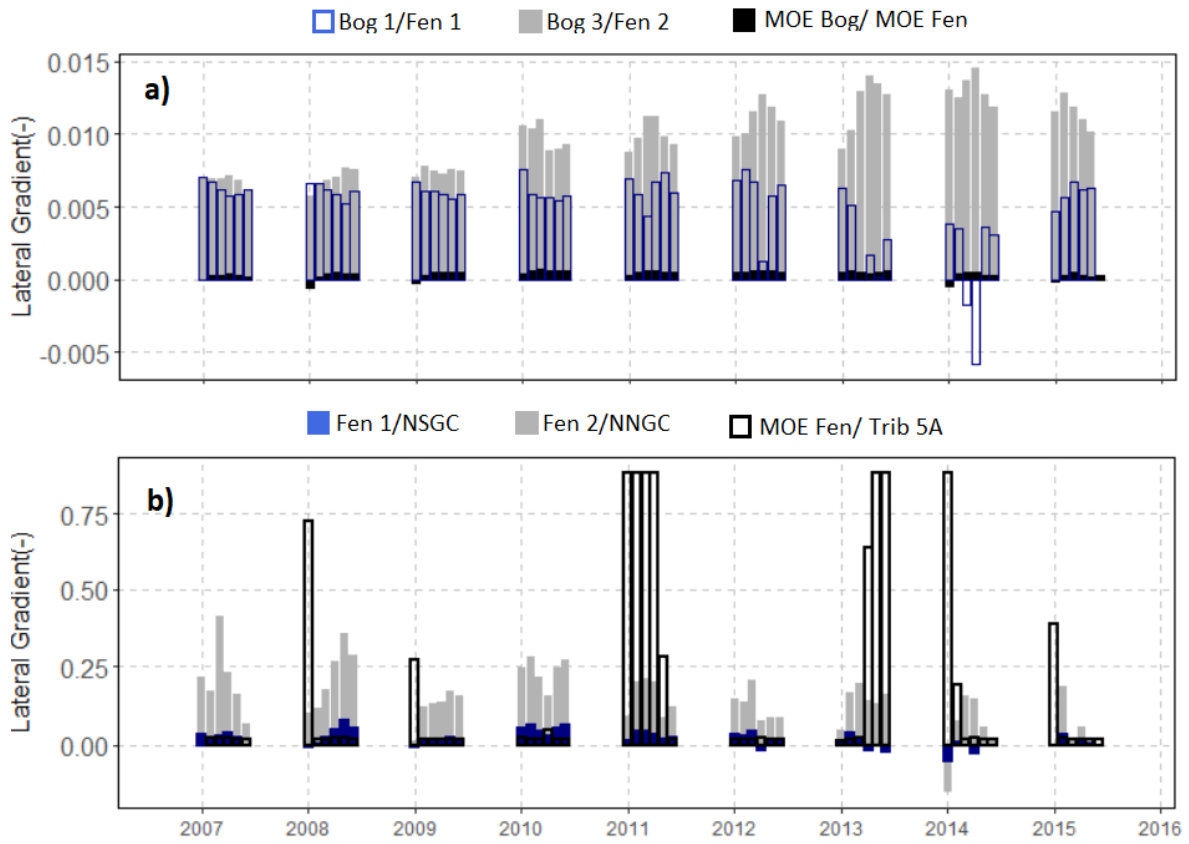
Figure C2. Monthly average lateral hydraulic gradients at of a) the bog/fen interface, and b) fen outlets. Gradients are positive in the bog to fen and fen to tributary direction.

Marine Sediment · **Snow** · **Spring Rain** · **Summer Rain** · **Fall Rain**

Species	Upper Limit	Lower Limit	Units
DOC	19.9	0.00	mg/L
Li$^+$	0.03	0.00	mg/L
Na$^+$	231.4	0.00	mg/L
NH$_4^+$	0.65	0.00	mg/L
K$^+$	4.44	0.00	mg/L
Mg^{2+}	27.03	0.00	mg/L
Ca^{2+}	114.6	0.01	mg/L
F$^-$	0.53	0.00	mg/L
Cl$^-$	56.1	0.00	mg/L
NO$_3^-$	0.41	0.00	mg/L
SO$_4$2-	268.2	0.00	mg/L
δ^{18}O$_{VSMOW}$	-8.08	-24.27	‰
δ^{2}H$_{VSMOW}$	-54.37	-179.58	‰
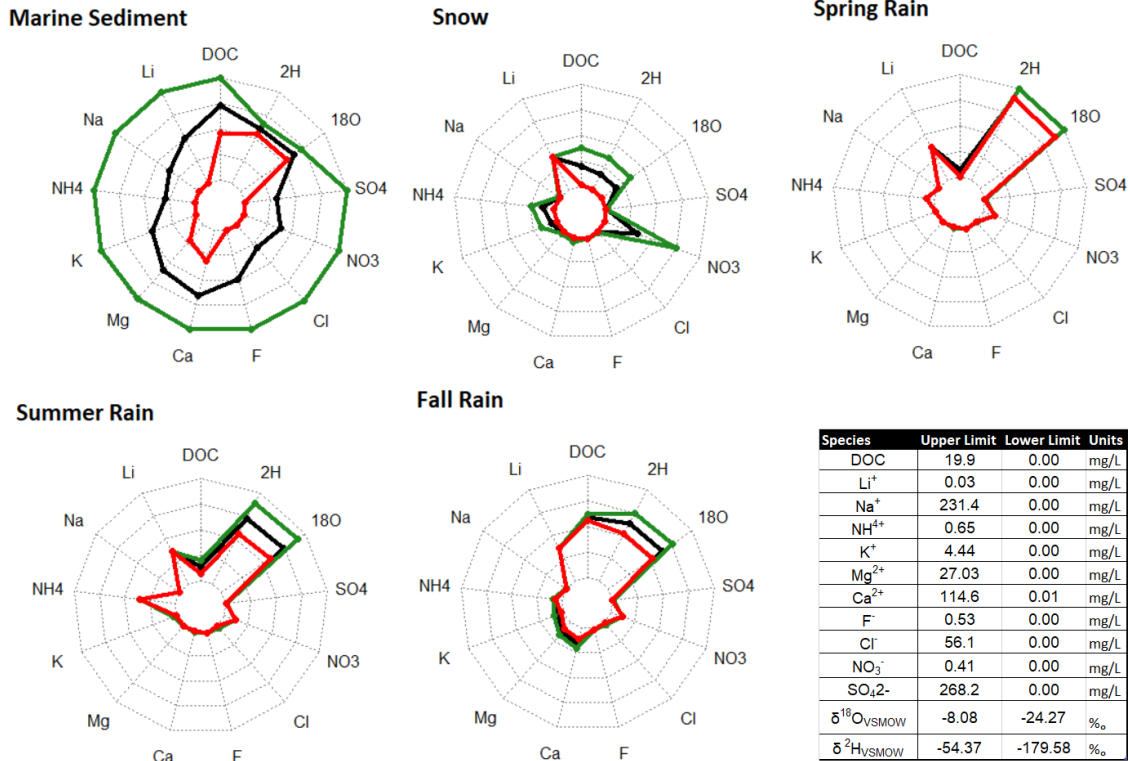
Figure C3. Radar plots showing average (black lines) ± standard devotion (green and red lines) measurements for chemical species testing above detection limits in the water sources.
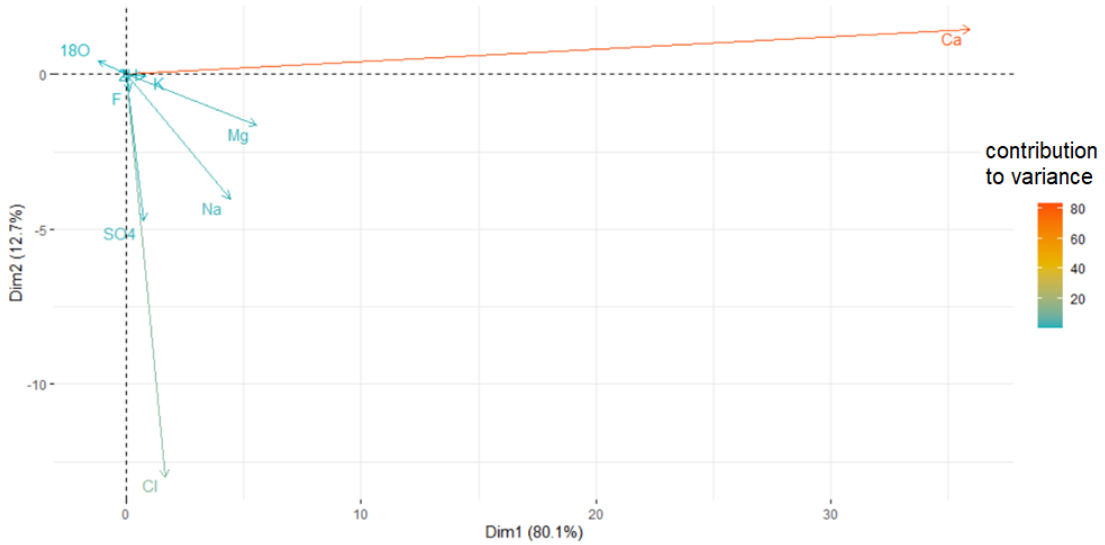
Figure C4. Primary (x axis) and secondary (y axis) principle components of the PCA analysis, and associated contributions of each included ion.

125
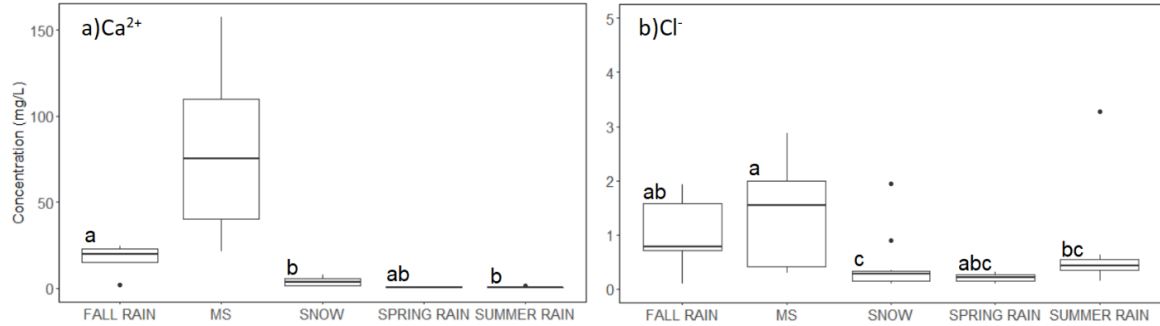
Figure C5. Calcium (a) and chloride (b) concentration distributions water sources. Letters denote distributions which were not significantly different for each chemical species. * 8 outliers were outside of scale bounds for Cl in the MS (165, 160, 66, 40, 26, 22, and 12 mg/L).
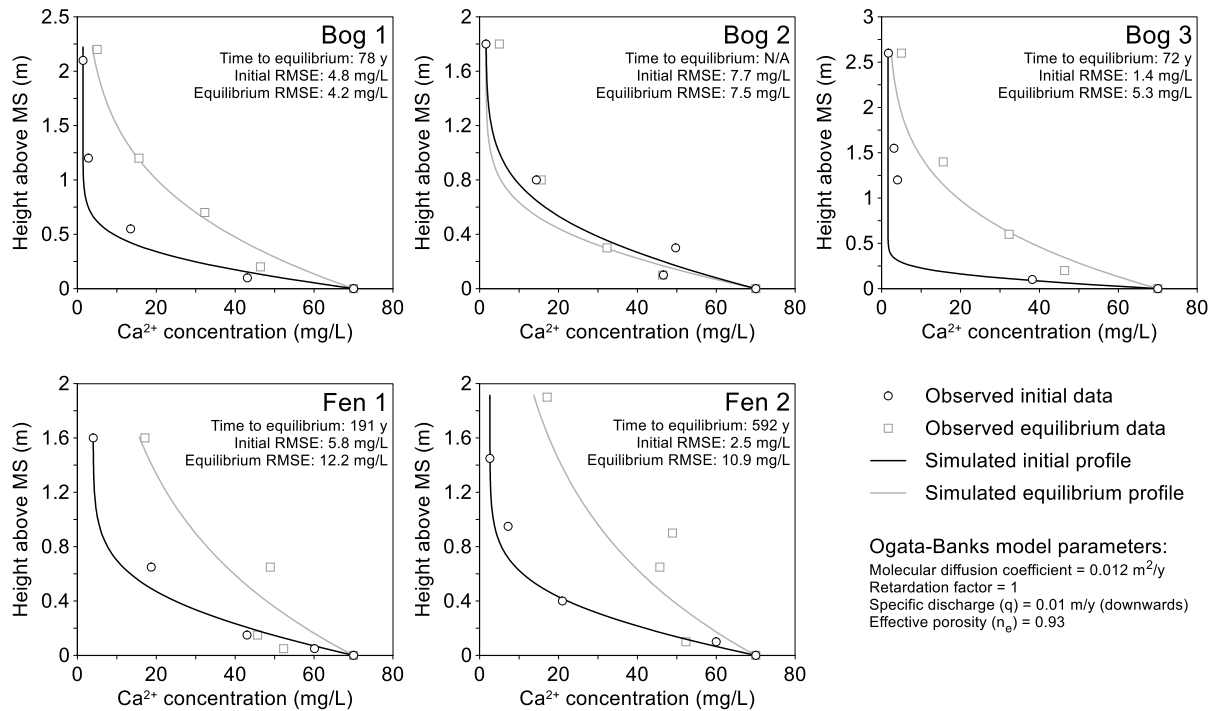
Figure C6. Observed (points) and simulated (lines) initial and equilibrium calcium concentrations at impacted Bog 1, 2 and 3, and Fen 1 and 2. The one-dimensional diffusion modelling used the analytical expression of Ogata and Banks (1961) to provide an estimate of the timeline associated with the reestablishment of pre-disturbance geochemical conditions along the peat profile. This model assumed a constant downward seepage rate of 10 mm/year, which reflects the loss of water along the interface between deep peat and marine sediment under a natural hydrologic regime

(i.e., when mine dewatering is not occurring). This seepage rate counteracts upward diffusion from the MS, and prolongs the time for geochemical conditions to return to equilibrium. Molecular diffusion was the only process that contributed to hydrodynamic dispersion (longitudinal dispersivity was ignored). The effective diffusion coefficient was calculated based on the free-water molecular diffusion for Ca^{2+} from Li and Gregory (1974) and the diffusional tortuosity of deep peat derived from Gharedaghloo and Price (2018). An effective porosity of 0.93 was used for bogs and fens and assumed to equal total porosity since the crucial transport process being considered in this model is diffusion. Adsorption processes were ignored, thus calcium was considered a non-reactive solute in this model. In reality, there would be adsorption between the Ca^{2+} and peat, which could prolong the length of time for equilibrium conditions to re-establish. However, the absence of studies that characterize Ca^{2+} isotherms for bog peat preclude the representation of sorption. All simulations assumed that diffusion could occur for the entire year.

The model was spun-up from an initially homogeneous Ca^{2+} concentration equal to the minimum concentration observed at each site (Bog 1-3 and Fen 1-2), until it approximated the solute profile at each site (more specifically, until it minimized the RMSE with the observed data). Then the model was run until it matched the concentration distribution at the unimpacted site for its respective peatland type; MOE Bog or MOE Fen, which were considered to be representative of equilibrium geochemical conditions. The time to obtain equilibrium Ca^{2+} concentrations along the profile was calculated as the difference in time between the initial and final models. In the case of Bog 2, the difference in time was slightly negative (-5 years), which indicated that Bog 2 exhibited the equilibrium conditions that were expected of an unimpacted Ca^{2+} profile.

Table C1. Fitting parameters for regressions between Main Transect wells/ tributary stages with those measured as part of the De Beers Victor Mine monitoring program

PEATLAND	NEST	VICTOR WELL	R^2
BOG 1	SB+0100	MS8-1R	0.82
FEN 1	SB+0180	MS8-1H	0.72
FEN 1	SB+0365	MS8-1H	0.76
FEN 1	SB+0540	MS8-1D	0.70
BOG 2	SB+0645	MS8-1R	0.72
FEN 2	SB+1005	MS8-1H	0.71

FEN 2	SB+1130	MS8-1H	0.76
BOG 3	SB+1295	MS8-1F	0.73
BOG 3	SB+1485	MS8-1H	0.73
NGCN	NGCN	NGC-3DS	0.77
NGCS	NGCS	NGC-3DS	0.83

Table C2. Yearly frequency of connection over the non-frozen period where continuous water table data were available (2007-2015). Where connection frequency (y) changed significantly over time (x) at the 95% confidence interval, lines of best fit for the change in connectivity over time, and fitting statistics, are shown.

	% OF TIME CONNECTED							
	MOE BOG	**BIO BOG**	**BOG 1**	**BOG 2**	**BOG 3**	**MOE FEN**	**FEN 1**	**FEN 2**
2007	100	100	90	100	10	100	100	35
2008	95	100	80	100	0	100	100	75
2009	100	100	85	100	0	100	100	80
2010	100	100	40	90	0	100	55	0
2011	100	45	60	85	0	75	50	0
2012	100	95	60	75	0	75	40	0
2013	95	100	30	35	0	90	30	10
2014	70	100	5	25	0	100	0	0
2015	100	100	60	85	0	100	40	0
FITTING STATISTICS			$y=-0.0199x+861.97$ ($r^2=0.51$, $p=0.03$)	$y=-0.0196x+873.27$ ($r2=0.48$, $p=0.04$)			$y=-0.0317x+1343.9$ ($r^2=0.79$, $p<0.01$)	$y=-0.0231+957.12$ ($r^2=0.48$, $p=0.04$)

Table C3. Outcomes of Kruskal-Wallace and Dunn post hoc tests comparing Ca2+ distributions for a given peatland measurement depth, categorized by season and year to determine temporal variability of concentrations. Distributions which were significantly different under each category (p<0.05) are italicized.

SITE/SOURCE	DEPTH	p (Ca^{2+} vs, Season)	p (Ca^{2+} vs, Year)	Sample Size
MOE BOG	PW PEAT	0.12	0.13	23

MOE BOG	100 PEAT	0.17	0.78	37
MOE BOG	150 PEAT	0.24	0.61	42
MOE BOG	DEEP PEAT	0.07	0.66	29
MOE FEN	PW PEAT	0.43	-	25
MOE FEN	100 PEAT	0.22	0.72	44
MOE FEN	150 PEAT	0.15	0.61	37
MOE FEN	DEEP PEAT	0.12	0.06	34
BIO BOG	PW PEAT	-	-	2
BIO BOG	100 PEAT	0.34	-	6
BIO BOG	150 PEAT	0.51	-	5
BIO BOG	DEEP PEAT	0.43	-	3
MS	-	0.32	0.66	35
FALL RAIN	-	-	-	46
SPRING RAIN	-	-	-	4
SUMMER RAIN	-	-	0.14	8
SNOW	-	-	0.17	11
BOG 1	PW PEAT	-	-	1
BOG 1	100 PEAT	-	-	6
BOG 1	150 PEAT	0.51	-	8
BOG 1	DEEP PEAT	0.87	0.22	11
BOG 2	PW PEAT	0.47	-	5
BOG 2	100 PEAT	0.1	0.1	12
BOG 2	150 PEAT	0.11	0.12	14
BOG 2	DEEP PEAT	0.48	0.56	5
BOG 3	PW PEAT	-	-	7
BOG 3	100 PEAT	0.22	0.38	16
BOG 3	150 PEAT	0.6	0.12	17
BOG 3	DEEP PEAT	-	-	4
FEN 1	PW PEAT	0.87	-	13
FEN 1	100 PEAT	0.85	0.86	27
FEN 1	150 PEAT	0.94	0.12	25

FEN 1	DEEP PEAT	0.8	0.88	12
FEN 2	PW PEAT	0.48	0.08	5
FEN 2	100 PEAT	0.09	0.14	20
FEN 2	150 PEAT	0.86	0.56	23
FEN 2	DEEP PEAT	0.24	0.25	9